

**DESIGN, SIMULATION & IMPLEMENTATION OF
EMBEDDED CONTROLLER FOR INDUCTION
MELTING MACHINE EMPLOYING OPTIMAL
RESONANT CONVERTER**

*A thesis submitted for the award of the
Degree of*

DOCTOR OF PHILOSOPHY
in
Electrical Engineering

By

Mr. Hiren M. Shah



**ELECTRICAL ENGINEERING DEPARTMENT
FACULTY OF TECHNOLOGY & ENGINEERING
THE MAHARAJA SAYAJIRAO UNIVERSITY OF BARODA
VADODARA – 390 001
GUJARAT, INDIA**

December 2012

Dedicated

To

My Family

**DESIGN, SIMULATION & IMPLEMENTATION OF
EMBEDDED CONTROLLER FOR INDUCTION
MELTING MACHINE EMPLOYING OPTIMAL
RESONANT CONVERTER**

*A thesis submitted for the award of the
Degree of*

DOCTOR OF PHILOSOPHY
in
Electrical Engineering

By

Mr. Hiren M. Shah



**ELECTRICAL ENGINEERING DEPARTMENT
FACULTY OF TECHNOLOGY & ENGINEERING
THE MAHARAJA SAYAJIRAO UNIVERSITY OF BARODA
VADODARA – 390 001
GUJARAT, INDIA**

December 2012

SYNOPSIS

For the Ph.D. thesis

“Design, Simulation & Implementation of Embedded Controller For Induction Melting machine employing optimal Resonant converter”

Guide:

Prof. Satish K Shah

Research Scholar:

Mr. Hiren M. Shah



**ELECTRICAL ENGINEERING DEPARTMENT
FACULTY OF TECHNOLOGY & ENGINEERING
THE MAHARAJA SAYAJIRAO UNIVERSITY OF BARODA
VADODARA – 390 001**

October, 2011

Synopsis

“Design, Simulation & Implementation of Embedded Controller For Induction Melting machine employing optimal Resonant converter”

Guide:

Prof. Satish K Shah

Research Scholar:

Mr. Hiren M. Shah

All Induction Melting applied systems are developed using electromagnetic induction which was first discovered by Michael Faraday. Electromagnetic induction refers to the phenomenon by which electric current is generated in a closed circuit by the fluctuation of current in another circuit placed next to it. The basic principle of induction heating, which is an applied form of Faraday's discovery, is the fact that AC current flowing through a circuit affects the magnetic movement of a secondary circuit located near it. Heat loss, occurring in the process of electromagnetic induction, could be turned into productive heat energy in an electric heating system by applying this law. Many industries have benefited from this new breakthrough by implementing induction heating for furnacing, quenching and welding.

In these applications, induction heating has made it easier to set the heating parameters without the need of an additional external power source. This substantially reduces heat loss while maintaining a more convenient working environment. Absence of any physical contact to heating devices precludes unpleasant electrical accidents. High energy density is achieved by generating sufficient heat energy within a relatively short period of time.

The demand for better quality, safe and less energy consuming products is rising. Such systems are described in the literature but no commercial design is available. Theoretical aspects are well understood but the practical utility and cost analysis are to be investigated.

The different types of electric heating/melting are Resistance heating, Conduction heating, Infrared Radiation heating, Induction heating, Dielectric Hysteresis heating, Electric Arc heating, Plasma heating, Electron Beam heating & Laser heating.

Resistance heating is the most common type of electric process heating. It uses the relationship between the voltage and current of resistance in Joule's Law.

Conduction heating exploits the heat energy generated when an object is placed between two electric poles, which is another application of Joule's Law. In this case, however, a different relationship exists between voltage and current, especially when the circuit current is high, because the object itself contains both resistance and inductance features.

Induction heating refers to the generation of heat energy by the current and eddy current created on the surface of a conductive object (according to Faraday's Law and the skin effect) when it is placed in the magnetic field, formed around a coil, where the AC current flows through (Ampere's Law).

Generally, semiconductor switching devices operate in Hard Switch Mode in various types of PWM DCDC converters and DC-AC inverter topology employed in a power system. In this mode, a specific current is turned on or off at a specific level of voltage whenever switching occurs. This process results in switching loss. The higher is the frequency the more are the switching loss, which obstructs efforts to raise the frequency. Switching also causes an EMI problem, because a large amount of di/dt and dv/dt is generated in the process.

By raising the switching frequency, you can reduce the size of a transformer and filter, which helps build a smaller and lighter converter with high power density. But as presented earlier, switching loss undermines the efficiency of the entire power system in converting energy, as more losses are generated at a higher frequency. Higher energy conversion efficiency at high frequency switching can be obtained by manipulating the voltage or current at the moment of switching to become zero. This is called "Soft Switching", which can be subcategorized into two methods: Zero-voltage switching and Zero-current switching. Zero-voltage switching refers to eliminating the turn-on switching loss by having the voltage of the switching circuit set to zero right before the circuit is turned on. Zero-current switching [1] is to avoid the turn-off switching loss by allowing no current to flow through the circuit right before turning it off. The voltage or current administered to the switching circuit can be made zero by using the resonance created by an L-C resonant circuit. This topology is named a "resonant converter." [5]

As a resonant converter provides most of the energy conversion efficiency in a power system by minimizing switching loss, it is widely used in a variety of industries. And this is also the reason why the converter is adopted in the Induction Melting Power System Topology, which is the major area of work for this thesis.

The resonant converter can be further classified into two major types: a half-bridge series resonant converter and a quasi-resonant converter. Due to single switch requirements the quasi-resonant converter is chosen for the work.

Refractory material is required between the charge and the induction heating work coil[2]. This can be either a rammed monolithic refractory or of a preformed-crucible construction. Conducting crucibles are essentially reformed high temperature refractory pots made in different shapes and sizes, which have relatively-low electrical resistivity ranging typically from $10^{-5} \Omega\text{m}$ to $6 \times 10^{-4} \Omega\text{m}$ at room temperature. Conducting crucibles made of carbon-bonded silicon carbide have resistivity from $10^{-5} \Omega\text{m}$ to $10^{-4} \Omega\text{m}$, whereas the resistivity of clay-bonded graphite crucibles is up to $6 \times 10^{-4} \Omega\text{m}$ at room temperature. The flexibility of production associated with the melting of nonferrous metals in portable crucibles or tilting furnaces with preformed crucible linings is well suited to foundries where relatively small amounts (typically less than 200 kg) of different metals or alloys are required.

Project envisages the development of Embedded Controller to improve the performance of Induction Melter. Ideas of the practical application of such a Melter for Gold & other metals with all next generation facilities and cost benefit analysis have to be looked in to detail. The project provides sufficient insight into these aspects. The technical report discusses technical and economical competitiveness of the prototype. Commercialization of the technology is positive. For the proposed work LPC2478 ARM controller was chosen for its following features.

NXP Semiconductors designed the LPC2478 microcontroller, powered by the 16-bit/32-bit ARM7TDMI-S core with real-time emulation, to be a highly integrated microcontroller for a wide range of applications that require advanced communications and high quality graphic displays. The LPC2478 microcontroller has 512 kB of on-chip high-speed flash memory. This flash memory includes a special 128-bit wide memory interface and accelerator architecture that enables the CPU to execute sequential instructions from flash memory at the maximum 72 MHz system clock rate. The LPC2478, with real-time debug interfaces that include both JTAG and embedded trace, can execute both 32-bit ARM and 16-bit Thumb instructions.[39,42]

The LPC2478 microcontroller incorporates a TFT controller, a 10/100 Ethernet Media Access Controller (MAC), a USB full-speed Device/Host/OTG Controller with 4 kB of endpoint RAM, four UARTs, two Controller Area Network (CAN) channels, an SPI interface, two Synchronous Serial Ports (SSP), three I2C interfaces, and an I2S interface. The very high speed execution & all modern

peripheral support the need of next generation facilities and powerful controlling can be accomplished using LPC2478 ARM controller.

The use of software development support tools [24] such as MATLAB, SIMULINK and Tool Boxes [25,26] makes simulation study as well design of graphical user interface simpler.

The work described in the thesis includes:

1. Design and implementation of 3-ph power circuit based on a new-generation of power semiconductor devices (IGBT's) & driver cards.
2. Development of MMI & controller board around LPC2478 ARM processor.
3. Designing of Coil, Capacitor, power circuit & developing controller hardware.
4. Proposal and implementation of modification in quasi-resonant power circuit to eliminate large amount of filter capacitors.
5. Simulation study of the design setup including power circuit & control circuit.
6. Development of Controller software.
7. Developing algorithm for auto-tuning PID using Ziegler-Nichols Frequency Domain method.
8. Software development using Keil Real-View for LPC2478 ARM processor. [27,28]
9. To explore new concept to melt gold/silver.

The thesis is organized in the form of ten chapters as follows:

- Chapter: 1** Overview: The chapter provides a preview and the context for the remainder of the thesis.
- Chapter: 2** Introduces the induction melting application and problem, which presents a brief state-of-art survey of research work carried out in the area of induction melting. Various power topologies are presented and the need for resonant converter is explained. The various resonant topologies have been presented for switching devices. The latest development on melting application and problem has been reviewed and lays down the motivation behind the research work carried out.
- Chapter:3** A quasi-resonant converter has been proposed, to reduce total switching loss. The design and implementations of a quasi-resonant converter for melting at a high temperature has been carried out.
- Chapter: 4** A modified quasi-resonant converter is proposed to eliminate large amount of filter capacitors. Simulation study of control strategy using MATLAB/SIMULINK.
- Chapter: 5** Discusses Design, Analysis and Simulation of power circuit for the proposed topology. The chapter includes the implementation of Power circuit.
- Chapter: 6** Describes the development of the control circuit for quasi-resonant converter. It also contains the development and design of main generator card with new generation SCALE-2 IGBT-driver circuits.
- Chapter: 7** It discusses the software implementation for micro-controller board & ARM-7 board. As well as development and design of MMI with TFT, touch screen and all modern

facilities are presented.

- Chapter: 8** It deals with the experimental verification of proposed induction Melter. The auto-tuning algorithm, the temperature accuracy and efficiency is verified.
- Chapter: 9** Final conclusions and future extension of the work and future scope in this field are elaborated in this chapter.
- Chapter:10** Thesis ends with Bibliography which includes the list of references used in each chapter and list of publications and presentations done based on this work.

References

1. K.H.Liu and F.C.Lee, "Resonant switches-A unified approach to improve performances of switching converters", IEEE INTELEC Conference Record, pp.344~351, 1984.
2. M.R. Kargahi, L. Hobson, "Theoretical investigations into the use of conducting crucibles in medium-frequency metal melting", IEE PROCEEDINGS, Vol. 132, Pt. B, No. 5, SEPTEMBER 1985
3. K.H.Liu and F.C.Lee, "Zero-voltage switching technique in DC-DC converters", IEEE Power Electronics Specialists Conference Record, pp.58~70, 1986.
4. W.A.Tabisz, P.Gradzki and F.C.Lee, "Zero-voltage-switched buck and flyback converters- Experimental results at 10MHz", IEEE Power Electronics Specialists Conference, pp.404~413, 1987.
5. K.H.Liu, R.Oruganti and F.C.Lee, "Resonant switches-Topologies and characteristics", IEEE Power Electronics Specialists Conference Record, pp.106~116, 1985.
6. W.A.Tabisz and F.C.Lee, "Zero-voltage switching multi-resonant technique in DC-DC converters", IEEE Power Electronics Specialists Conference Record, pp.9~17, 1988.
7. W.A.Tabisz and F.C.Lee, "Development of power supply for induction heating", Annual Project Report for ERL/ITRI of VPEC, July 1991.
8. L.Grajales, W.A.Tabisz and F.C.Lee, "Development of power supply for induction heating", Annual Project Report for ERL/ITRI of VPEC, July 1992.
9. W.C.Moreland, "The induction range:Its performance and its development problems", IEEE Transactions on Industry Applications, vol.IA-9, pp.81~85, 1973.
10. P.H.Peters, "A portable cool-surface induction cooking appliance", IEEE Transactions on Industry Applications, vol.IA-10, no.6, pp.814~822, 1974.
11. L.Grajales, K.R.Wang and F.C.Lee, "Development of power supply for induction heating", Annual Project Report for ERL/ITRI of VPEC, July 1993.
12. H.Omori, M.Nakaoka, H.Yamashita and T.Marubishi, "A novel type induction-heating singleended resonant inverter using new bipolar darlington transistor", IEEE PESC Proc., pp.590~599, 1985.
13. P.Jain and S.B.Dewan, "Starting problems associated with a transformer coupled load in a series inverter", IEEE Transactions on Magnetics, vol.24, no.6, pp.2895~2897, 1988.
14. G.Zaiser, G.Fischer, M.Bruckmann and H.Doht, "ZVS driver for voltage-controlled switches in resonant converters", Power Conversion, June 1995 Proceedings, pp.481~489.
15. H.W.Koertzen, J.D.van Wyk and J.A.Ferreira, "Design of the half-bridge series resonant converter for induction heating", IEEE PESC Record, vol.2, pp.729~735, 1995.

16. S.Hinchliffe and L.Hobson, *Review of solid state devices and circuits for HF electric process heating applications:Part_ devices*, Int'l Journal of Electronics, vol.61,no.2,pp.143~167, 1986.
17. S.Hinchliffe and L.Hobson, *Review of solid state devices and circuits for HF electric process heating applications:Part_ circuit*, Int'l Journal of Electronics, vol.61,no.3,pp.261~279, 1986.
18. M.Orfeuil & A.Robin, *Electric Process Heating*, Battelle Press, 1987
19. J.Davies, *Induction Heating Handbook*, McGraw-Hill, 1979
20. M.G.Loizinskii, *Industrial Applications of Induction Heating*, Pergamon Press, 1969
21. N.Mohan, T.M.Undeland & W.P.Robbins, *Power Electronics: Converters, Applications, and Design*, John Wiley & Sons, 1989
22. “Induction-Heated Cooking Appliance Using New Quasi-Resonant ZVS-PWM Inverter With Power Factor Correction” By Shengpei Wang, Kiyoshi Izaki, Izuo Hirota, Hidekazu Yamashita, Hideki Omori, and Mutsuo Nakaoka, IEEE Transactions on Industry Applications, Vol. 34, No, 4, JULY/AUGUST 1998 705
23. Review of Project at Purdue University... “Fuzzy logic and Genetic Algorithm Synergism to Control & Identification of Dynamical System” by Yonghan Lee & Prof. Stanislaw H. Zak. – Project sponsored by National Science Foundation

REFERENCE MANUALS

- | | |
|--------------------------------------|--------------------|
| 1. MATLAB® R13/R14: DOCUMENTATION CD | The Mathworks Inc. |
| 2. Using MATLAB7: User Guide | The Mathworks Inc. |
| 3. Using SIMULINK5: User Guide | The Mathworks Inc. |
| 4. Keil Real-View ARM | KEIL |
| 5. MCB2470 EVM board | Embedded Artists |

**DESIGN, SIMULATION & IMPLEMENTATION OF
EMBEDDED CONTROLLER FOR INDUCTION
MELTING MACHINE EMPLOYING OPTIMAL
RESONANT CONVERTER**

*A thesis submitted for the award of the
Degree of*

DOCTOR OF PHILOSOPHY
in
Electrical Engineering

By

Mr. Hiren M. Shah



**ELECTRICAL ENGINEERING DEPARTMENT
FACULTY OF TECHNOLOGY & ENGINEERING
THE MAHARAJA SAYAJIRAO UNIVERSITY OF BARODA
VADODARA – 390 001
GUJARAT, INDIA**

December 2012

Declaration

I, **Mr. Hiren M. Shah** hereby declare that the work reported in this thesis entitled “**Design, Simulation & Implementation of Embedded Controller For Induction Melting machine employing optimal Resonant converter**” submitted for the award of the degree of **DOCTOR OF PHILOSOPHY** in Electrical Engineering Department, Faculty of Technology & Engineering, The M. S. University of Baroda, Vadodara is original and has been carried out in the Department of Electrical Engineering, Faculty of Technology & Engineering, M. S. University of Baroda, Vadodara. I further declare that this thesis is not substantially the same as one, which has already been submitted in part or in full for the award of any degree or academic qualification of this University or any other Institution or examining body in India or abroad.

December 2012

Mr. Hiren M. Shah

Certificate

This is to certify that the thesis entitled, **“Design, Simulation & Implementation of Embedded Controller For Induction Melting machine employing optimal Resonant converter”** submitted by **Mr. Hiren M. Shah** in fulfillment of the degree of **DOCTOR OF PHILOSOPHY** in Electrical Engineering Department, Faculty of Technology & Engineering, The M. S. University of Baroda, Vadodara is a bonafide record of investigations carried out by him in the Department of Electrical Engineering, Faculty of Technology & Engineering, M. S. University of Baroda, Vadodara under my guidance and supervision. In my opinion the standards fulfilling the requirements of the Ph.D. Degree as prescribed in the regulations of the University has been attained.

December 2012

Prof. Satish K. Shah

Department of Electrical Engineering,
Faculty of Technology & Engineering,
The Maharaja Sayajirao University of Baroda,
Vadodara – 390 001

ACKNOWLEDGEMENTS

I express my thanks to god for providing me inspirations, strength, energy and patience to start and accomplish my work with the support of all concerned a few of them I am trying to acknowledge.

I would like to express my sincerest gratitude towards **My Guide and Head of Electrical Engineering Department Prof. Satish K. Shah**, Faculty of Technology and Engineering, The M. S. University of Baroda, who gave me an opportunity to work on this problem, and did not fail in trusting in my commitment. Of course, this work would not have been possible without his full and whole hearted support as an advisor, well wisher.

I would like to convey my sincere thanks to Mr. Viral N. Parikh, Director of Delmer Products Ltd., Vadodara, who not only supported financially but also gave me mental support on each and every stage of the work.

I heartily thank to Mr. Promod Nagraj, Mr. Mohan Tilvalli and Prof. M. M. Pathan who have given their endless support, and gave me guidance whenever I need it.

I would like to thank my colleagues for their help and throughout support, to teaching and non teaching staff of Electrical Engineering Department, Faculty of Technology and Engineering, The M. S. University of Baroda for providing me co-operative environment.

I also acknowledge my personal dedication towards **MY FAMILY** who have always supported in bad and good times and have been dedicated to my success.

Hiren M. Shah

ABSTRACT

In recent days the gold price is on a big hike which has lead to increase in recycling process. The melting is the first stage of recycling. Thus a requirement is generated for development of optimized Embedded controller for Induction Melting machine.

Electromagnetic induction refers to the phenomenon by which electric current is generated in a closed circuit by the fluctuation of current in another circuit placed next to it. In the melting applications, induction heating has made it easier to set the heating parameters without the need of an additional external power source. This substantially reduces heat loss while maintaining a more convenient working environment. Absence of any physical contact to heating devices precludes unpleasant electrical accidents. High energy density is achieved by generating sufficient heat energy within a relatively short period of time.

The demand for better quality, safe and less energy consuming products is rising. Such systems are described in the literature but no commercial design is available. Theoretical aspects are well understood but the practical utility and cost analysis are to be investigated.

As a resonant converter provides most of the energy conversion efficiency in a power system by minimizing switching loss it is widely used in a variety of industries. And this is also the reason why the converter is adopted in the Induction Melting Power System Topology, which is the major area of work for this thesis.

The main objective of the research work is to propose and implement the modified quasi-resonant converter. Project envisages the development of Embedded Controller to improve the performance of Induction Melter. Proposed strategies employing soft computing are simulated using development support tools such as: MATLAB/SIMULINK. Ideas of the practical application of such a Melter for Gold & other metals with all next generation facilities and cost benefit analysis are looked into detail. The project provides sufficient insight into these aspects. The technical report discusses technical and economical competitiveness of the prototype. Commercialization of the technology is positive.

A prototype model is developed to evaluate the scheme and to generate experimental results.

Table of contents

List of Figures	IV
List of Tables	VIII
1. Introduction	1-5
1.1 General	1
1.2 State of The Art	2
1.3 Motivation	4
1.4 Thesis Organization	5
2. Principle Of Induction Melting & Survey of Power Topologies & Different Tuning Methods for PID	6-23
2.1 Introduction	6
2.2 Types of Electric Process Heating	7
2.3 Principle of Induction Melting	8
2.4 Electromagnetic Induction	9
2.5 Skin Effect	9
2.6 PWM Techniques	10
2.7 Resonant Topologies	12
2.7.1 Series or Parallel Loading	13
2.7.2 Fixed or Variable Frequency	13
2.7.3 Discontinuous Resonance	14
2.7.4 Zero Current Switch	14
2.7.5 Zero Voltage Switch	15
2.8 Survey of different tuning methods for PID	16
2.9 Summary	23
3. Design & Implementation of A Quasi-Resonant Converter	24-37
3.1 Introduction	24
3.2 Resonant Converter	25
3.3 Power System of Induction Melter	27
3.4 Half-bridge Series Resonant Converter	28
3.4.1 Main Power Circuit	29
3.4.2 Operation Theory	30
3.5 Quasi-resonant Converter	32
3.5.1 Main power circuit	32
3.5.2 Operating Concept	32

3.6 Simulation of Quasi-resonant Converter	34
3.7 Summary	37
4. Proposal & Implementation of Modified Quasi-Resonant Converter	38-45
4.1 Introduction	38
4.2 Modified Quasi Resonant Converter	38
4.2.1 Main Power Circuit	39
4.2.2 Operation Theory	39
4.3 Simulation of Modified Quasi-resonant Converter	40
4.4 Summary	45
5. Design And Implementation of Power Circuit	46-56
5.1 Introduction	46
5.2 Steps of Design of Tank Circuit	46
5.3 Summary	56
6. Development And Design of The Control Circuit for Quasi-Resonant Converter	57-74
6.1 Introduction	57
6.2 Control	57
6.3 Current Sensing Technology Overview	58
6.4 Micro-controller Board (AT89C51ED2)	61
6.5 Embedded controller (ARM-7) Board (LPC2478)	66
6.6 Coreless IGBT Gate Driver	67
6.7 New Generation Scale-2 IGBT-Driver Circuits	68
6.8 Summary	74
7. Software Implementation	75-98
7.1 Introduction	75
7.2 Low-level software for Micro-controller Board	75
7.2.1 Main program	75
7.2.2 Timer-0 Interrupt at 1ms	78
7.2.3 Timer-1 Interrupt for maximum on-cycle time	80
7.2.4 Timer-2 Interrupt at 40ms	81
7.2.5 Interrupt on external falling edge (generated by Load Tuning Circuit of Figure 6-7)	86
7.2.6 Serial port Interrupt	86

7.3 High-level software for Embedded controller (ARM-7) Board	90
7.3.1 Graphical User Interface	90
7.3.2 Main program (MAIN.C)	93
7.3.3 Interrupt Routines (IRQ1.C)	95
7.3.4 Serial Port Routines (UART.C)	98
7.4 Summary	98
8. Experimental Verification	99-107
8.1 Introduction	99
8.2 Experimental System	99
8.3 Protection Considerations	103
8.4 Experimental Results	103
8.5 Summary	107
9. Conclusion & Future Scope	108-111
9.1 General	108
9.2 Summary of Important Findings	108
9.3 Scope for Further Research	111
10.Bibliography	112-119
Appendix A: Using Development Tools	120-127
A.1 Programming AT89C51ED2	120
A.2 Keil Real View Project Creation	121
A.3 Eagle Schematic Design	123
A.3 Datasheet of IGBT	124
Appendix B: Photo Gallery	128-137

List of Figures

Figure No.	Name of Figure	Page No.
2-1a	Equivalent circuit of a transformer	8
2-1b	Secondary short	8
2-1c	Basics of Induction Melting	8
2-2	Waveform of a Switching Device	11
2-3	Basic Resonant Converter	13
2-4	Zero-current switch - topology and waveforms	15
2-5	Zero-voltage switch - topology and waveforms	15
2-6	A SIMULINK setup for Example 1	21
2-7	Oscillation captured from scope	21
2-8	Step response from PID values given by ZNFD method	22
2-9	How a point on Nyquist curve is moved with PID control	23
3-1	Operating Principle	24
3-2a	Series Resonant	25
3-2b	Parallel Resonant	25
3-3	Frequency Curve	27
3-4	Power System Using Half-bridge Series Resonant Converter	28
3-5	Main Power Circuit	29
3-6	Equivalent Circuit	29
3-7	Equivalent of Main Power Circuit	30
3-8	Waveforms of Main Power Circuit	31
3-9	Power Circuit of Quasi-resonant Converter	32
3-10	Equivalent Circuit	33
3-11	Waveforms of Main Power Circuit	33
3-12	Simulation of Quasi-resonant converter	35
3-13	Simulation Result of Inductor Current	36
4-1	Power Circuit of Modified Quasi-resonant Converter	38

4-2	Equivalent Circuit	39
4-3	Waveforms of Main Power Circuit	39
4-4	Simulink Block of Quasi-resonant converter	41
4-5	Simulation Result of Inductor Current	42
4-6	Simulation Result of IGBT Current	43
4-7	Simulation Result of voltage across IGBT	44
5-1	Tank Capacitor Bank	47
5-2	Modified Tank Capacitor Bank	48
5-3	Tank Inductor	49
5-4	L-C Tank Circuit	50
5-5	Three phase transformer	51
5-6	Three Phase Bridge Rectifier	52
5-7	Filter Choke	52
5-8	Set of Output Characteristics for two IGBT's with different Saturation Voltages	54
5-9	The TC of the Set of Output Characteristic Curves	55
5-11	RCD Snubber	56
6-1	Control Scheme	57
6-2	Variable Load	58
6-3	Representation of the Hall effect and its electrical parameters	59
6-4	Basic Topology of Open Loop Hall Effect Current Sensor	59
6-5	Basic Topology of Close Loop Hall Effect Current Sensor	60
6-6	Hall Effect Current Sensor Panel Mounting Type HT300M	61
6-7	Load Tuning and Over Current Protection Circuit	62
6-8	Waveform of Load Tuning Circuit	63
6-9	Micro-controller Circuit	64
6-10	Measurement of DC-Link Voltage & Current	65
6-11	Measurement of Crucible Temperature	65
6-12a	ARM-7 control board (top part)	66
6-12b	ARM-7 control board (bottom part)	67
6-13	Block diagram of the coreless gate drive system	67
6-14	Basic Schematic of the gate drive board with 2SC0435T driver	68

6-15	Turn-on characteristic of an IGBT	69
6-16	Typical characteristic at IGBT turn-off	69
6-17	Principle of an IGBT driver with Active Clamping	70
6-18	Principle of an IGBT driver with Advanced Active Clamping	71
6-19	Principle of a central driver	71
6-20	Principle of driving parallel connected IGBTs with individual drivers	71
6-21	Electrical characteristics of 2SC0435T	72
6-22	Final Schematic of the gate drive board with 2SC0435T driver	73
7-1	Monitor Page of GUI	90
7.2	Setup Page of GUI	91
7-3	Snapshot of Melder Project in Keil Real View	92
7-4	Closed Loop System with <i>PID</i> controller	95
7.5	<i>PID</i> controller schematic	95
8-1	Micro-controller (AT89C51ED2) Board	99
8-2	Gate firing section of Micro-controller Board	100
8-3	IGBT driver board placed near IGBT assy.	100
8-4	Comparator section of Micro-controller Board	101
8-5	CS5460(ADC) section of Micro-controller Board	101
8-6	ARM-7 controller Board	102
8-7	Gate drive board with 2SC0435T driver	102
8-8	Copper work pieces kept into crucible	103
8-9	Gate Pulse v/s Tank current	104
8-10	Gate Pulse v/s DC-Link current	105
8-11	Gate Pulse v/s DC-Link voltage	105
8-12	DC-Link Current	106
8-13	Power Factor Reading 0.999	106
8-14	Melted work pieces	107
A-1	Crystal Programmer	120
A-2	Programming window	121
A-3	New Project wizard	121
A-4	Configuration wizard	122

A-5	Project Creation with Different groups	122
A-6	Schematic Design in Eagle 5.4	123
A-7	Datasheet of FZ600R12KE4 IGBT	124
B-1	LPC2478 OEM Board	128
B-2	Thermocouple Mounting	129
B-3	Meters & DSO	129
B-4	LCD display of Mirco-controller Board (POWER-OFF)	130
B-5	LCD display of Mirco-controller Board (POWER-ON)	130
B-6	Title Screen of Embedded Controller	131
B-7	Monitor Screen of Embedded Controller	131
B-8	Screen of Embedded Controller showing START of Melter Power	132
B-9	Screen of Embedded Controller for going into Parameter Menu	132
B-10	Parameter Screen of Embedded Controller	133
B-11	Snapshot of D.S.O. showing Tank Current	133
B-12	Whole setup for metering	134
B-13	Prototype Model of Induction Melter	134
B-14	Testing of Induction Melter in Progress-1	135
B-15	Testing of Induction Melter in Progress-2	135
B-16	Work Pieces of Copper	136
B-17	Work Pieces in Crucible	136
B-18	Insertion of long copper piece to show effect of load inductance changes	137
B-19	Melted work pieces	137

List of Tables

Table No.	Name of Table	Page No.
2.1	Effect of PID parameter on closed loop system	17
2.2	Parameters for ZN (OL)	18
2.3	Parameters for ZN (CL)	20
7.1	Main program listing (Micro-controller board)	78
7.2	Timer-0 Interrupt service subroutine listing	80
7.3	Timer-1 Interrupt service subroutine listing	81
7.4	Timer-2 Interrupt service subroutine listing	86
7.5	External Interrupt service subroutine listing	86
7.6	Serial Port Interrupt service subroutine listing	89
7.7	MAIN.C Part-1 listing	93
7.8	MAIN.C Part-2 listing	94
7.9	MAIN.C Part-3 listing	94
7.10	C code for PID algorithm	96
7.11	C code for computing a & T_u for Autotuning.	97
7.12	UART.C subroutines listing	98
8.1	Experimental Verification Summaries	104

Chapter 1

INTRODUCTION

1.1 General

All Induction Melting applied systems are developed using electromagnetic induction which was first discovered by Michael Faraday. Electromagnetic induction refers to the phenomenon by which electric current is generated in a closed circuit by the fluctuation of current in another circuit placed next to it. The basic principle of induction heating, which is an applied form of Faraday's discovery, is the fact that AC current flowing through a circuit affects the magnetic movement of a secondary circuit located near it. Heat loss, occurring in the process of electromagnetic induction, could be turned into productive heat energy in an electric heating system by applying this law. Many industries have benefited from this new breakthrough by implementing induction heating for furnacing, quenching and welding.

In these applications, induction heating has made it easier to set the heating parameters without the need of an additional external power source. This substantially reduces heat loss while maintaining a more convenient working environment. Absence of any physical contact to heating devices precludes unpleasant electrical accidents. High energy density is achieved by generating sufficient heat energy within a relatively short period of time.

The demand for better quality, safe and less energy consuming products is rising. Such systems are described in the literature but no commercial design is available. Theoretical aspects are well understood but the practical utility and cost analysis are to be investigated.

The different types of electric heating/melting are Resistance heating, Conduction heating, Infrared Radiation heating, Induction heating, Dielectric Hysteresis heating, Electric Arc heating, Plasma heating, Electron Beam heating & Laser heating.

Resistance heating is the most common type of electric process heating. It uses the relationship between the voltage and current of resistance in Joule's Law.

Conduction heating exploits the heat energy generated when an object is placed between two electric poles, which is another application of Joule's Law. In this case, however, a different relationship exists between voltage and current, especially when the circuit current is high, because the object itself contains both resistance and inductance features.

Induction heating refers to the generation of heat energy by the current and eddy current created on the surface of a conductive object (according to Faraday's Law and the skin effect) when it is placed in the magnetic field, formed around a coil, where the AC current flows through (Ampere's Law).

Generally, semiconductor switching devices operate in Hard Switch Mode in various types of PWM DCDC converters and DC-AC inverter topology employed in a power system. In this mode, a specific current is turned on or off at a specific level of voltage whenever switching occurs. This process results in switching loss. The higher the frequency the more the switching loss, which obstructs efforts to raise the frequency. Switching also causes an EMI problem, because a large amount of di/dt and dv/dt is generated in the process.

By raising the switching frequency, the size of a transformer and filter can be reduced, which helps build a smaller and lighter converter with high power density. But as presented earlier, switching loss undermines the efficiency of the entire power system in converting energy, as more losses are generated at a higher frequency. Higher energy conversion efficiency at high frequency switching can be obtained by manipulating the voltage or current at the moment of switching to become zero. which can be subcategorized into two methods: Zero-voltage switching and Zero-current switching. Zero-voltage switching refers to eliminating the turn-on switching loss by having the voltage of the switching circuit set to zero right before the circuit is turned on. Zero-current switching is to avoid the turn-off switching loss by allowing no current to flow through the circuit right before turning it off which was presented by K.H.Liu and F.C.Lee at IEEE INTELEC Conference & IEEE Power Electronics Specialists Conference [1],[2].

1.2 State of The Art

This section provides a comprehensive review of the literature pertaining to the different resonant topologies for induction heating, melting applications. Emphasis is given to both historical papers of classical importance, as well as to the current state of the art.

The voltage or current administered to the switching circuit can be made zero by using the resonance created by an L-C resonant circuit. As a resonant converter provides most of the energy conversion efficiency in a power system by minimizing switching loss, it is widely used in a variety of industries. And this is also the reason why the converter is adopted in the Induction Melting Power System Topology.

The resonant converter can be further classified into two major types: a half-bridge series resonant converter and a quasi-resonant converter. K.H.Liu, R.Oruganti and F.C.Lee proposed Resonant topologies & characteristic in IEEE Power Electronics Specialists Conference [3].

H.Ogiwara , A.Okuno and M.Nakaoka presented the paper which was mainly concerned with a resonant capacitor voltage-clamped type half-bridge topology of new instantaneous resonant current vector-regulated high-frequency inverter with phase-shifting control, which efficiently operates at zero-current soft-switched quasi-resonant and load resonant tank circuit sub-resonant hybrid soft-switching schemes. Its analytical results and performance evaluations were described through computer-aided simulating methods [4].

The efficient single ended type high-frequency induction-heating quasi resonant inverter circuit using a single advanced 2nd generation IGBT for soft-switching and its specially designed driver IC, which operates at a zero-voltage soft switching(ZVS)mode under PFM-based power regulation strategy was presented by Izuo Hirota, Hideki Omori, Kundu Arun Chandra and Mutsuo Nakaoka. The generic voltage-fed and current-fed circuit versions of single-ended resonant inverters for home power electronics appliances were systematically proposed and classified on the basis of the soft-switched PFM mode inverter family. These new technologies are especially developed for quasi-resonant ZVS high frequency inverter with working coil-linked induction - heating loads. This high-efficient high - frequency quasi-resonant inverter system with high-power factor correction and sine wave line current shaping functions is practically demonstrated including a high-frequency IGBT with reduced saturation voltage characteristics, and discussed on the basis of high-power density home-power electronic appliances in the next generation[5].

A New IGBT half-bridge inverter topology with active auxiliary resonant circuit (A'RC) was proposed by Ryoung-Kuk Lee, Jin-Woo Jung, Bum-Seok Suh and Dong-Seck Syun. The A'RC permits the large lossless turn-off snubber capacitor to be successfully used. Therefore, it makes IGBT be used efficiently in high power and high frequency induction heating system. The operation principle and the design procedures of the proposed A'RC are described in detail [6].

Wang, S.; Izaki, K.; Hirota, I.; Yamashita, H.; Omori, H.; Nakaoka, M. presented a new prototype of a voltage-fed quasi-load resonant inverter with a constant-frequency variable-power (CFVP) regulation scheme, which is developed for the next-generation high frequency high power induction heated appliances. This application specific high frequency single ended push pull inverter using new generation specially designed insulated gate bipolar transistors (IGBTs) can efficiently operate under a principle of zero-voltage switching pulse width modulation (ZVS-PWM) strategy [7].

1.2.1 Half-bridge Series Resonant Converter

The merits of a half-bridge series resonant converter are: stable switching, low cost, and a streamlined design. As the voltage of the circuit is limited to the level of the input voltage, the switching circuit can have low internal pressure, which helps reduce the cost. The design of the switching control component, inside a circuit, can be streamlined. There are also some demerits. As the half-bridge method requires two switching circuits, the overall working process becomes more complicated and the size of the heat sink and PCB should also be larger. In addition, the gate operating circuits must be insulated.

1.2.2 Quasi-resonant Converter

One of the merits of a quasi-resonant converter is that it needs only one switching circuit inside. This enables a relatively smaller design for the heat sink and PCB, making the working process far simpler. Another strong point is the fact that the system ground can be shared. A quasi-resonant converter is not free from defects. Most of all, switching is relatively unstable. And high internal pressure of the switching circuit, caused by the resonant voltage administered to both sides of the circuit, pushes the cost of the circuit higher. Besides, the design for the controlling component is more complicated. But as mentioned earlier, technological improvements in high frequency semiconductor switching devices has lead to innovation in terms of low price, high performance, and reliability.

1.3 Motivation

As a resonant converter provides most of the energy conversion efficiency in a power system by minimizing switching loss, it is widely used in a variety of industries. And this is also the reason why the converter is adopted in the Induction Melting Power System Topology, which is the major area of work for this thesis.

Project envisages the development of Embedded Controller to improve the performance of Induction Melter. Ideas of the practical application of such a Melter for Gold & other metals with all next generation facilities and cost benefit analysis have to be looked into detail. The project provides sufficient insight into these aspects. The technical report discusses technical and economical competitiveness of the prototype. Commercialization of the technology is positive.

Hence the motivation behind the research work reported in this thesis was

1. To design and implement 3-ph power circuit based on a new-generation of power semiconductor devices (IGBT's) & driver cards.
2. Development of MMI & Embedded controller board around LPC2478 ARM processor.
3. Designing of Coil, Capacitor, power circuit & developing controller hardware.

4. Proposal and implementation of modification in quasi-resonant power circuit to eliminate large amount of filter capacitors.
5. Simulation study of the design setup including power circuit & control circuit.
6. Development of Controller software.
7. Developing algorithm for auto-tuning PID using Ziegler-Nichols Frequency Domain method.
8. Software development using Keil Real-View for LPC2478 ARM processor.
9. To explore new concept to melt gold/silver.

1.4 Thesis Organization

The chapter 1 provides a preview and the context for the remainder of the thesis.

In chapter 2 the introduction is given on the induction melting application and problem, which presents a brief state-of-art survey of research work carried out in the area of induction melting. Various power topologies are presented and the need for resonant converter is explained. The various resonant topologies have been presented for switching devices. The latest development on melting application and problem has been reviewed and lays down the motivation behind the research work carried out.

In chapter 3 a quasi-resonant converter has been proposed, to reduce total switching loss. The design and implementations of a quasi-resonant converter for melting at a high temperature has been carried out.

In chapter 4 a modified quasi-resonant converter is proposed to eliminate large amount of filter capacitors. It also includes the simulation study of control strategy using MATLAB/SIMULINK.

Chapter 5 discusses Design, Analysis and Simulation of power circuit for the proposed topology. The chapter includes the implementation of Power circuit.

Chapter 6 describes the development of the control circuit for quasi-resonant converter. It also contains the development and design of main generator card with new generation SCALE-2 IGBT-driver circuits.

Chapter 7 discusses the software implementation for micro-controller board & Embedded controller (ARM-7) board. As well as development and design of MMI with TFT, touch screen and all modern facilities are presented. Chapter 8 deals with the experimental verification of proposed induction Melter. The auto-tuning algorithm, the temperature accuracy and efficiency is verified.

In chapter 9 final conclusions and future extension of the work and future scope in this field are elaborated.

Chapter 2

PRINCIPLE OF INDUCTION MELTING & SURVEY OF POWER TOPOLOGIES & DIFFERENT TUNING METHODS FOR PID

2.1 Introduction

In this chapter the introduction is given on the induction melting application and problem, which presents a brief state-of-art survey of research work carried out in the area of induction melting. Various power topologies are presented and the need for resonant converter is explained. The various resonant topologies have been presented for switching devices. The latest development on melting application and problem has been reviewed and lays down the motivation behind the research work carried out.

Electromagnetic induction refers to the phenomenon that electric current is generated in a closed circuit by the fluctuation of current in another circuit placed next to it. The basic understanding of induction heating, which is an applied form of Faraday's discovery, starts from the fact that the AC current flowing through a circuit affects the magnetic movement of a secondary located near to it. The fluctuation of current inside the primary was found to be the answer to the mysterious current generated in the neighboring secondary. The Faraday's discovery has served as a main starting point in developing electric motors, generators, transformers, wireless communications devices, etc. Its applications, however, have not been necessarily flawless. Heat loss that occurs during the induction heating process was a major headache undermining the overall function of a system. Researchers sought to minimize heat loss by laminating the magnetic frames placed inside a motor or transformer. The Faraday's Law was followed by a series of more advanced discoveries such as the Lenz's Law which explains the fact that inductive current flows in inverse to the direction of changes in induction magnetic movement.

Heat loss occurring in the process of electromagnetic induction could be turned into productive heat energy in an electric heating system by applying this law. Many different industries have benefited from this new breakthrough by implementing induction heating to furnacing, quenching, welding, etc. In these applications, induction heating has made it easier to set the heating parameters with no need of additional external power source. This substantially reduces heat loss while maintaining more convenient working environment. Absence of any physical contact to heating devices precludes

unpleasant electrical accidents, and high energy density is achieved by generating sufficient heat energy within a relatively short period of time.

As the demand for a better-quality and less energy-consuming product is getting higher, the electronic appliances have more advanced in terms of quality, safety, and energy consumption. Safety in use and efficient and fast heating/melting make them more attractive.

2.2 Types of Electric Process Heating

Before entering the description of induction heating, some types of electric process heating are provided below.

- Resistance Heating
- Conduction Heating
- Infrared Radiation Heating
- **Induction Heating**
- Dielectric Hysteresis Heating
- Electric Arc Heating
- Plasma Heating
- Electron Beam Heating
- Laser Heating

Resistance heating is the most common type of electric process heating, which applies the relationship between the voltage and current of resistance in the Joule's Law.

Conduction heating exploits the heat energy generated when an object is placed between two electric poles, which is another application of the Joule's Law. In this case, however, a different relationship exists between voltage and current, especially when the circuit current is high, because the object itself contains both resistance and inductance features.

The main topic of this document is induction heating/melting, which is a combination of electromagnetic induction, the skin effect, and the principle of heat transfer. In short, induction heating refers to the generation of heat energy by the current and Eddy current created on the surface of a conductive object (according to the Faraday's Law and the skin effect) when it is placed in the magnetic field formed around a coil where the AC current flows through (Ampere's Law). Detailed descriptions of induction heating are presented in the following sections of the document.

2.3 Principle of Induction Melting

Induction melting is comprised of three basics: electromagnetic induction, the skin effect, and heat transfer. The fundamental theory is similar to that of a transformer. In this section, electromagnetic induction and the skin effect are demonstrated. Figure 2-1 illustrates a very basic system consisting of inductive melting coils and current to explain electromagnetic induction and the skin effect.

Figure 2-1-a shows the simplest form of a transformer, where the Secondary current is in direct proportion to the primary current according to the turn ratio. The primary and secondary losses are by Resistance of Windings and the Link coefficient between the two circuits is 1. Magnetic current leakage is ignored here.

When the coil of the secondary is turned only once and short-circuited, there would be a substantial heat loss due to the increased load current (secondary current). This is demonstrated in Figure 2-1-b.

Figure 2-1-c shows a system where the energy supplied from the source is of the same amount as the combined loss of the Primary and secondary. In the figure, the inductive coil of the primary has many turns while the secondary is turned only once and short-circuited. The inductive heating coil and the load are insulated from each other by a small aperture.

As the primary purpose of induction heating is to maximize the heat energy generated in the secondary, the aperture of the inductive heating coil is designed to be as small as possible and the secondary is made with a substance featuring low resistance and high Permeability. Nonferrous metals will undermine energy efficiency because of their properties of high resistance and low Permeability.

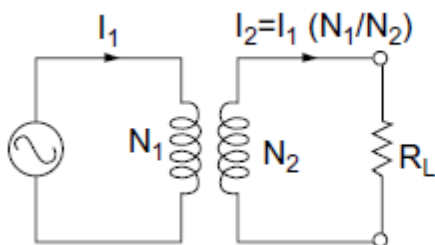


Figure 2-1a Equivalent circuit of a transformer

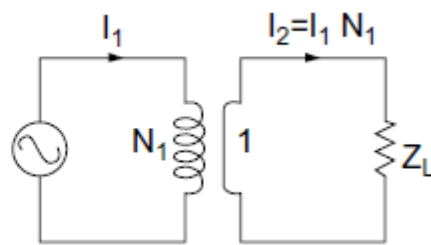


Figure 2-1b Secondary short

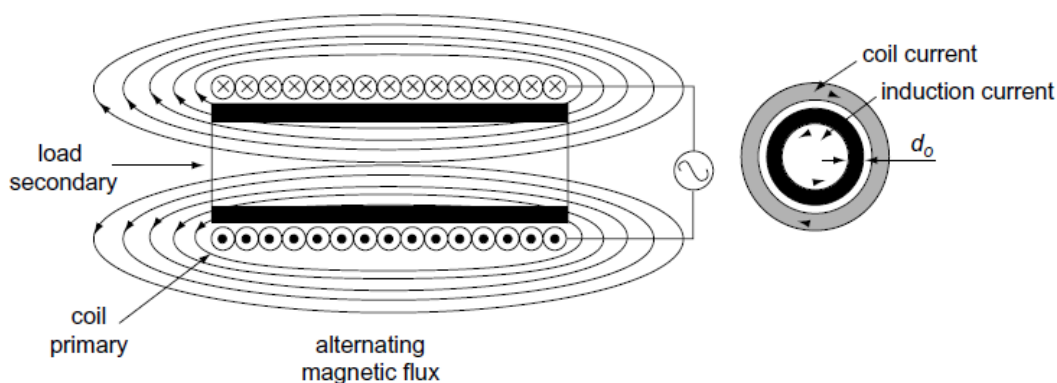


Figure 2-1c Basics of Induction Melting

2.4 Electromagnetic Induction

As shown in Figure 2-1, when the AC current enters a coil, a magnetic field is formed around the coil according to the Ampere's Law.

An object put into the magnetic field causes a change in the velocity of the magnetic movement.

The density of the magnetic field wanes getting closer to the center from the surface. According to the Faraday's Law, the current generated on the surface of a conductive object has an inverse relationship with the current on the inducing circuit as described in Formula 2-1. The current on the surface of the object generates Eddy Current.

$$E = N \frac{d\Phi}{dt} \quad (\text{Equation 2-1})$$

As a result, the electric energy caused by the induced current and Eddy Current is converted to heat energy as in Formula 2-2.

$$P = E^2 / R = i^2 R \quad (\text{Equation 2-2})$$

Here, resistance is determined by the resistivity (ρ) and permeability (μ) of the conductive object.

Current is determined by the intensity of magnetic field. Heat energy is in inverse relationship with Skin Depth.

2.5 Skin Effect

To reach the melting temperature of Gold/Silver (around 1064°C) in a short time the frequency of ac supply must be kept of the order of medium frequency.

The higher the frequency of the current administered to the coil, the more intensive becomes the induced current flowing around the surface of the load. The density of the induced current diminishes when flowing closer to the center as shown in Equation 2-3 and 2-4 below. This is called Skin Effect or Kelvin Effect. From this effect, one can easily infer that the heat energy converted from electric energy would be concentrated on the skin depth (surface of the object).

$$i_x = i_0 e^{-x/d_0} \quad (\text{Equation 2-3})$$

Here, i_x : distance from the skin (surface) of the object, current density at x .

i_0 : current density on skin depth ($x=0$)

d_0 : a constant determined by the frequency (current penetration depth or skin depth)

$$d_0 = \sqrt{\frac{2\rho}{\mu\omega}} \quad (\text{Equation 2-4})$$

Here, ρ : resistivity

μ : permeability of the object

ω : Frequency of the current flowing through the object

2.6 PWM Techniques

It is generally recognized that PWM inverters offer a number of advantages over rival convertor techniques. These advantages are usually gained at the expense of more complex control & power-ckt configuration. The cost & complexity of PWM inverter systems will significantly reduce with continuing developments in LSI technology, fast switching thyristors & power transistors, GTOs & FETs. Combining the computing power of the μp with the fast switching characteristics of the new power electronic devices provides the possibility of realizing the full potential & versatility of power electronic control techniques. Because of advances in solid state power devices and microprocessors [x1], [x1], [x1], [x1], switching power converters are used in more & more modern three phase induction load to convert and deliver the required energy to the objet. The energy that a switching power converter delivers to an induction load is controlled by modulation techniques.

The fundamental of the modulation techniques have been well established.[x2], [x2], [x2], [x2], [x2]. Pulse Width Modulated (PWM) signals are applied to the gates of the power devices. PWM signals are pulse trains with fixed frequency and magnitude and variable pulse width. There is one pulse of fixed magnitude in every PWM period. However, the width of the pulses changes from pulse to pulse according to a modulating signal. When a PWM signal is applied to the gate of power devices, it causes the turn-on and turn-off intervals of the power devices to change from one PWM period to another PWM period according to the same modulating signal. The frequency of a PWM signal must be much higher than that of the modulating signal, the fundamental frequency, such that energy delivered to the load depends mostly on the modulating signal[x3].

The basic PWM techniques are:

1. Single Pulse Width Modulation
2. Multi Pulse Width Modulation
3. Sinusoidal Pulse Width Modulation

But when the technology progresses some advanced modulation techniques are also proposed by the different researcher like:

1. Trapezoidal Modulation
2. Staircase Modulation
3. Stepped Modulation
4. Harmonic Injection Modulation
5. Delta Modulation
6. Space vector Modulation
7. Random PWM

Generally, semiconductor switching devices operate in Hard Switch Mode in various types of PWM DCDC converters and DC-AC inverter topology employed in a power system. In this mode, a specific current is turned on or off at a specific level of voltage whenever switching occurs, as shown in Figure 2-2. This process results in switching loss. The higher the frequency the more the switching loss, which obstructs efforts to raise the frequency. Switching loss can be calculated in a simple way as shown in Equation 2-5 below. Switching also causes an EMI problem, because a large amount of di/dt and dv/dt is generated in the process.

$$P_{sw} = \frac{1}{2} V_{sw} I_{sw} f_s (t_{on} + t_{off}) \quad (\text{Equation 2-5})$$

where, P_{sw} : switching loss [W]

V_{sw} : switching voltage [V]

I_{sw} : switching current [A]

f_s : switching frequency [kHz]

t_{on} : switch turn-on time [s]

t_{off} : switch turn-off time [s]

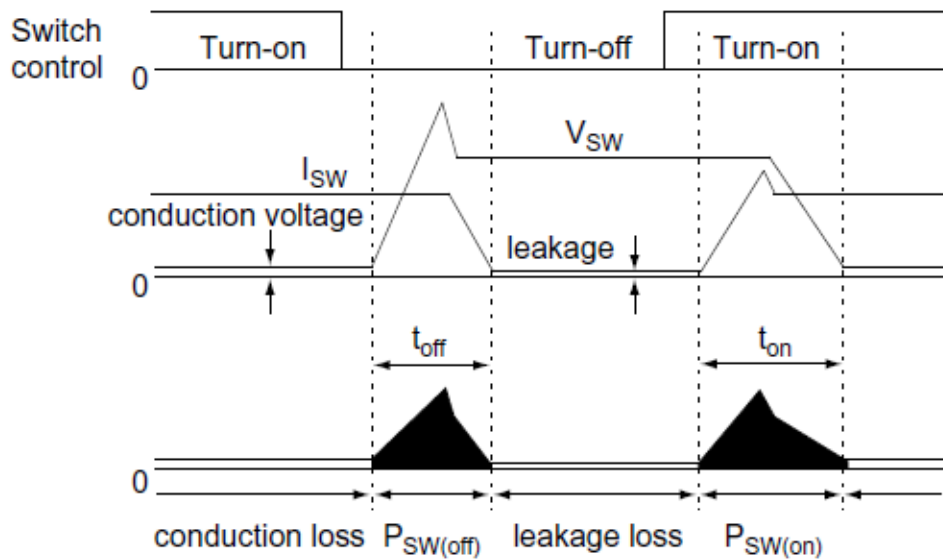


Figure 2-2 Waveform of a Switching Device

By raising the switching frequency, the size of a transformer and filter can be reduced, which helps build a smaller and lighter converter with high power density. But as presented earlier, switching loss undermines the efficiency of the entire power system in converting energy, as more losses are generated at a higher frequency. Higher energy conversion efficiency at high frequency switching can

be obtained by manipulating the voltage or current at the moment of switching to become zero which can be subcategorized into two methods: Zero-voltage switching and Zero-current switching. Zero-voltage switching refers to eliminating the turn-on switching loss by having the voltage of the switching circuit set to zero right before the circuit is turned on. Zero-current switching is to avoid the turn-off switching loss by allowing no current to flow through the circuit right before turning it off which was presented by K.H.Liu and F.C.Lee at IEEE INTELEC Conference & IEEE Power Electronics Specialists Conference [1],[2].

The voltage or current administered to the switching circuit can be made zero by using the resonance created by an L-C resonant circuit. This topology is named a “resonant converter”.

In Zero-current switching, the existing inductance is absorbed into the resonant circuit, eliminating the surge in voltage in a turn-off situation. A voltage surge resulting from an electric discharge of junction capacitance, which occurs upon turning on the switching circuit, cannot be avoided. This method has a defect of causing switching loss ($0.5CV^2f$). Zero-voltage switching, however, is free from such a defect by making both the existing inductance and capacitance to be absorbed by the resonant circuit. This eliminates any chance of causing a surge in current both at turn-off (caused by inductance) or turn-on (by capacitance) conditions. Zero-voltage switching enables switching with less loss while substantially reducing the problem of EMI at high frequency. This difference in features makes Zero-voltage switching more desirable than Zero-current switching.

As a resonant converter provides most of the energy conversion efficiency in a power system by minimizing switching loss, it is widely used in a variety of industries. And this is also the reason why the converter is adopted in the Induction Melting Power System Topology.

2.7 Resonant Topologies

First let us define a resonant converter as a power conditioning system which utilizes a resonant L-C circuit as a part of the power conversion process. All resonant converters operate in essentially the same way: a square pulse of voltage or current is generated by the power switches and this is applied to a resonant circuit. Energy circulates in the resonant circuit and some or all of it is then tapped off to supply the output. While basically simple, this principle can be applied in a wide variety of ways, creating a bewildering array of possible circuits and operating modes.

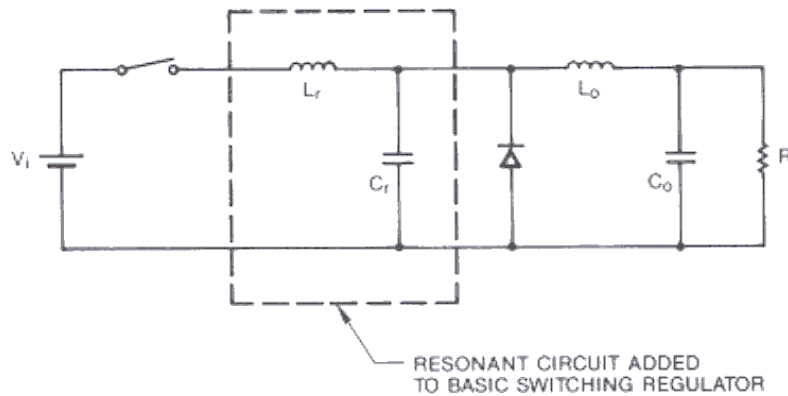


Figure 2-3 Basic Resonant Converter

A resonant switch consists of a switching device (a transistor with a steering diode, for example) in combination with a two-element resonant circuit. This resonant switch may be configured in several different ways, but they always perform the same function as the conventional switch in a square wave converter. It is a useful concept as most resonant mode circuit topologies can be visualized as a conventional PWM circuit with the power switch replaced with a resonant switch.

2.7.1 Series or Parallel Loading:

Since resonant converters operate by putting energy into a resonant circuit and then transferring some or all of it into the load, there are two ways this may be accomplished. If the load is in series with the resonant circuit elements, we call it a series loaded converter and the operating characteristics tend toward a current source with a high impedance output.

Parallel loading is the opposite, with a low impedance voltage source output.

Both modes have application to power systems with high voltage outputs usually using series loaded current source drive and low voltage supplies using parallel loading.

2.7.2 Fixed or Variable Frequency:

Resonant converters may be configured for either constant or variable frequency operation, but these choices infer significant differences in their operation. Fixed frequency control systems use conventional pulse width modulation to change the output in response to a control input. This forces a fixed-frequency system to have at least one non-zero switching transition and possibly two, thereby voiding one of the more significant reasons for choosing to use a resonant mode topology. This would usually preclude its use unless system considerations required a synchronized frequency operation.

Variable frequency operation, however, needs to be subdivided by the third classification: whether the resonant circuit current is continuous or discontinuous. A circuit operating in the continuous resonant mode uses the slope of the resonant circuit impedance curve to control the output. The circuit can

operate either above or below resonance but the principle is the same: that the control circuit changes the frequency to move either toward or away from resonance, and thereby controls the amount of energy which is transferred into the resonant circuit and therefore to the load.

While many practical systems have used continuous conduction, variable frequency operation, there are several disadvantages:

1. The non-zero switching adds stress to the transistors.
2. As the frequency approaches resonance, peak currents or voltages can get very high, adding stress to the resonant components.
3. The control transfer function is very nonlinear following the resonant impedance curve.

The major advantage of the continuous mode of operation is that the frequency varies over a much smaller range than with the discontinuous mode.

2.7.3 Discontinuous Resonance:

The discontinuous operating mode works by supplying constant packets of energy to the load with the rate, i.e. frequency, determined by load power demand.

Perhaps the most popular and important class of resonant converters with variable frequency and discontinuous current is often called Quasi-Resonance. Within the Quasi- Resonant converter category there are still many variations in circuit operation.

Quasi-resonant circuit waveforms are not sinusoidal, but have two essentially linear portions interspersed with two sinusoidal portions.

A quasi-resonant converter control loop is usually configured with a pulse generator driving the resonant circuit at a repetition rate defined by the control circuit. The pulse generator may be set for constant pulse width defined by the resonant circuit -or set to sense zero crossing of either current or voltage. With maximum loading and low line voltage, a quasi-resonant converter can approach continuous resonance as a limit when the individual pulses run together.

Within the variable frequency, discontinuous mode of operation there are two remaining decisions a designer must make which will have significant effect on the characteristics of his power supply:

Zero current or Zero voltage switching.

2.7.4 ZERO CURRENT SWITCH

A typical Zero Current Switch consists of a switch S , in series with the resonant inductor L_{RES} and the resonant capacitor C_{RES} connected in parallel. Energy is supplied by a current source. The circuit and waveforms are shown in figure 2-4.

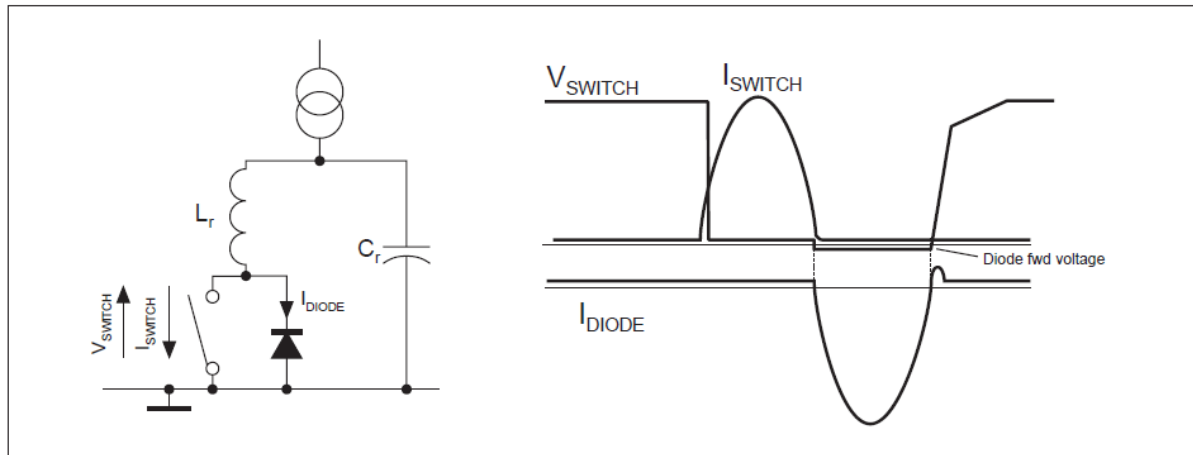


Figure 2-4 Zero-current switch - topology and waveforms

When the switch S is off, the resonant capacitor is charged up with a more or less constant current, and so the voltage across it rises linearly.

When the switch is turned on, the energy stored in the capacitor is transferred to the inductor, causing a sinusoidal current to flow in the switch. During the negative half wave, the current flows through the anti-parallel diode, and so in this period there is no current through or voltage across the switch; and it can be turned off without losses.

2.7.5 ZERO VOLTAGE SWITCH

A typical Zero Voltage Switch consists of a switch in series with a diode. The resonant capacitor is connected in parallel, and the resonant inductor is connected in series with this configuration. A voltage source connected in parallel injects the energy into this system. The circuit and waveforms are shown in figure 2-5.

When the switch is turned on, a linear current will flow through the inductor. When the switch turns off, the energy that is stored in the inductor flows into the resonant capacitor. The resulting voltage across the capacitor and the switch is sinusoidal. The negative half-wave of the voltage is blocked by the diode. During this negative half wave, the current and voltage in the switch are zero, and so it can be turned on without losses.

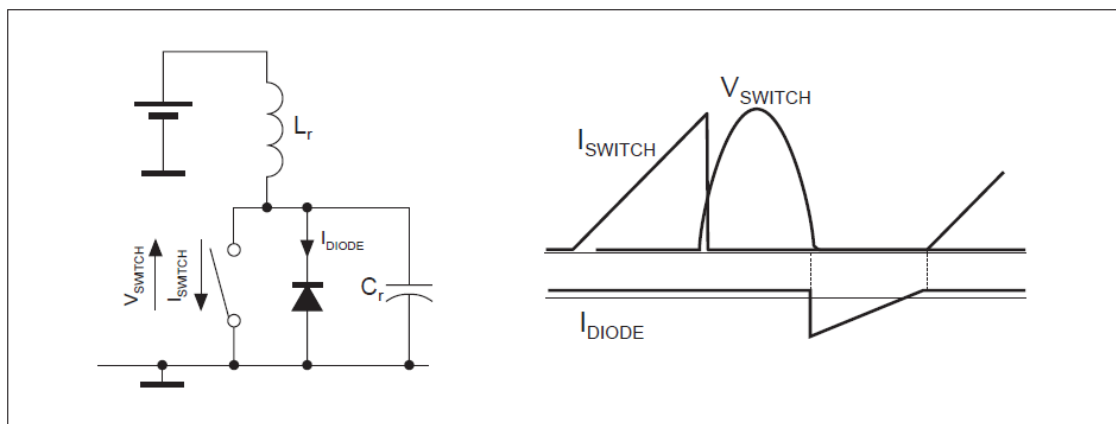


Figure 2-5 Zero-voltage switch - topology and waveforms

2.8 Survey of different tuning methods for PID

Proportional-Integral-Derivative (PID) control is still widely used in industries because of its simplicity. No need for a plant model. No design to be performed. The user just installs a controller and adjusts 3 gains to get the best achievable performance. Most PID controllers nowadays are digital.

Different forms of PID

A standard equation of PID controller is

$$u(t) = K \left\{ e(t) + \frac{1}{Ti} \int_0^t e(t) dt + Td \frac{de(t)}{dt} \right\} \quad (\text{Equation 2-6})$$

where the error $e(t)$, the difference between command and plant output, is the controller input, and the control variable $u(t)$ is the controller output. The 3 parameters are K (the proportional gain), Ti (integral time), and Td (derivative time).

Proportional:

The proportional term, also called gain, must have a value greater than zero for the control loop to operate. The value of the proportional term is multiplied by the error (e) to generate the proportional contribution to the output.

If proportional is acting alone, with no integral, there must always be an error or the output will go to zero. A great deal must be known about the load, sensor, and controller to compute a proportional constant K_p . Most often, the proportional setting is determined by trial and error. The proportional setting is part of the overall control loop gain, as well as the heater range and cooling power. The proportional setting will need to change if either of these changes.

Integral:

In the control loop, the integral term, also called reset, looks at error over time to build the integral contribution to the output.

By adding integral to the proportional contribution, the error that is necessary in a proportional-only system can be eliminated. When the error is at zero, controlling at the set point, the output is held constant by the integral contribution. The integral setting (I) is more predictable than the proportional setting. It is related to the dominant time constant of the load. Measuring this time constant allows a reasonable calculation of the integral setting.

Derivative:

The derivative term, also called rate, acts on the change in error with time to make its contribution to the output.

By reacting to a fast changing error signal, the derivative can work to boost the output when the set point changes quickly; reducing the time it takes for temperature to reach the set point. It can also see the error decreasing rapidly when the temperature nears the set point and reduce the output for less overshoot. The derivative term can be useful in fast changing systems, but it is often turned off during steady state control because it reacts too strongly to small disturbances or noise. The derivative setting (D) is related to the dominant time constant of the load.

The proportional controller (KP) will have the effect of reducing the rise time and will reduce, but never eliminate, the steady state error. An integral controller (KI) will have the effect of eliminating the steady state error, but it may make the transient response worse. A derivative control (KD) will have the effect of increasing the stability of the system, reducing the overshoot and improving the transient response.

Closed loop response	Rise time	Overshoot	Settling time	Steady state error	Stability
Increasing Kp	Decrease	Increase	Small increase	Decrease	Degrade
Increasing Ki	Small decrease	Increase	Increase	Large decrease	Degrade
Increasing Kd	Small decrease	Decrease	Decrease	Minor change	Improve

Table-2.1 Effect of PID parameter on closed loop system

Controller Tuning

The selection of a controller type (P, PI, PID) and its parameters (K, Ti, Td) is intimately related to the model of the process to be controlled. The adjustment of the controller parameters to achieve satisfactory control is called *tuning*.

In the process-control field, it is quite common to first install a PID controller on a process with little analytical study being done beforehand, and then set the controller parameters by experiment. This 'experimental design' of controller settings is known as *controller tuning*.

Auto-tuning PID controllers

The ability of a controller to select and adjust the control parameters automatically via an algorithm is called "*Auto-tuning*" or "*Self-tuning*". So, self-tuning controllers are capable of automatically readjusting the controller tuning settings. They are often referred to as auto-tuning controllers.

Numbers of the industrial processes are controlled by PID-proportional integral derivative controllers. The various settings of the controller have profound effect on loop performance. Proper tuning of a controller is not only essential to its correct operation but also improves product quality, reduces scrap, shortens downtime and saves money. Procedures for tuning conventional PID controllers are well established and simple to perform. Any time a controller is replaced; the new instrument must be re-tuned, which can be difficult under certain running conditions. Hence the need arises for a controller with auto tuning feature.

As previously said, it is important for the controller to be tuned when it is installed first. It also becomes a necessity when it is controlling a critical process. Proper tuning of parameters helps in controlling the process quickly and efficiently which requires trial and error. So, the main advantage of using auto-tuner is that it simplifies tuning drastically and thus contributes to improved control quality.

Different Tuning Method

- Ziegler & Nichols with Step Identification [ZN(OL)]
- Internal Model Control [IMC]
- Ziegler & Nichols with Relay Identification [ZN(CL)]
- Iterative feedback tuning

Ziegler & Nichols with Step Identification [ZN (OL)]:

The first Ziegler and Nichols method tunes the parameter of the PID according to the following table, on the basis of the parameters identified for a First Order PID with Delay Time model.

	K	Ti	Td
P	T/mL	0	0
PI	0.9T/mL	3L	0
PID	1.2T/mL	2L	0.5L

Table-2.2 Parameters for ZN (OL)

In the original version of method, the tuning formulas are given with respect to some characteristic of the process identified in terms of the points where the tangent to the step response in the point of maximum slope intersects the step response. However here the modified version has been used since it is more robust with respect to noise.

Internal Model Control [IMC]:

The principle of this method is explained in Astrom and Hagglund, 1995. The system is approximated by a model of the form,

$$G(s) = K_p / (1 + sT)e^{-sL} \quad (\text{Equation 2-7})$$

If the actual system is unknown, the static gain K_p , the apparent time constant T and the apparent dead time L are determined from an open loop step response, from which an IMC controller is then computed. The controller given by the IMC method can be interpreted as a PID controller with the following choices:

$$K = 2T + L / (2K_p(T_f + L)) \quad (\text{Equation 2-8})$$

$$T_i = T + L / 2 \quad (\text{Equation 2-9})$$

$$T_d = TL / 2T + L \quad (\text{Equation 2-10})$$

Here the design parameter T_f corresponds to the desired closed-loop time constant. In each of our four simulations, we have optimized over this design parameter to achieve an IMC controller with minimum settling time. This optimization was performed by trial and error.

Ziegler & Nichols with Relay Identification [ZN (CL)]:

The Ziegler-Nichols tuning rules are based on what is called the ultimate sensitivity method" (Astrom and Witten mark, 1997). It consists of determining the point where the Nyquist plot of the open loop system intersects the negative real axis. This point is obtained by connecting a purely proportional to the system, and by increasing the controller gain until the closed-loop system reaches the stability limit, at which oscillations occur. The oscillation period is denoted T_c and the corresponding critical gain by K_c . The Ziegler-Nichols choice for the three PID parameters is then

$$K = K_c/17$$

$$T_i = T_c/2$$

$$T_d = T_c/8$$

The second Ziegler and Nichols method tunes the parameter of the PID according to the following table, on the basis of a point of the frequency response identified by a relay experiment. The period of oscillation is denoted as T_u , while the gain margin is $K_u = 4A_s/\pi \cdot A$.

	K	Ti	Td
P	$0.5K_u$	0	0
PI	$0.4K_u$	$0.8T_u$	0
PID	$0.6K_u$	$0.5T_u$	$0.125T_u$

Table-2.3 Parameters for ZN (CL)

In the original version of method, the identification of the point requires to apply proportional control and increase the controller gain until the process output reaches a sustained oscillation. However it is a dangerous practice since it leads the model near the stability limit.

The Iterative Feedback Tuning (IFT) method:

For the simulations presented in the next section, the IFT method with mask was applied, with a mask of length t_0 . Unless otherwise specified, no weighting was applied to the control input in the criterion. Thus, the following criterion was minimized:

$$J(\rho) = E \left\{ \sum_{t=t_0}^N \left(y_t(\rho) - y_t^d \right)^2 \right\}.$$

The initial values of the PID parameters were chosen in such a way as to give an initial response that was very slow, and with no overshoot. The length t_0 of the mask was initially chosen to correspond with the settling time of this very slow response. This length was then successively reduced until oscillations appeared in the closed loop step response.

Tuning by Ziegler-Nichols Frequency Domain (ZNFD) method

There are some variants of autotuning methods suggested in the literature. Here we have used one of them, the relay feedback, which is closely related to a manual tuning scheme known as Ziegler-Nichols Frequency Domain (ZNFD) method.

To tune a PID controller manually by ZNFD method, we start by turning off both the integral and derivative terms. Then K is to be set up to the point that the closed-loop system starts to oscillate. At

this point, the plant output will swing in a constant sinusoid motion, not growing and not dying out. Write this value down on a paper as K_u . Then find a way to measure the period of oscillation. Note this period as T_u . That's all. Suggested values of the 3 parameters can be found from Table-2.3. Example 1 demonstrates this procedure in simulation.

Example 1: We want to experiment ZNFD method on this plant

$$P(s) = \frac{1}{(s+1)^3} \quad (\text{Equation 2-11})$$

Figure 2.6 shows a SIMULINK setup used for this simulation. We turn off the I and D terms and adjust K until $K = 8$, the output oscillates. Figure 2.7 captures the oscillation. Hence $K_u = 8$, and from Figure 2.7 $T_u = 3.5$. Using Table 2.3, we get $K = 4.8$, $T_i = 1.75$ and $T_d = 0.4375$. Figure 2.8 shows a step response when these values are used. Note that the overshoot is quite excessive (50%). In a sense, ZNFD just gives us some good values to start with. We can often fine-tune the PID to improve the response.

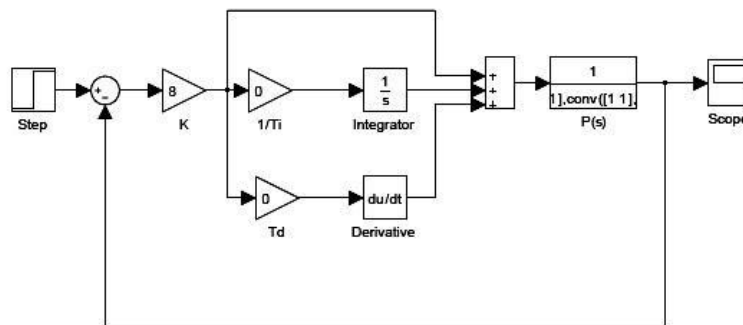


Figure 2-6 A SIMULINK setup for Example 1

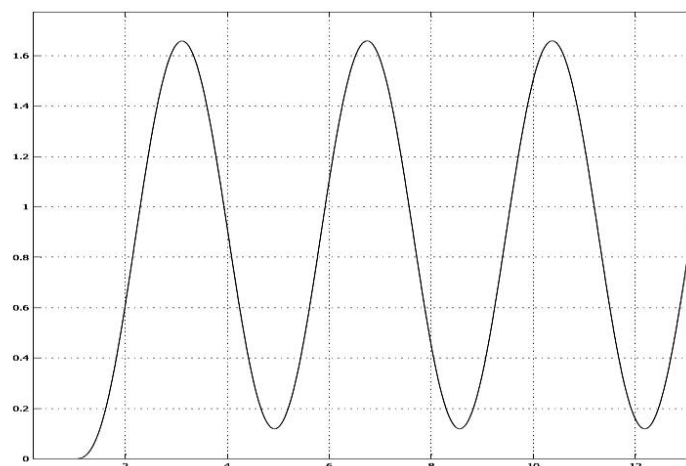


Figure 2-7 Oscillation captured from scope

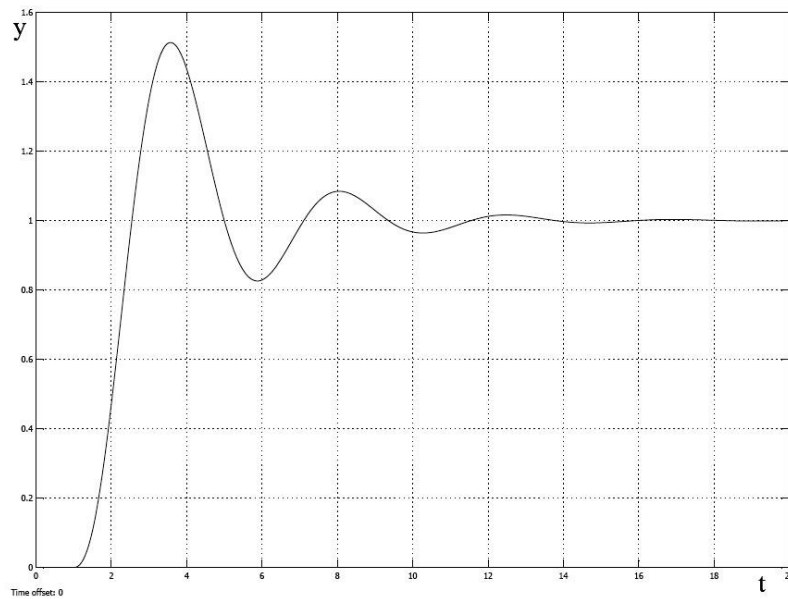


Figure 2-8 Step response from PID values given by ZNFD method

The ZNFD method could be explained using a Nyquist diagram in Figure 2.9. The diagram shows how a point x on the curve is moved related to the P, I, and D terms. Using the P term alone, x could be moved in radial direction only. The I and D terms help provide more freedom to move perpendicular to the radius. It can be shown that by using ZNFD method, the critical point $(-1/K_u, 0)$ is moved to the point $-0.6 - 0.28i$. The distance of this point to the critical point is 0.5. So the sensitivity peak is at least 2. This explains the high overshoot in the step response.

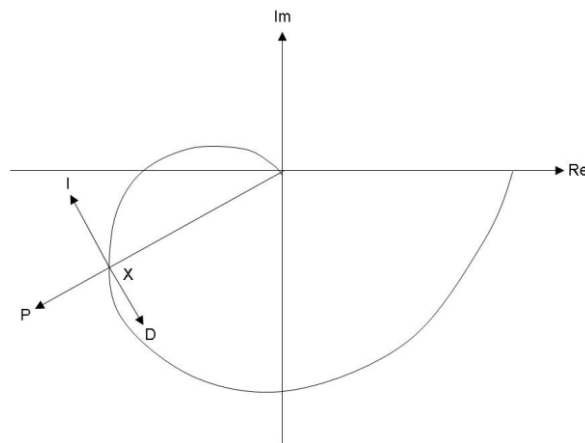


Figure 2-9 How a point on Nyquist curve is moved with PID control

2.9 Summary

The main finding of this chapter reveals following:

1. As a resonant converter provides most of the energy conversion efficiency in a power system by minimizing switching loss, they are best suited for DC-AC converters as compared to PWM converters.
2. Due to skin effect the high frequency switching creates heat on the surface of the load, hence medium switching frequency is used for melting applications.
3. Zero-voltage switching refers to eliminating the turn-on switching loss by having the voltage of the switching circuit set to zero right before the circuit is turned on.
4. Zero-current switching is to avoid the turn-off switching loss by allowing no current to flow through the circuit right before turning it.
5. Different Tuning methods for PID loop are surveyed. It is found that the Ziegler and Nichols method for tuning is simple, accurate and can be easily implemented in digital PID control.

Chapter 3

DESIGN AND IMPLEMENTATION OF A QUASI-RESONANT CONVERTER

3.1 Introduction

The concept of induction heating employed in the application of gold melting can be simplified as the following. First, convert the AC current coming from the power source to DC using a rectifier. Then, connect this DC current to a high frequency switching circuit to administer high frequency current to the heating coil. According to the Ampere's Law, a high frequency magnetic field is created around the heated coil. If a conductive object, e.g. the graphite crucible with gold/silver metal, is put inside the magnetic field, induced Voltage and Eddy current is created on the skin depth as a result of Skin Effect and the Faraday's Law, generating heat energy.

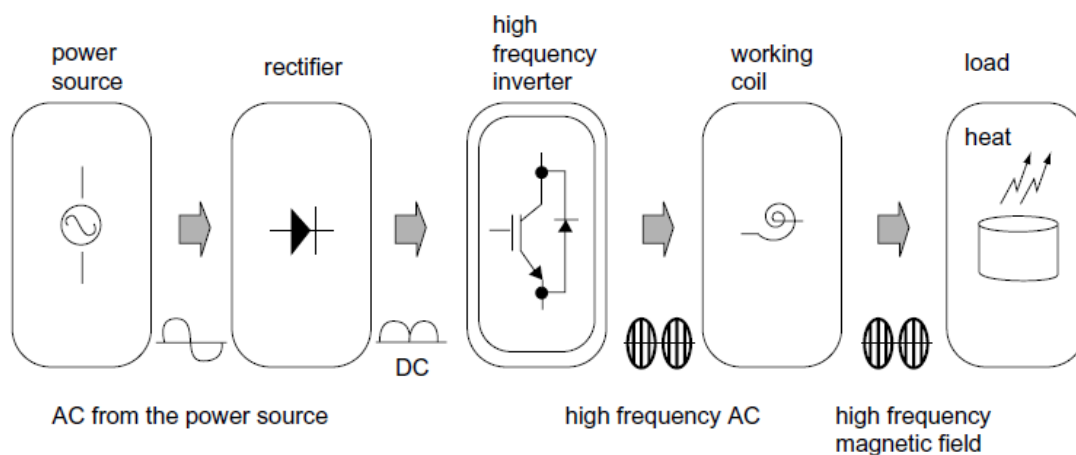


Figure 3-1 Operating Principle

Increasing the frequency of operation of power converters is desirable, as it allows the size of magnet circuit and capacitors to be reduced, leading to cheaper and more compact circuits. However, increasing the frequency of operation also increases switching losses and hence reduces system efficiency. One solution to this problem is to replace the "chopper" switch of a standard SMPS topology (Buck, Boost etc.) with a "resonant" switch, which uses the resonances of circuit capacitances and inductances to shape the waveform of either the current or the voltage across the switching element, such that when switching takes place, there is no current through or voltage across it, and hence no power dissipation.

A circuit employing this technique is known as a resonant converter (or, more accurately, a quasi-resonant converter, as only part of the resonant sinusoid is utilized).

3.2 Resonant Converter

The resonant circuit of a resonant converter consists of a capacitor, an inductor, and resistance and there are two types of resonant converter generally used: a series resonant circuit and a parallel resonant circuit.

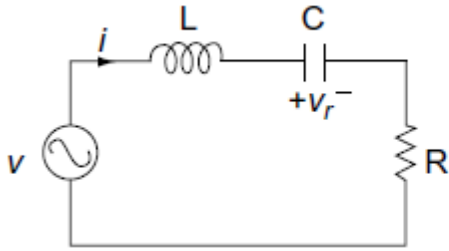


Figure 3-2a Series Resonant

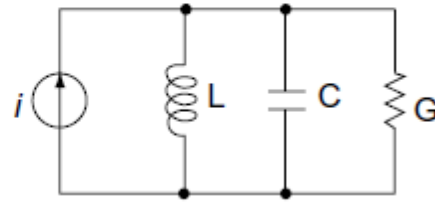


Figure 3-2b Parallel Resonant

Figure 3-2a & 3-2b shows these two common types. When power is connected, electric energy as in Equation 3-3 is stored in the inductor and transferred to the capacitor. Equation 3-4 simplifies the calculation of the amount of the energy stored in the capacitor, to be sent to the inductor. Resonance occurs while the inductor and the capacitor exchange the energy. And the total amount of energy stored in the circuit during resonance remains unchanged. This total amount is the same as the amount of energy in peak stored in the inductor or capacitor.

$$i = \sqrt{2}I \sin \omega t \text{ [A]} \quad (\text{Equation 3-1})$$

$$V_c = -\frac{\sqrt{2}I}{\omega C} \cos \omega t \text{ [V]} \quad (\text{Equation 3-2})$$

$$E_L = \frac{1}{2} Li^2 = LI^2 \sin^2 \omega t \text{ [J]} \quad (\text{Equation 3-3})$$

$$E_C = \frac{1}{2} CV_c^2 = \frac{I^2}{\omega^2 C} \cos^2 \omega t = LI^2 \cos^2 \omega t \text{ [J]} \quad (\text{Equation 3-4})$$

$$E_L + E_C = LI^2 (\sin^2 \omega t + \cos^2 \omega t) = LI^2 \text{ [J]} \quad (\text{Equation 3-5})$$

As, some energy is lost by the resistance in the process of resonance, the total amount of energy stored in the inductor decrements in each resonant exchange. The resonance frequency, which is the speed of energy transfer, is determined by capacitance (C) and inductance (L) as in Equation 3-9.

Chapter 3 DESIGN AND IMPLEMENTATION OF A QUASI-RESONANT CONVERTER

The inductive reactance and the capacitive reactance are summarized in Equation 3-6, and 3-7, respectively, and the size of impedance in a series resonant circuit is determined as in Equation 3-8.

$$X_L = j2\pi fL \quad (\text{Equation 3-6})$$

$$X_C = \frac{1}{j2\pi fC} \quad (\text{Equation 3-7})$$

$$|Z| = \sqrt{R^2 + (\omega L - \frac{1}{\omega C})^2} \quad (\text{Equation 3-8})$$

At the resonance frequency, the inductive reactance of Equation 3-6 and the capacitive reactance of Equation 3-7 become the same, i.e. the voltage of the power source and the current in the circuit stay on the same level. The resonance frequency can be summarized as in Equation 3-9. The current in the circuit reaches its peak when the source frequency becomes identical to the resonance frequency. It decrements when the source frequency gets higher or lower than the resonance frequency.

$$f_0 = \frac{1}{2\pi\sqrt{LC}} \text{ [Hz]} \quad (\text{Equation 3-9})$$

And the selection ratio of a half-bridge series resonant circuit is as in the following Equation 3-10.

$$Q = \frac{\omega_0 L}{R} = \frac{1}{\omega_0 CR} = \frac{Z}{R} \quad (\text{Equation 3-10})$$

As shown in the formula above, the smaller becomes the resistance than the inductance, i.e. when the source frequency gets closer to the resonance frequency, the sharper gets the frequency curve of Figure 3-3 and the bigger becomes the value of Q. The numerator is the energy accumulated in the inductor during resonance and the denominator is the average amount of energy consumed in resistance in each cycle. The frequency curve below demonstrates the relationship between current/output energy and the source frequency when the source voltage of the resonant circuit is set equal. The current and output energy reaches its maximum value at the resonance frequency.

In the area where the switching frequency is lower than the resonance frequency, the inductive reactance has a direct relationship with the switching frequency, in other words, the lower the frequency, the smaller the inductive reactance. And according to Equation 3-7, the capacitive reactance is in inverse relationship with the frequency. As the reactance becomes more capacitive, the current gets higher than the voltage in status. When the switching frequency increases (in Equation 3-8), impedance gets bigger, enlarging the amount of output energy as in Figure 3-3. In the opposite

situation, a lower switching frequency leads to smaller impedance, causing the output energy to decrement.

In the area where the switching frequency is higher than the resonance frequency, the higher the switching frequency the bigger is the inductive reactance. Here, the value of the capacitive reactance gets smaller according to Equation 3-7. The more inductive reactance causes the current to be lower than the voltage in status. In this situation, a higher switching frequency is accompanied by an increase of impedance (Equation 3-8), causing the output energy to be lower (as in Figure 3-3). When the switching frequency goes down, the impedance is decreased, raising the output energy (as in Equation 3-8).

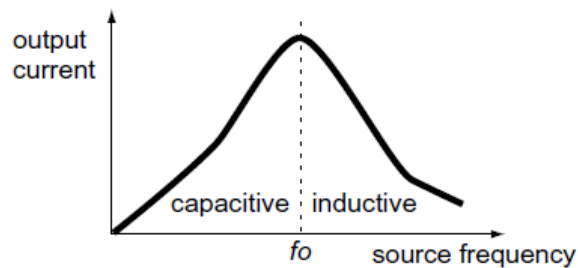


Figure 3-3 Frequency Curve

3.3 Power System of Induction Melter

There are two kinds of topology used in a power system, a half-bridge series resonant converter and a quasi-resonant converter. These two topologies have their own merits and demerits.

The merits of a half-bridge series resonant converter are: stable switching, low cost, and a streamlined design. As the voltage of the circuit is limited to the level of the input voltage, the switching circuit can have low internal pressure, which helps reduce the cost.

The design for the switching control part inside a circuit can be streamlined. There are also some demerits. As the half-bridge method requires two switching circuits, the overall working process becomes more complicated and the size of heat sink and PCB should be also bigger. In addition, the gate operating circuits must be insulated.

One of the merits of a quasi-resonant converter is that there needs only one switching circuit inside. This enables a relatively smaller design for the heat sink and PCB, making the working process far simpler. Another strong point is the fact that the system ground can be shared. A quasi-resonant converter is not free from defects. Most of all, switching is relatively unstable. And high internal pressure of the switching circuit, caused by the resonant voltage administered to both sides of the circuit, pushes the cost of the circuit higher. Besides, the design for the controlling part is more complicated. But as mentioned earlier, technological development in high frequency semiconductor switching devices has lead to an innovation in terms of low price, high performance, and reliability.

Quasi-resonant converters are now more generally used because of the smaller heat sink and PCB size and simpler operation process. We discuss in following section the operation of a half-bridge series resonant converter and a quasi-resonant converter.

3.4 Half-bridge Series Resonant Converter

A number of designing methods are available for a power system using a half-bridge series resonant converter. The power system demonstrated in Figure 3-4 is comprised of the AC power supply, main power circuit, control circuit, input current detection circuit, resonant current detection circuit, and gate operation circuit. The following figure illustrates the operation of a power system as a whole.

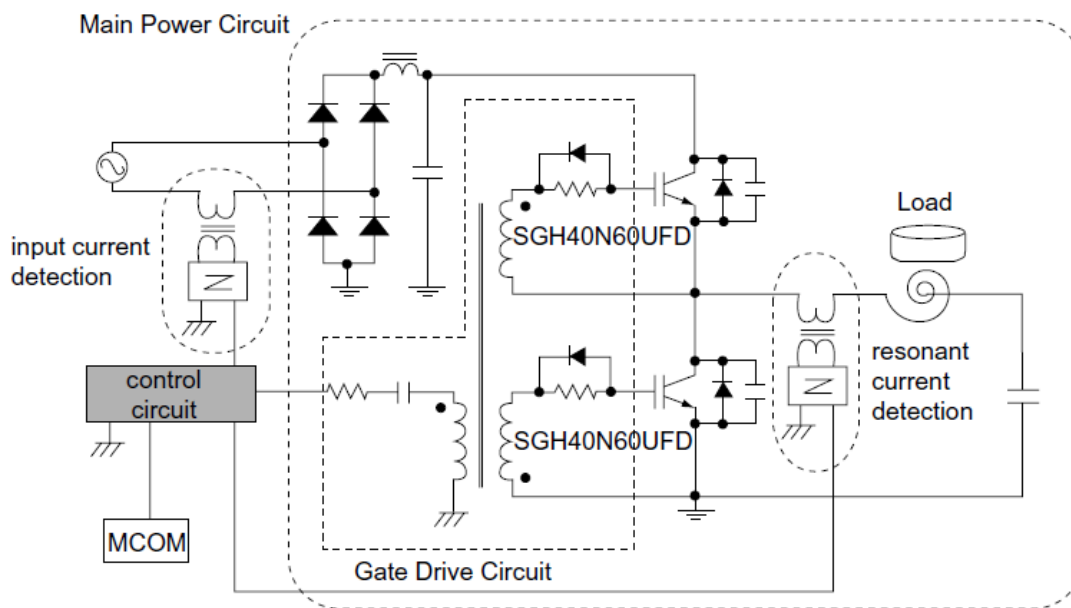


Figure 3-4 Power System Using Half-bridge Series Resonant Converter

The AC power passes through the rectifier to be transmitted to the capacitor. In this system, the leveling capacitor serves as a filter preventing the high frequency current flowing toward the inverter from entering the input part. Input current becomes the average of the inverter current, and the ripples flow to the leveling capacitor.

The voltage passing the leveling capacitor is turned into square wave in the process of high frequency switching in the inverter. The high frequency harmonics contained in the square wave are eliminated by the Lr, Cr filter. The square wave enables resonance in the resonant circuit, which, in turn, creates a magnetic field around the resonant inductor affecting the load. Eddy currents are formed around the surface of the object, generating heat energy.

The input current flowing through the AC input section to the rectifier and the resonant current flowing through the inverter to the resonant circuit are input to the control circuit. In order to control the maximum level of input and resonant current, the control circuit sets the switching frequency of the inverter, administering it to the gate of the inverter switch via the gate operating circuit.

Microcontroller allows the detection circuit to examine the input current to determine the presence of a conductive object, protecting the system by manipulating the on/off status of the control circuit. More detailed demonstrations of each part are presented below.

3.4.1 Main Power Circuit

The main power circuit employs a half-bridge series converter switching at a high frequency as shown in Figure 3-5. The switching circuit consists of an IGBT (Insulated-gate Bipolar Transistor). Zero voltage/current turn-on switching is enabled by turning on the IGBT while the diode is in turn on period. The resonant circuit comprises resonant inductance (L_r) and resonant capacitance (C_r). The capacitors, C_1 and C_2 , are the lossless turn-off snubber for the switches, S_1 and S_2 .

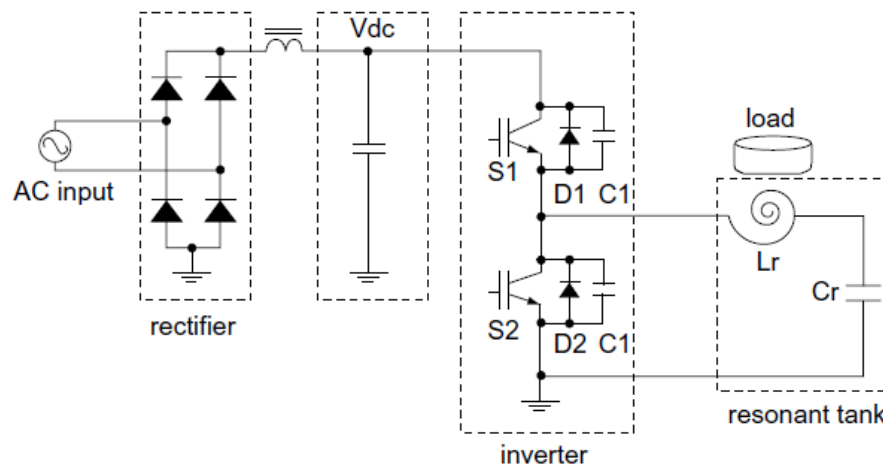


Figure 3-5 Main Power Circuit

Equivalent circuits to a resonant circuit are described in Figure 3-6. The load in circuit (a) is equivalent to the circuit in (b) where the transformer has resistance connected to the secondary circuit. And this can more simplified as in the circuit (c), where R^* , L^* , and C_r are directly connected. R^* in (c) indicates the resistance of the primary circuit of the transformer converted from the secondary. L^* means the inductor on the primary side of the transformer (L_r), which is a resonant inductor combining the leakage inductor and the secondary inductor.

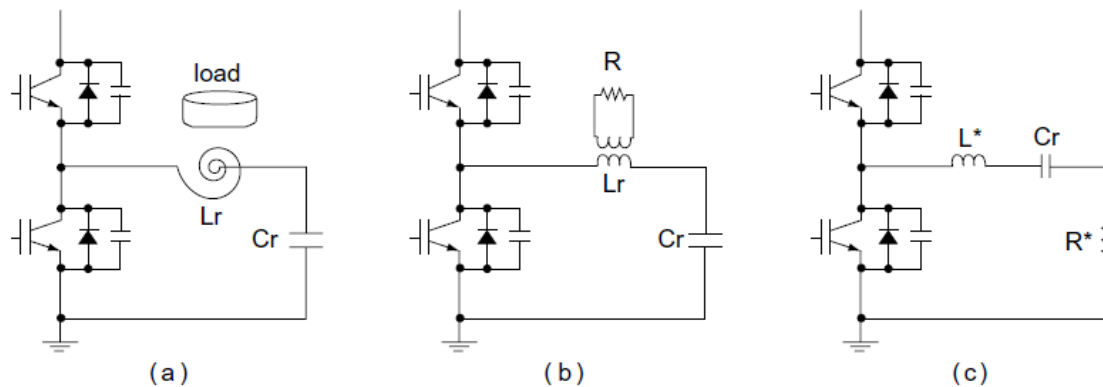


Figure 3-6 Equivalent Circuit

3.4.2 Operation Theory

By connecting the IGBT switching circuit, S1 and S2, in parallel to diodes, D1 and D2, current loss can be minimized. When S1 is turned-off, D2 helps S2 stay on zero voltage/current before being turned on, substantially reducing current loss (this is also the same case with S1). There occurs no reverse-recovery problem as the voltage on both sides remains zero after the diode is turned off.

However, as the switching circuit is turned off at around the upper limit of voltage and current, some switching loss results on turn-off. The capacitors, C1 and C2, acting as a turn-off snubber connected in parallel to S1 and S2, can check the level of this loss to a minimum level. Upon turn on, the switching circuit starts from zero voltage/current, so these turn-off snubbers operate as lossless turn-off snubbers.

The configuration of a half-bridge series resonant converter (Figure 3-5) can be simplified as an equivalent circuit illustrated in Figure 3-7. Figure 3-8 is a wave form of a frequency cycle in each part of the main power circuit. Turn on S1, when the current of the L*-Cr resonant circuit flows in opposite direction through D1 (S1 and S2 remain off).

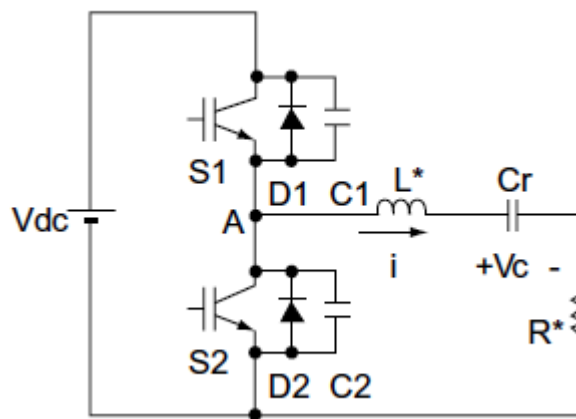


Figure 3-7 Equivalent of Main Power Circuit

MODE I: t_0 - t_1

The resonant current flowing in inverse direction changes its direction at the point of $t=t_0$ flowing through S1. In this mode, DC-LINK voltage of V_{dc} lets the resonant circuit accumulate energy by supplying power through S1.

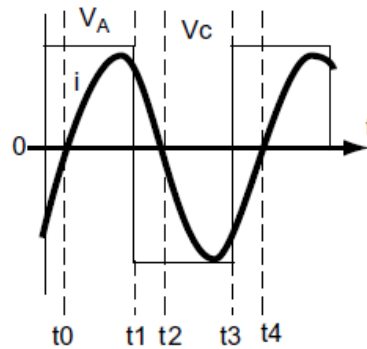


Figure 3-8 Waveforms of Main Power Circuit

MODE II: t_1 - t_2

When S_1 is turned off at the point of $t=t_1$, the resonant current flowing through S_1 begins freewheeling through the D_2 diode. In this process, a small amount of switching turn-off loss occurs as the S_1 switch is turned off while retaining some values in voltage and current. For the following mode, S_2 is turned on when $t_1 < t < t_2$. As the S_2 switch remains at zero voltage/current, no switching loss takes place upon turn-on. And the reverse-recovery of D_1 does not necessarily have to be fast.

MODE III: t_2 - t_3

Right after $t=t_2$, the current freely resonates flowing in inverse direction through S_2 which is already turned on. Here, the resonant capacitor, C_r , serves as a source of voltage.

MODE IV: t_3 - t_4

When S_2 is turned off at $t=t_3$, the resonant current flowing through S_2 starts freewheeling through the D_1 diode. In this process, a small amount of switching loss occurs on turn-off. For the following mode, the S_1 switch is turned on at a proper point ($t_3 < t < t_4$). At this point, there happens no switching loss upon turn-on as the S_1 switch remains at zero voltage/current. And the reverse-recovery of D_2 does not have to be fast. In this mode, the energy of the resonant circuit is converted to V_{dc} , passing D_1 . The operating mode after $t > t_4$ repeats Mode I through IV, explained above.

3.5 Quasi-resonant Converter

The following Figure 3-9 features a block diagram of a quasi-resonant converter in a streamlined form.

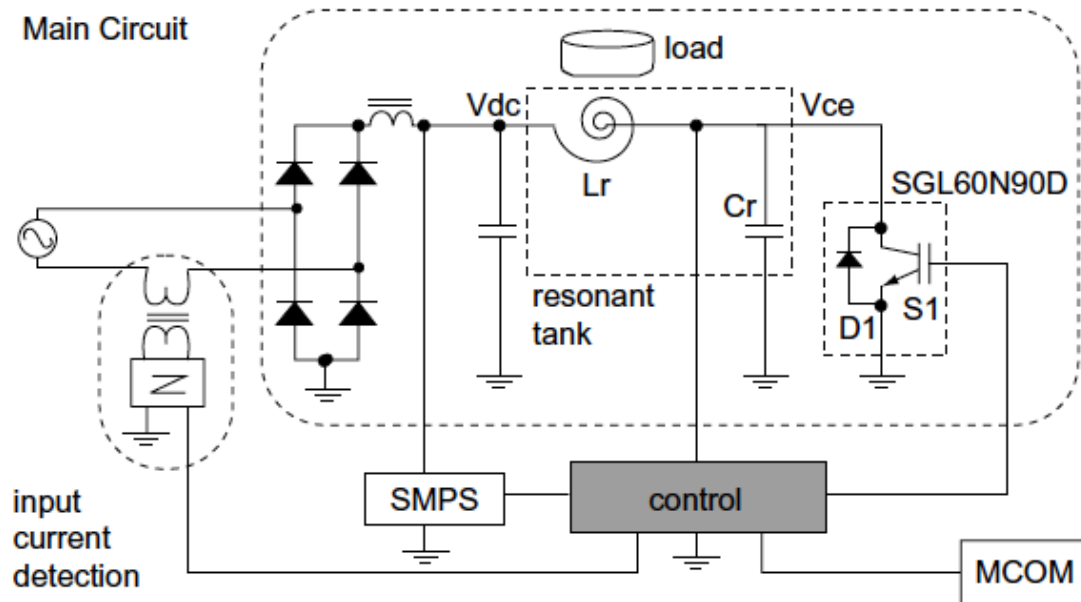


Figure 3-9 Power Circuit of Quasi-resonant Converter

The total system block is comprised of main power circuit, input current detection circuit, control circuit, and SMPS circuit, as shown in Figure 3-9. The basic operating concept of quasi-resonant circuit is similar to that of half-bridge series resonant converter in the fact that heat energy is generated. However, the methods of controlling the gate in the switching circuit are totally different. Major functions of each block are as follows.

3.5.1 Main power circuit

The main power circuit features a quasi-resonant converter consisting of the IGBT and a diode connected to it in parallel the circuit executes high frequency switching. By turning on the IGBT while the diode is in turn-on it is possible to do a turn-on switching with the voltage and current remaining at zero. The resonant circuit is composed of resonant inductance (L_r) and resonant capacitance (C_r).

3.5.2 Operating Concept

Figure 3-10 illustrates an equivalent of the main power circuit. When D1, connected to the S1 switching circuit, is turn-on a zero voltage turn-on switching is available as V_{ce} of the circuit becomes zero. In this circuit, the switch must be endurable to high internal pressure to accommodate the high voltage of V_{ce} administered to the both ends of the switch.

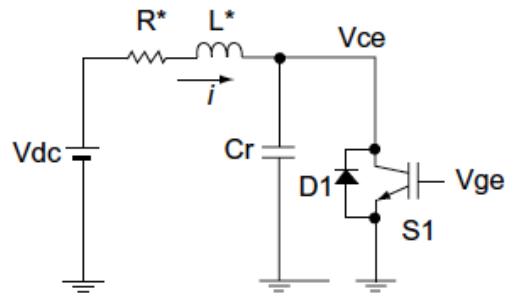


Figure 3-10 Equivalent Circuit

Figure 3-11 shows the waveforms of each block of the main power circuit in a cycle. In the initial stage, S1 is turned off by the control circuit when the current flowing through L^* and S1 reaches its peak. At this point, $V_c(0)=0V$. There are four modes available.

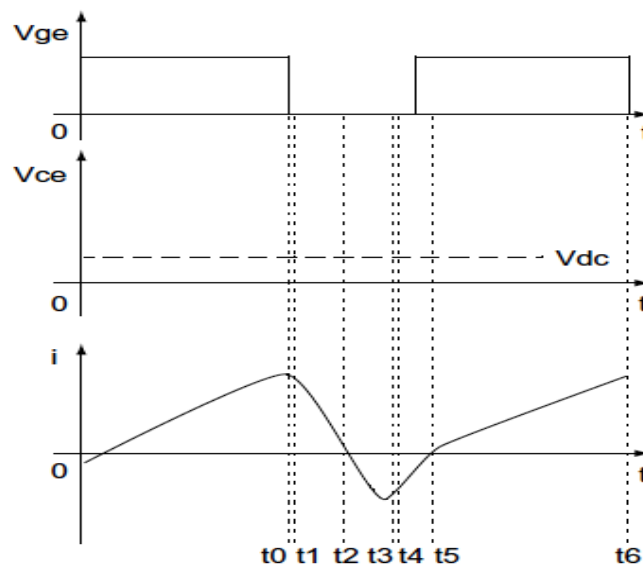


Figure 3-11 Waveforms of Main Power Circuit

MODE I: t_0 - t_1

As mentioned earlier, the switching circuit is turned off at the point the resonant current flowing through the circuit comes to its peak, i.e. at t_0 . In this process, a turn-off switching loss occurs. V_{ce} level is rapidly increased by the capacitor (C_r) to become DC-LINK (V_{dc}) at t_1 .

Even when the switch is turned off at t_0 , the current keeps incrementing to reach its peak at t_1 , when V_{ce} becomes equal to V_{dc} , as DC-LINK is higher than the resonant voltage. At this point, the energy stored in the inductor begins to be transferred to the capacitor.

MODE II: t_1 - t_4

As V_{dc} is lower than V_{ce} after t_1 , the current decreases to be zero at t_2 , when the resonant voltage reaches its maximum. This is also the point when the transfer of the energy stored in the inductor to the capacitor is completed. The peak level of the resonant voltage has a direct relationship with the turn-on time of the switch (MODE IV: t_5 - t_6).

After t_2 , the capacitor starts discharging the energy to the inductor, which causes the voltage and the current flowing in inverse to decrement and to reach its minimum level at t_3 , i.e. $V_{ce}=V_{dc}$, respectively. Passing t_3 , the resonant current increases as $V_{ce}<V_{dc}$ and the discharge is completed at t_4 .

MODE III: t_4 - t_5

After t_4 , the energy sent by the capacitor and stored in the inductor is converted to DC-LINK as the D1 diode is forward biased. The resonant current is flowing through D1, during the time S1 is turned on.

MODE IV: t_5 - t_6

As the switching circuit remains turned on while the current is freewheeling through D1, the current flows in the right direction through the circuit and the inductor starts to store the energy, which makes it possible to do a zero voltage turn-on switching.

At t_6 , the switching circuit is turned off, returning to MODE I. As the peak level of the voltage is in direct relationship with the on-duty frequency, one can manipulate this level, i.e. output energy, by adding or reducing the on-duty frequency.

3.6 Simulation of Quasi-resonant Converter

Simulation results were performed using Simulink block as shown in Figure 3-12. To limit the stresses in switching device to 600V & to isolate the main supply the 3-ph ac is stepped down using a 3-ph step down transformer from 415V to 140V. This is further rectified using a 3-ph rectifier and smoothened using an inductor & capacitor. The resonant circuit is composed of resonant inductance (L_r) and resonant capacitance (C_r). Simulation results of dc-link voltage & the inductor current are shown in Figure 3-13.

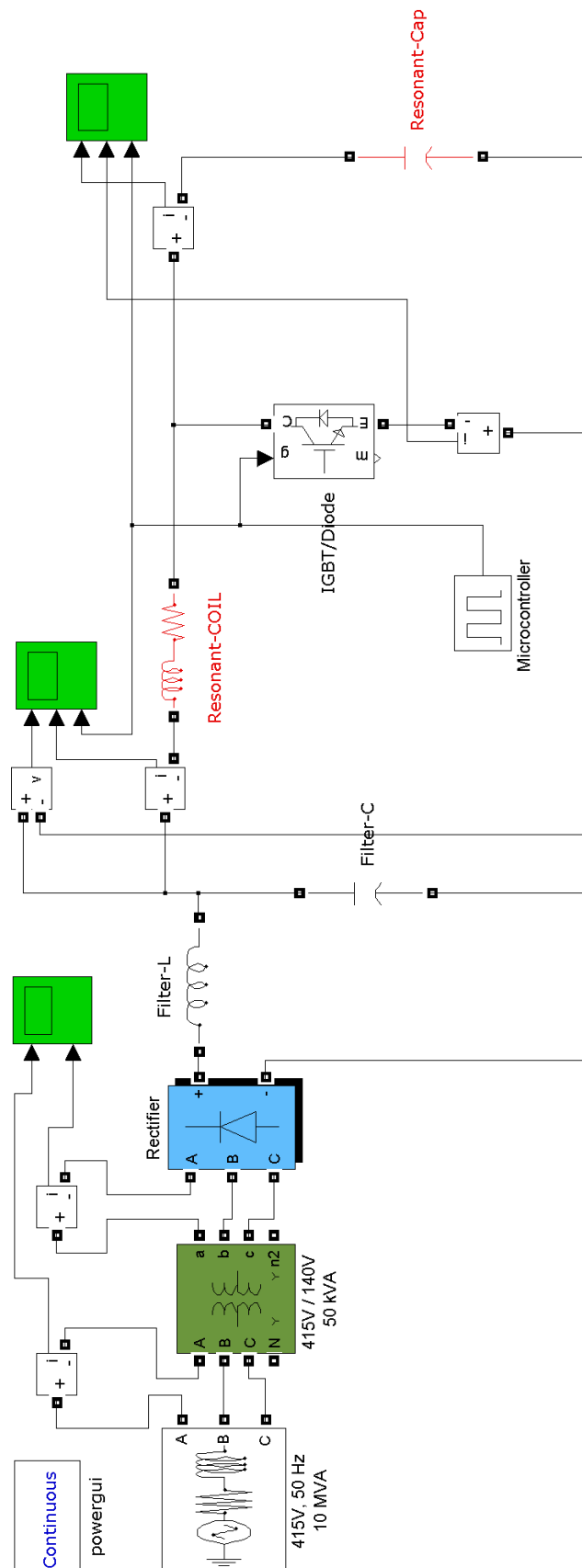


Figure 3-12 Simulation of Quasi-resonant converter

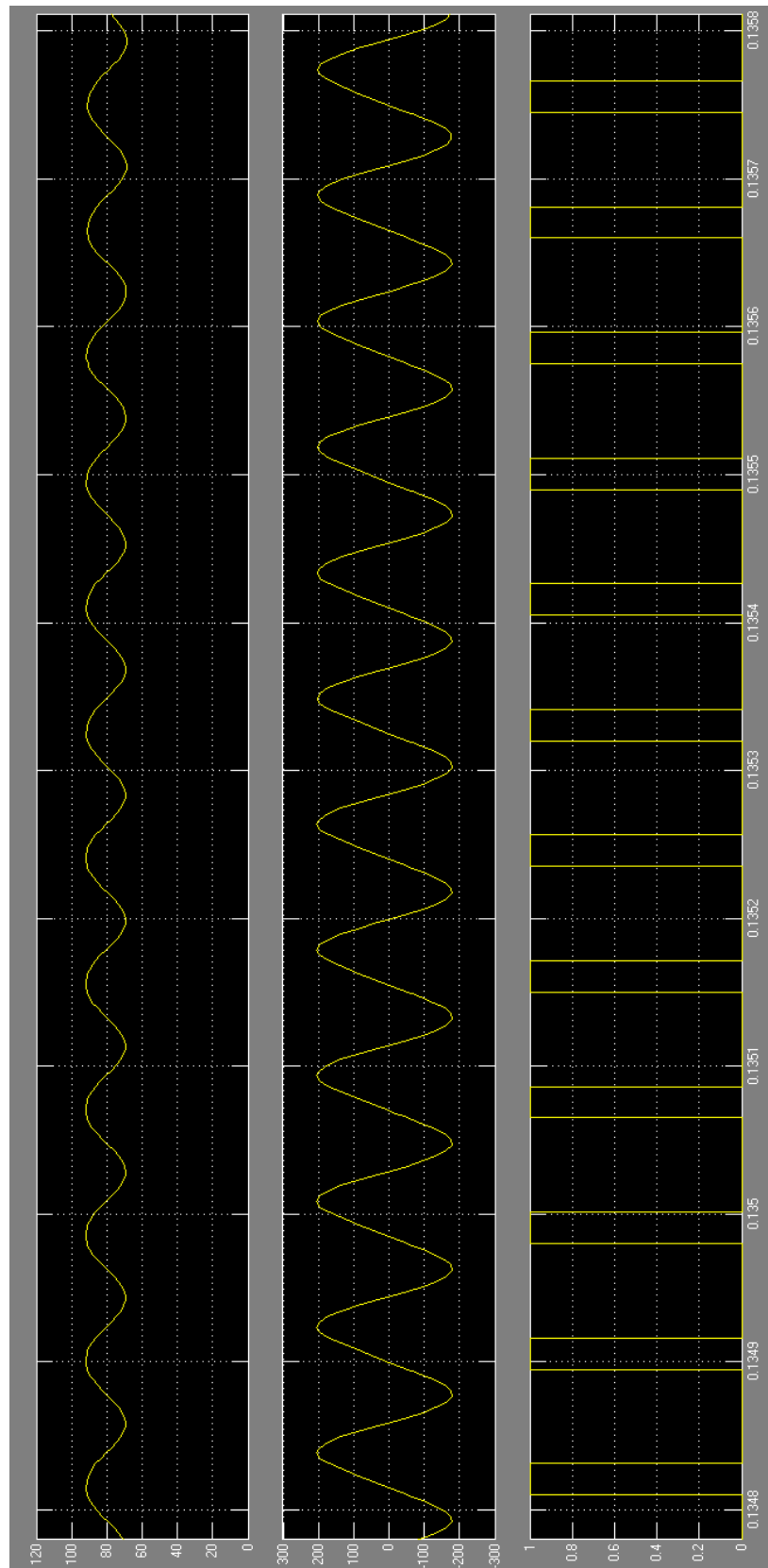


Figure 3-13 Simulation Result of Inductor Current

3.7 Summary

The main findings of this chapter reveals following:

1. The half-bridge series resonant converter is having stable switching & low cost. As the voltage of the circuit is limited to the level of the input voltage, the switching circuit can have low internal pressure, which helps reduce the cost.
2. As the half-bridge method requires two switching circuits, the overall working process becomes more complicated and the size of heat sink and PCB should be also bigger. In addition, the gate operating circuits must be insulated.
3. As compared to half-bridge series resonant converter the quasi-resonant converter needs only one switching circuit inside. This enables a relatively smaller design for the heat sink and PCB, making the working process far simpler. Another strong point is the fact that the system ground can be shared.
4. In case of quasi-resonant converter the high internal pressure of the switching circuit, caused by the resonant voltage administered to both sides of the circuit, pushes the cost of the circuit higher. But as mentioned earlier, technological development in high frequency semiconductor switching devices has lead to an innovation in terms of low price, high performance, and reliability. Quasi-resonant converters are now more generally used because of the smaller heat sink and PCB size and simpler operation process.

Chapter 4

PROPOSAL & IMPLEMENTATION OF MODIFIED QUASI-RESONANT CONVERTER

4.1 Introduction

As seen in Figure 3-9 the quasi resonant converter requires a Capacitor to provide the path of return current. In Mode-III after t_4 , the energy sent by the capacitor and stored in the inductor is converted to DC-LINK as the D1 diode is forward biased. During this period the current flows through filter capacitor.

A new approach to quasi resonant converter is proposed in following section so as to remove filter capacitor.

4.2 Modified Quasi Resonant Converter

The following Figure 4-1 features a block diagram of a modified quasi-resonant converter.

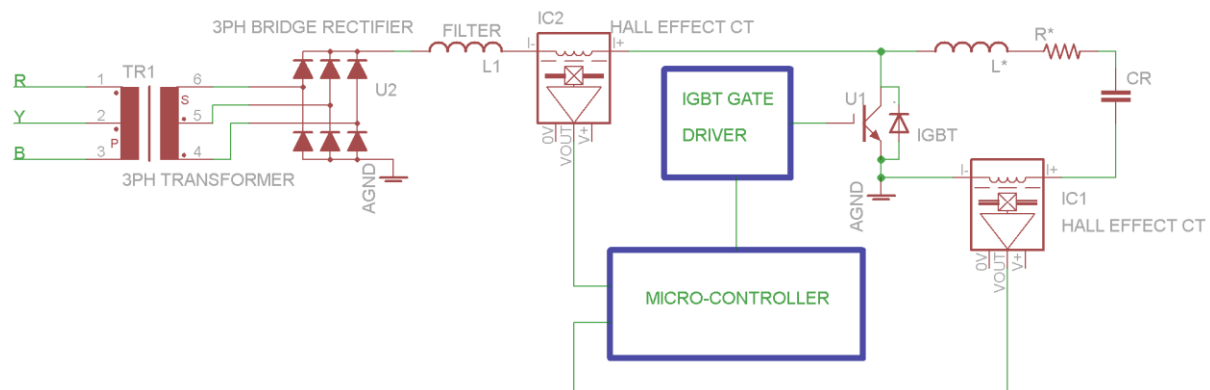


Figure 4-1 Power Circuit of Modified Quasi-resonant Converter

The total system block is comprised of main power circuit, dc-link & tank current detection circuit and microcontroller as shown in Figure 4-1. The basic operating concept of modified quasi-resonant circuit is similar to that of quasi-resonant converter in the fact that heat energy is generated. However, the methods of controlling the gate in the switching circuit are totally different.

Major functions of each block are as follows.

4.2.1 Main power circuit

The main power circuit features a quasi-resonant converter consisting of the IGBT and a diode connected to it in parallel the circuit executes high frequency switching. By turning off the IGBT while the diode is in turn-on it is possible to do a turn-off switching with the voltage and current remaining at zero. The resonant circuit is composed of equivalent inductance (L^*), equivalent resistance (R^*) and resonant capacitance (CR).

4.2.2 Operating Concept

Figure 4-2 illustrates an equivalent of the main power circuit. When D1, connected to the S1 switching circuit, is turn-on a zero voltage turn-off switching is available as V_{ce} of the circuit becomes zero.

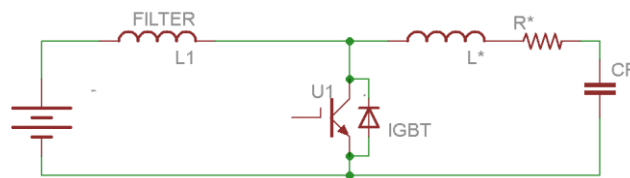


Figure 4-2 Equivalent Circuit

Figure 4-3 shows the waveforms of each block of the main power circuit in a cycle. In the initial stage U1 is off. And CR is charged fully by the current flowing through L1, L^* and R^* . Following are the four modes available.

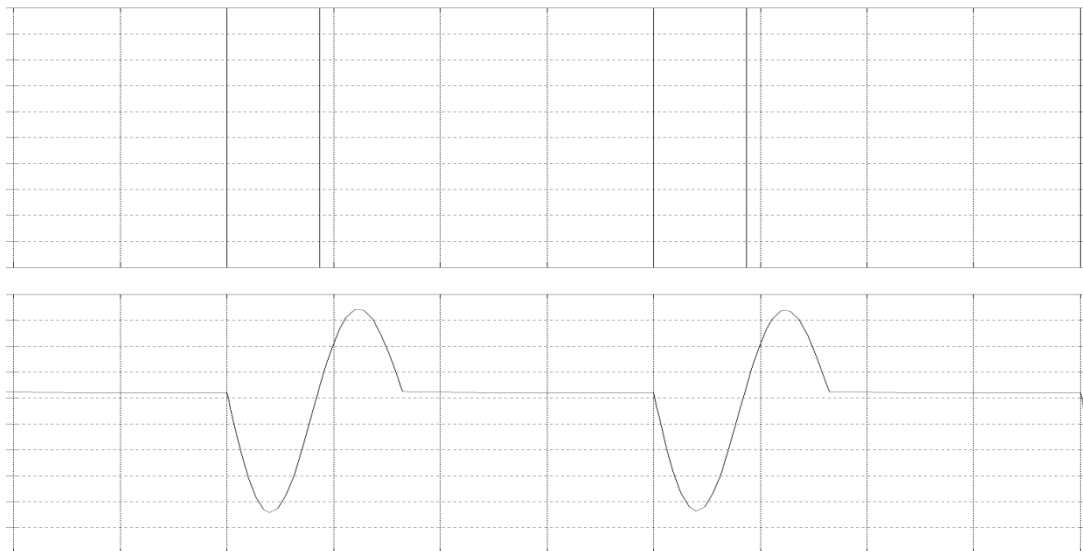


Figure 4-3 Waveforms of Main Power Circuit

MODE I:

At time t_0 the switching circuit is turned on. In this process, a turn-on switching loss occurs. At this point the capacitor starts discharging the energy to the inductor through switching circuit. Thus the current increases in the negative direction. The current reaches to its maximum value when the capacitor is discharged.

MODE II:

At this point, the energy stored in the inductor begins to be transferred to the capacitor. So the current starts decreasing in negative direction. Once the capacitor is fully charged in negative direction the current becomes zero. This is also the point when the transfer of the energy stored in the inductor to the capacitor is completed.

MODE III:

After this point, the capacitor starts discharging the energy to the inductor, which causes the current flowing in the positive direction through the diode. At this point as the resonant current is flowing through freewheeling diode the voltage & current in the switching device is zero, and can be switched off to have zero turn-off switching loss. The current reaches to maximum when the discharge is completed.

MODE IV:

After this point, the energy stored in the inductor begins to be transferred to the capacitor so that current starts decreasing in positive direction. The current becomes zero when the energy transfer is completed. At this point or later the switching circuit can be turned on, returning to MODE I.

The frequency of operation can be varied depending upon required power by increasing/decreasing the turn-on instant of switching circuit.

4.3 Simulation of Modified Quasi-resonant Converter

Simulation results were performed using Simulink block as shown in Figure 4-4. To limit the stresses in switching device to 600V & to isolate the main supply the 3-ph ac is stepped down using a 3-ph step down transformer from 415V to 140V. This is further rectified using a 3-ph rectifier and smoothened using an inductor. As there is no return path required for current the filter capacitor is not required. The resonant circuit is composed of resonant inductance (L_r) and resonant capacitance (C_r). Simulation result of the inductor current is shown in Figure 4-5. Figure 4-6 shows the simulation result of current through IGBT. And that of dc-link voltage is shown in Figure 4-7. The DC-link voltage of 200V is applied to the input of the converter.

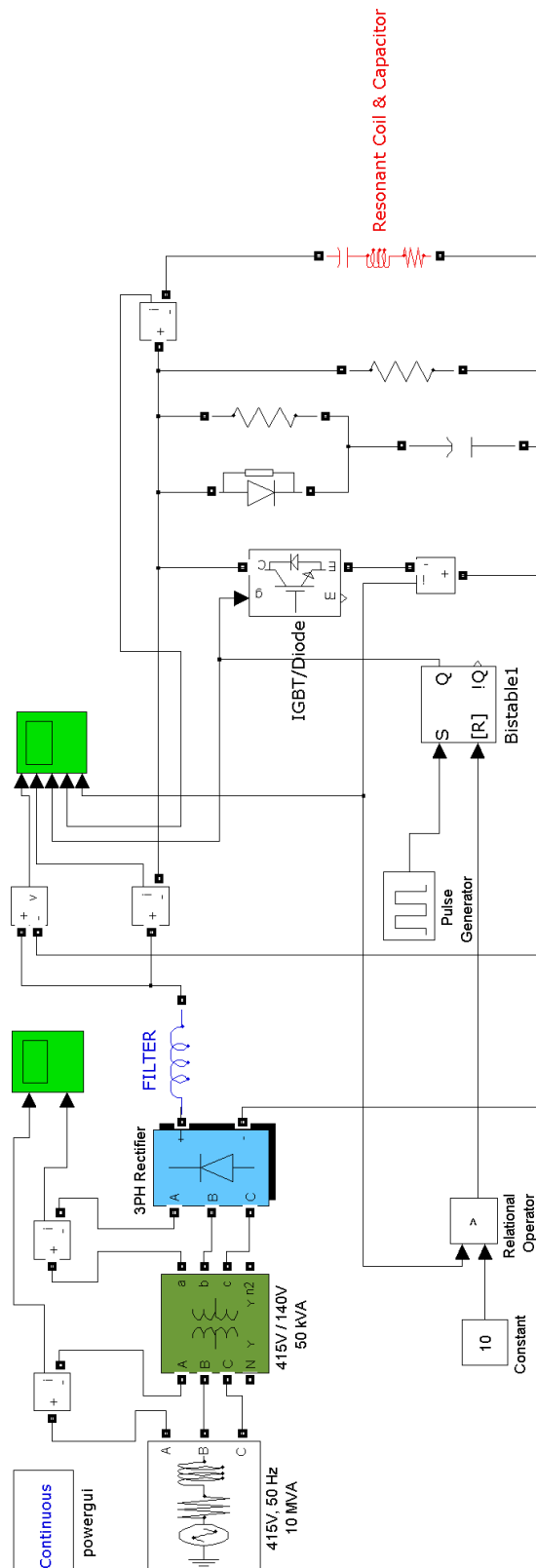


Figure 4-4 Simulink Block of Quasi-resonant converter

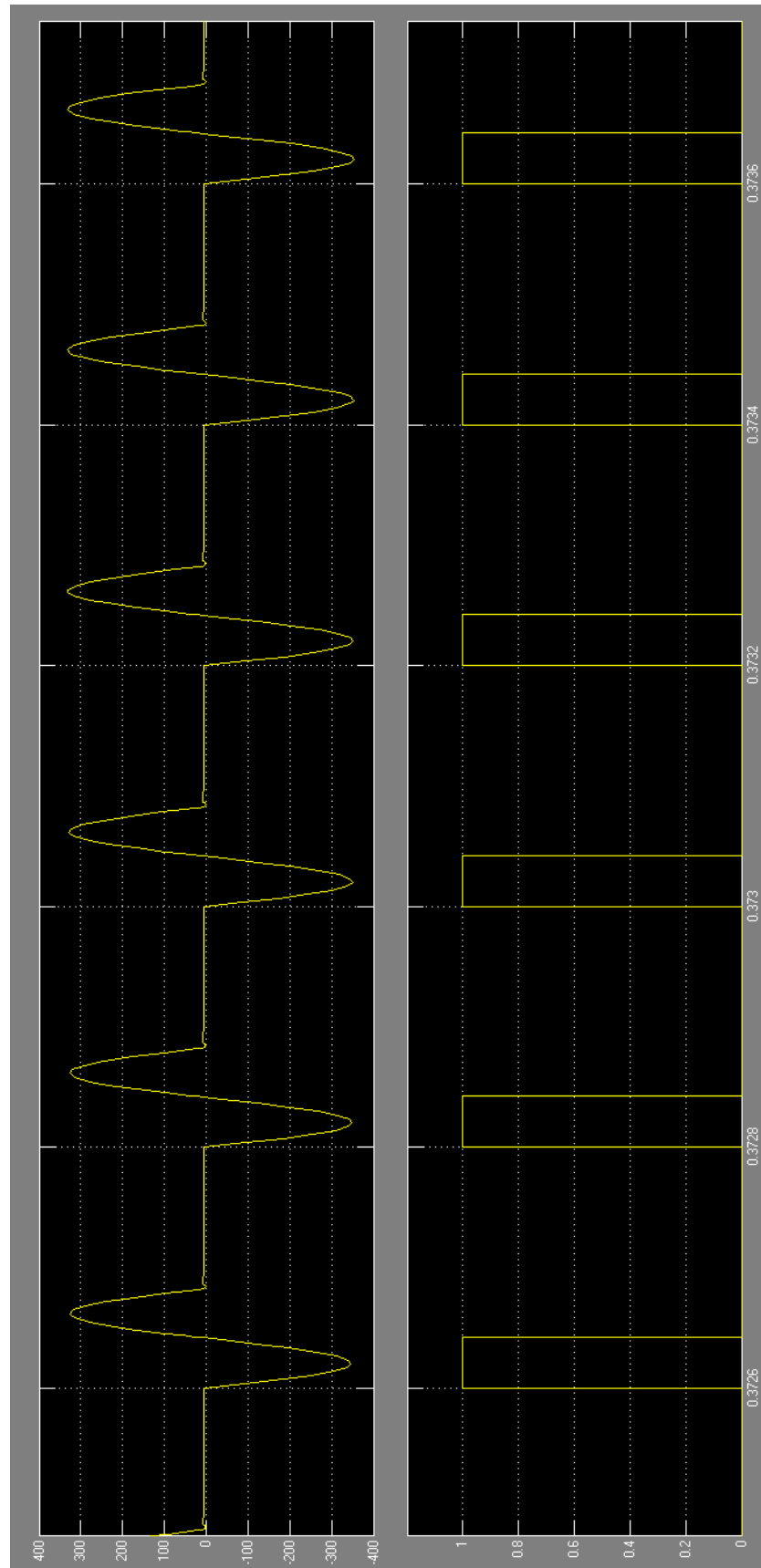


Figure 4-5 Simulation Result of Inductor Current

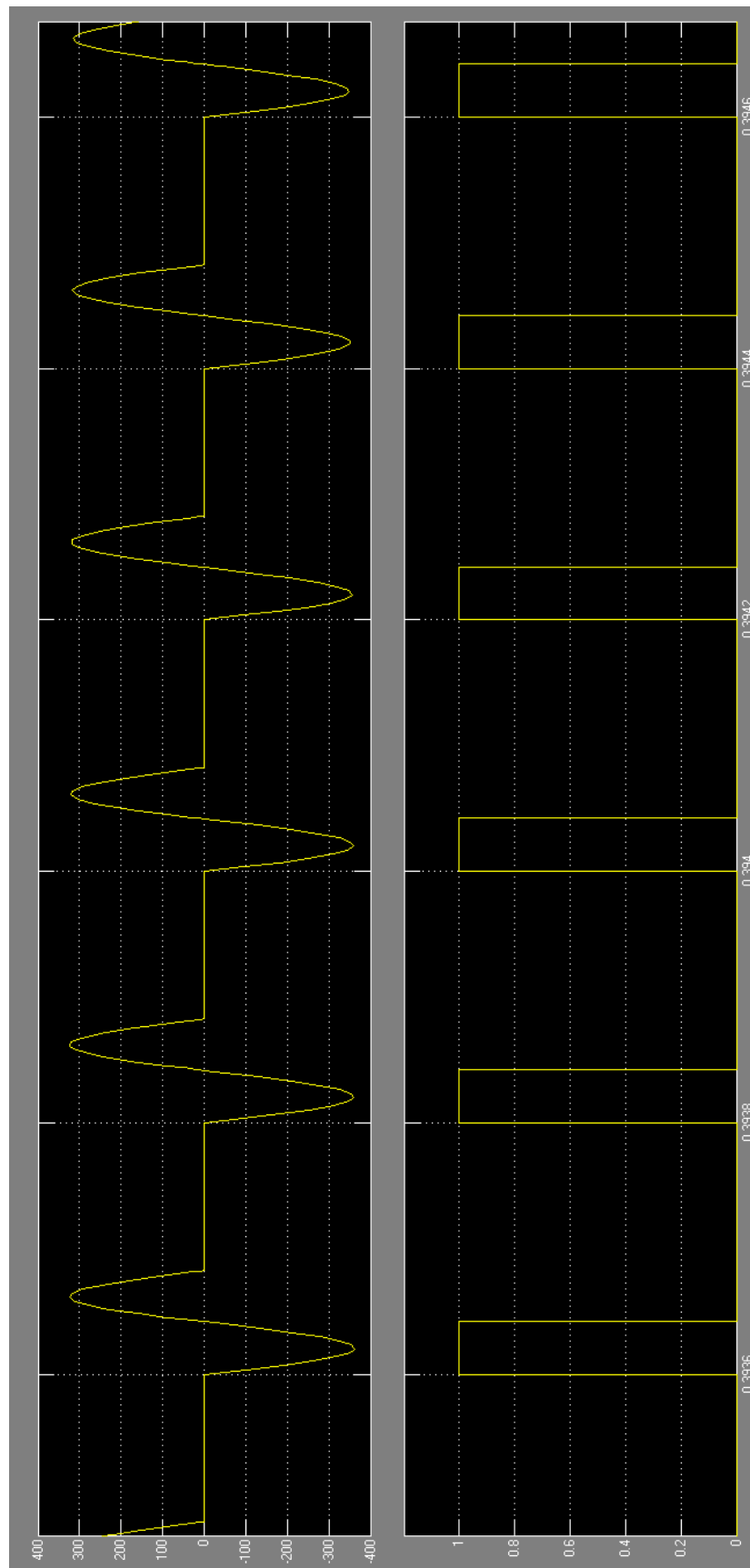


Figure 4-6 Simulation Result of IGBT Current

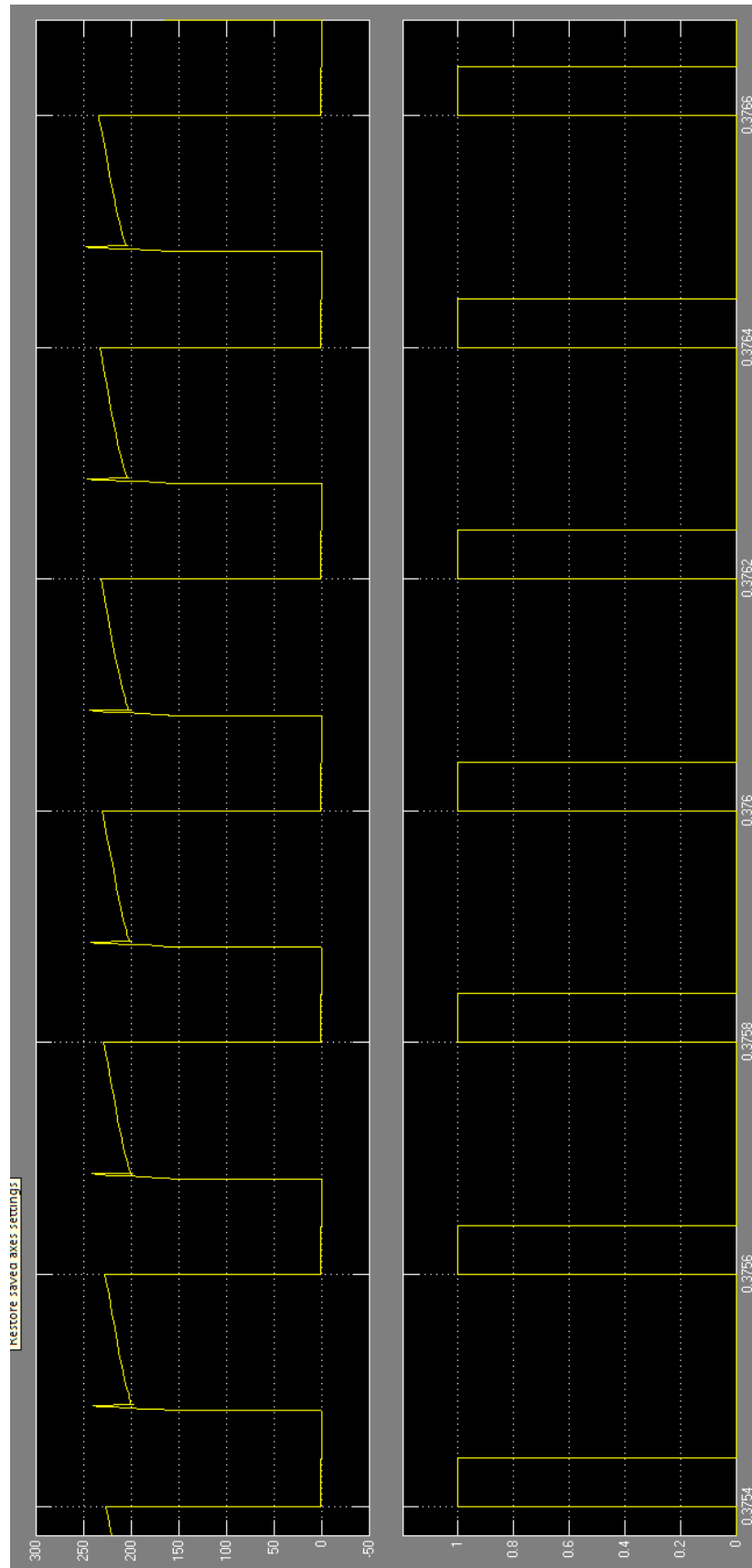


Figure 4-7 Simulation Result of voltage across IGBT

4.4 Summary

This chapter has presented analysis, modeling and simulation of the modified Quasi-resonant converter. The main findings of this chapter reveals following:

1. The modified quasi resonant converter is low cost as the filter capacitor is eliminated as compared to quasi resonant converter. This new scheme also requires one switching device which maintains the advantage of a relatively smaller design for the heat sink and PCB.
2. This new scheme is more advantageous as the positive & negative current flows through the same resonant path resulting into a pure sine wave of current.
3. This system has advantages like low switching losses, reduced stress and increased power density.
4. The variation in power can easily be obtained by changing the operating frequency of IGBT gate pulses.
5. The simulation results are in line with the predictions.

Chapter 5

DESIGN

AND IMPLEMENTATION

OF POWER CIRCUIT

5.1 Introduction

The overall performance and the cost of the Melter will be one of the important issues to be considered during the design process for the next generation of Induction Melting applications. The power circuit of Melter applications must achieve high efficiency and high reliability.

The quasi resonant converter presented in Chapter 4 has been used as the power circuit. The power circuit includes 3ph transformer, 3ph rectifier, filter choke, Igbt, snubber circuit, resonant tank capacitor & resonant tank coil.

5.2 Steps of Design of Tank Circuit

As heat energy is generated in the process of energy exchange between the inductor and the capacitor in the resonant circuit, the level of inductance and capacitance is a very important factor. The following is a description of some factors determining the value of this level.

Power Consumption:

As the most common design of Melter is 5 to 8kg, the overall power supply is designed based on this capacity, which is at maximum of 10kw. In order to get proper stirring effect the resonant frequency is set as 12khz for following calculations.

Current:

The Input current is the average of the resonant current. Hence for 10kw maximum power the Input current can be calculated as follows:

$$I = \frac{2\pi P}{V} = \frac{2\pi \times 10000}{140 \times \sqrt{2}} = 317.3A$$

C (Capacitance):

The Capacitance of the resonant circuit is determined as follows:

$$C = \frac{I}{2\pi fV} = \frac{317.3}{2 \times \pi \times 12000 \times 140 \times \sqrt{2}} = 21.25 \mu F$$

Thus a capacitor bank is formed using 10 pieces of $2.0\ \mu\text{F}$ capacitors in parallel, which totals to $20.0\ \mu\text{F}$. Firstly the capacitor bank was made as shown in figure 5-1.



Figure 5-1 Tank Capacitor Bank

To reduce the overall space & to do proper connections with inductance and to take care of cooling of inductor the new capacitor bank is formed as shown in figure 5-2. In this bank the first terminal of each capacitor is touching the front plate and the second terminal is touching the back plate, thus connecting them in parallel.



Figure 5-2 Modified Tank Capacitor Bank

L (Inductance):

The Inductance of the resonant inductor is computed with the above value of Capacitance.

$$L = \frac{1}{(2\pi f)^2 C} = \frac{1}{(2\pi \times 12000)^2 \times 20.0 \times 10^{-6}} = 8.79 \mu H$$

The inductor is made with a hollow pipe wound with 10 turns to get the required inductance. Water is passed through the hollow pipe for cooling purpose. The high temperature refractory cement is applied on the outer surface of coil to protect it from heat produced in the crucible.



Figure 5-3 Tank Inductor

Finally the L-C tank resonant circuit is formed as shown in figure 5-4 in such a way that no wires are required to complete the circuit. The tails of coil are themselves acting as interconnecting wires.



Figure 5-4 L-C Tank Circuit

3 Phase Transformer:

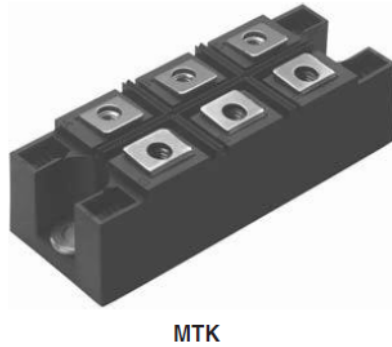
As the Melter is designed for 10kw the rating for 3ph transformer is chosen slightly higher than the maximum rating. Thus a 13kva transformer is used which steps down the 415v Line voltage to 140v Line voltage. The purpose is to operate the power circuit at low voltage and also to get isolation. Figure 5-5 shows the 3phase transformer in 3 limb construction with primary & secondary wound in star-star connection.



Figure 5-5 Three phase transformer

Three Phase Rectifier:

A three phase bridge rectifier of 160A & maximum repetitive peak reverse voltage of 1600V is used to rectify the output of transformer. Figure 5-6 depicts the features of the bridge rectifier.

**FEATURES**


- Package fully compatible with the industry standard INT-A-PAK power modules series
- High thermal conductivity package, electrically insulated case
- Excellent power volume ratio
- 4000 V_{RMS} isolating voltage
- UL E78996 approved 
- Totally lead (Pb)-free
- Designed and qualified for industrial level

Figure 5-6 Three Phase Bridge Rectifier

Filter Choke:

Figure 5-7 Filter Choke

Switching Device (IGBT):

The insulated-gate bipolar transistor (IGBT) has accrued success as a high-power solid-state switching device due to its combination of fast switching, low conduction loss, and high-impedance gate control. Manufacturers are therefore motivated to develop switches with extended voltage ratings and current carrying capability. Currently, commercial off-the-shelf (COTS) high-voltage IGBTs are rated up to 6.5 kV from multiple manufacturers. High voltage (> 1200 V) IGBTs are commonly sold as modules with ratings from 200 to over 2000 A.

The IGBTs implemented in the IGBT stack are non punch through (NPT)-type devices. The NPT IGBT is a common type of IGBT due to excellent thermal properties such as negative temperature coefficient of resistivity and high-thermal reliability, which are favorable qualities for the synchronized switching of devices in series and parallel arrangement [12].

Today state of the art IGBTs are trench / field-stop devices.

Trench IGBT

The MOS channel of a Trench IGBT compared with a planar IGBT is rotated by 90° . Thus, a higher channel density can be realized at the chip top side which leads to a higher inundation of the top/emitter side with charge carriers. A maximum channel density would not only worsen the short circuit robustness but also increase the turn off losses dramatically. A good combination of a suitable trench density, a low backside emitter efficiency (collector doping) and a high charge carrier life time leads to a clear reduction of the saturation voltage without increase of turnoff losses [14].

Field-stop IGBT

In a field-stop IGBT, an additional n^+ layer is introduced close to the collector. This layer, named field-stop, brings down the electric field within a very short spatial dimension. Therefore, it is possible to make the chips thinner and in such a way to reduce the static and dynamic losses. However, during switching events the silicon volume not affected by carrier extraction through the electric field is determining the amount of carriers contributing to the tail current.

This tail carrier/charge is crucial for the softness of an IGBT. In case of high transient over voltages the space charge region reaches far into the field stop and the residual/tail charge is very small. For a critical voltage the tail current disappears and the current flow snaps off. Such a snap-off results in high and hardly controllable over voltages. This, so far, was a big challenge for the design-in of trench field stop modules in high power applications.

Thus a 62mm C-Series module with Trench/Fieldstop IGBT4 (FZ600R12KE4) is selected with 600A DC-collector current & 1200V collector-emitter voltage. To achieve a 1200A current two of them are connected in parallel.

IGBT'S in parallel:

Apart from looking for an IGBT which is designed for a particular power range there is also the possibility, particularly at high currents, of connecting two or more smaller IGBTs in parallel. Noteworthy advantages of this are a more flexible and individual organization of the layout, the heat sources can be distributed so that higher levels of power loss can be dissipated, and possibly also cost advantages by comparison with module attachments, depending on the device type and power.

The disadvantage is the unequal split in losses. The main reason for this lies in the uneven current split between devices which results from differences in V_{CEsat} , g_{fs} and V_{th} (variability in parameter values), which are manufacturer-dependent. Differences can arise in addition due to asymmetrical power and drive circuits, which are exhibited chiefly in the dynamic switching behavior.

The blocking characteristics of parallel-connected IGBTs can be ignored, because in relation to the conducting state behavior many small sources of power loss have very little effect. For the behavior in the conducting state, then when the gate-emitter voltage is constant the static current split is determined by the conducting state voltage. Figure 5-8 shows the output characteristics for two PT IGBTs with different collector-emitter saturation voltages. The conducting state voltage across the parallel-connected IGBTs is the same. The static current ($I_{load} = I_{C2} + I_{C1}$) splits as determined by the set of output characteristics.

The different split of the current between the devices results in different heating, and different power losses, for the IGBTs. When connected in parallel, the IGBT with the smaller saturation voltage must carry the greater partial current, has higher conducting-state losses and gets warmer.

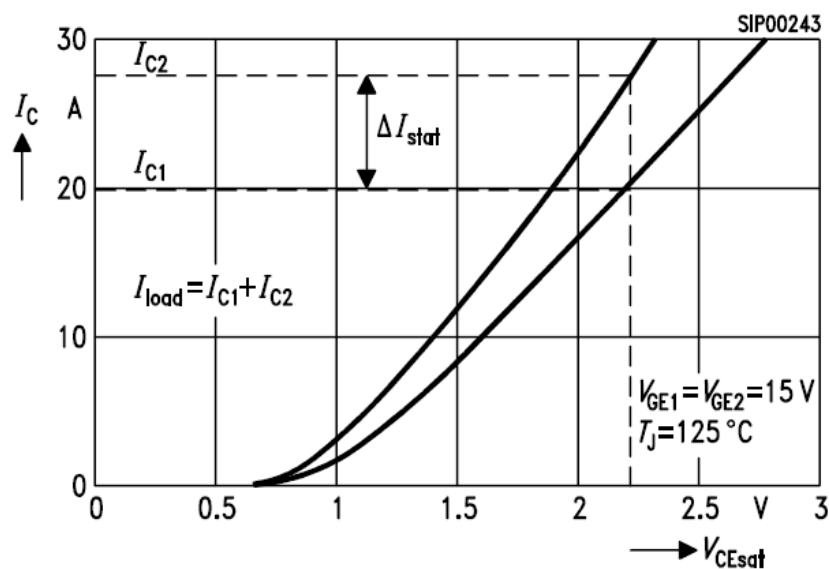


Figure 5-8 Set of Output Characteristics for two IGBT's with different Saturation Voltages

Another point affecting the current split is the temperature coefficient (TC) of the set of output characteristics Figure 5-9.

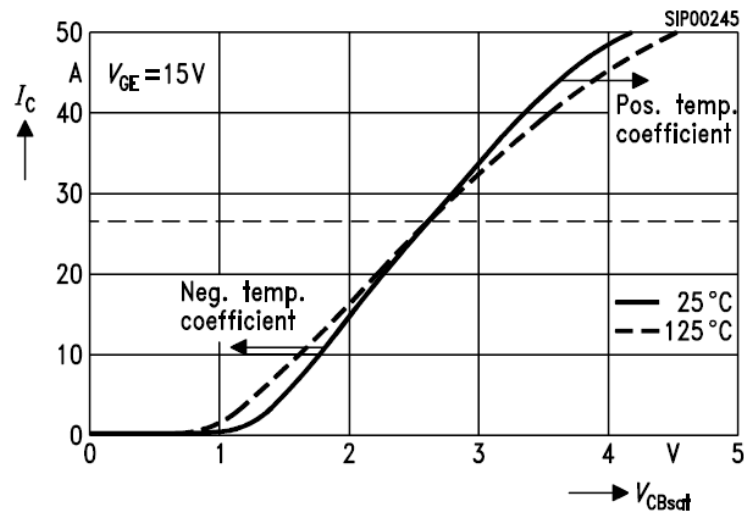


Figure 5-9 The TC of the Set of Output Characteristic Curves

The IGBTs should have a symmetrical layout with respect to IGBT current paths & gate driver. The most sensitive parameter is the emitter stray inductance in the gate circuit. For the same drive voltage (V_{drive}), unequal emitter stray inductances produce different gate-emitter voltages (V_{GE}) during switching. This results in an asymmetrical dynamic split of the current or different switching losses. In addition, the switching behavior can be balanced by using separate gate dropping resistors. There should be symmetrical cooling conditions (identical heat-sink temperature and flow rate below the paralleled devices).

To achieve above requirements & to get equal distribution of current the two IGBT's are fitted on same heatsink & are connected using busbar as shown in Figure 5-10

Snubber Circuit:

Power semiconductors are the heart of power electronics equipment. Snubber is a circuit which is placed across semiconductor devices for protection and to improve performance. Snubber can do many things:

- Reduce or eliminate voltage or current spikes
- Limit dI/dt or dV/dt
- Shape the load line to keep it within the safe operating area (SOA)
- Transfer power dissipation from the switch to a resistor or a useful load
- Reduce total losses due to switching
- Reduce EMI by damping voltage and current ringing

There are many different kinds of snubber but the two most common ones are the resistor-capacitor (RC) damping network and the resistor-capacitor-diode (RCD) turn-off snubber.

An RC snubber, placed across the switch, can be used to reduce the peak voltage at turn-off and to damp the ringing. In most cases a very simple design technique can be used to determine suitable values for the snubber components (R_s and C_s).

RC snubbers are very useful for low and medium power applications but when the power level is more than a few hundred watts the loss in the snubber can be excessive and other types of snubbers need to be considered.

The RCD snubber has several advantages over the RC snubber:

- In addition to peak voltage limiting, the circuit can reduce the total circuit loss, including both switching and snubber losses.
- Much better load lines can be achieved, allowing the load line to pass well within the SOA.
- For a given value of C_s , the total losses will be less

The key feature of this RCD snubber is that the switch voltage rises slowly as the switch current falls. This means that the high peak power associated with simultaneous maximum voltage and current is eliminated. The net result is much lower peak stress and switching loss.

Looking at all above advantages an RCD snubber is used which is connected across IGBT as shown in Figure 5-11.

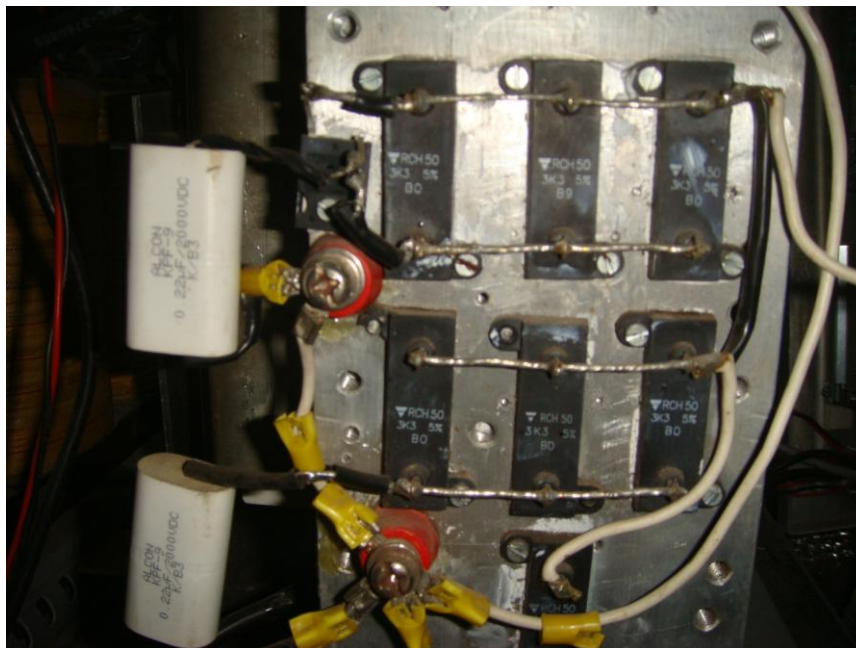


Figure 5-11 RCD Snubber

5.3 Summary

In this chapter the design & implementation of power circuit is presented. The calculations are shown & how to prepare inductor & capacitor are explained. The IGBT's are introduced & their types are explained. The new generation Trench/Fieldstop IGBT4 is selected and it is described how to connect two IGBT's in parallel. The need and details of RCD snubber is explained.

Chapter 6

DEVELOPMENT AND DESIGN OF THE CONTROL CIRCUIT FOR QUASI-RESONANT CONVERTER

6.1 Introduction

This chapter describes the basic principles of operation and control of quasi-resonant converter for induction melting application. In induction melting application the load is variable which depends on the type & quantity of metal to be melted. Thus the output frequency should be automatically adjusted to suit changing load condition, so that the converter always operates at the resonance frequency of tank circuit.

6.2 Control

Control of the output frequency and output power of the converter is effected by command triggers to the converter. The control scheme is shown in Figure 6-1.

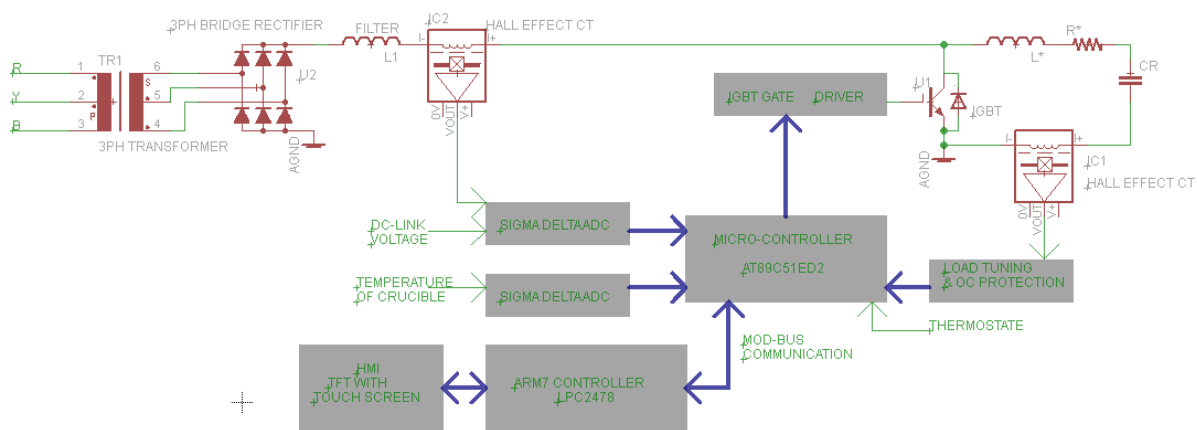


Figure 6-1 Control Scheme

Three distinct control loops are utilized in controlling the output of the converter.

They are:

1. Self control of the ON duty cycle by timing the converter switching from the induction load,
2. Control of output frequency and power by closed loop control through D-C Link power feedback.
3. Current limit for mishaps of short circuits by closed loop control.



Figure 6-2 Variable Load

Self-controlling the output frequency allows the converter to adjust itself to compensate for variations encountered with induction loads as shown in Figure 6-2. When the driving frequency is the resonant frequency of the tank circuit, the capacitive and inductive currents cancel each other, the input power factor is unity, and the generator supplies only real current and real power to the load. If the magnetic work piece is heated through the Curie temperature, or if it is removed from the crucible, the magnetic permeability of the flux path inside the coil is reduced to unity, and the coil inductance is decreased. The inductor current increases, the capacitor current no longer equaling it, and the generator is forced to supply a large lagging current. Thus compensation is required to be automatically made by control which should sense the increase in the tank natural resonant frequency and should speed up the switching rate of the converter.

As shown in Figure 6-1, the hall effect CT is used to sense the high frequency current in the tank circuit. The details about it are in the following topic.

6.3 Current Sensing Technology Overview

There are three technologies that are typically used for measuring current: sense resistors, current transformers and Hall effect sensors.

Sense resistors are simply a resistor placed in series with the load. By ohms law, the voltage drop across the device is proportional to the current. For low currents, these provide very accurate measurement given the resistance value has a tight tolerance.

Although sense resistors with high performance thermal packages have been developed for larger currents, they still result in insertion loss. In addition, they do not provide a measurement isolated from transient voltage potentials on the load. Sense resistors also require other circuitry such as instrumentation amplifiers to generate a distinguishable signal.

Current transformers are relatively simple to implement and are passive devices that do not require driving circuitry to operate. The primary current (AC) will generate a magnetic field that is coupled into a secondary coil by Faraday's Law. The magnitude of the secondary current is proportional to the number of turns in the coil, which is typically as high as >1000 . The secondary current is then sensed through a sense resistor to convert the output into a voltage.

There are two techniques for sensing current using Hall effect devices. According to the Hall effect, a magnetic field passing through a semiconductor resistor will generate a differential voltage proportional to the field (figure 6-3).

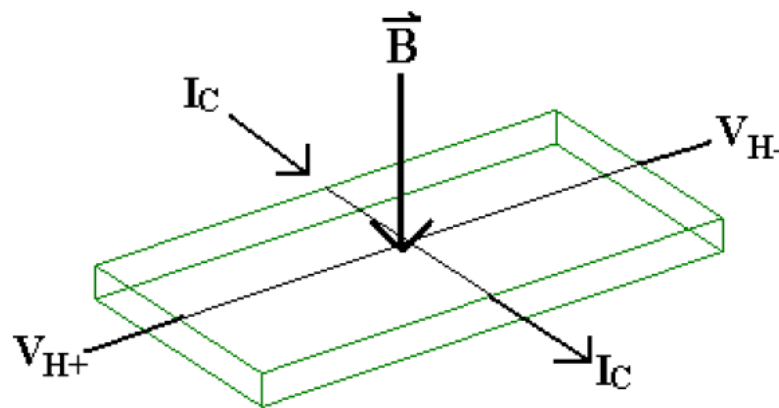


Figure 6-3 Representation of the Hall effect and its electrical parameters

Concentric magnetic field lines are generated around a current carrying conductor. Approximating the primary current conductor as infinitely long, the magnetic field strength may be defined $B = \mu_0 I / 2\pi r$, where μ_0 is the permeability of free space, I is the current and r is the distance from the center of the current conductor. In order to induce a larger signal out of the Hall element; the current conductor may be wrapped around a slotted ferrous toroid N number of times, such that $B = \mu_0 NI / 2\pi r$. In an open loop topology, the Hall element output is simply amplified and the output is read as a voltage that represents the measured current through a scaling factor as depicted in figure 6-4.

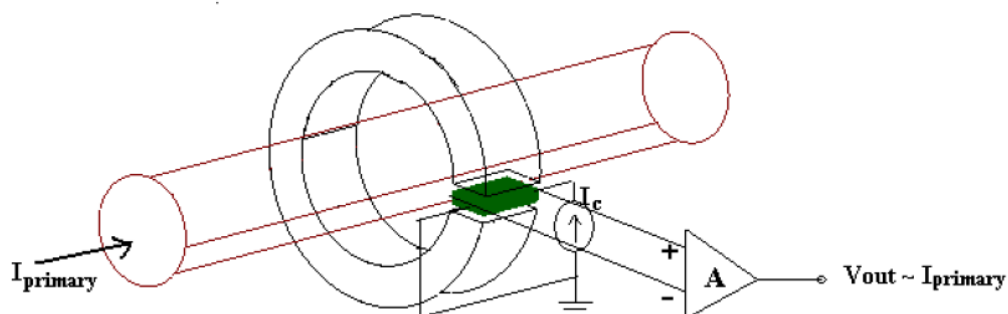


Figure 6-4 Basic Topology of Open Loop Hall Effect Current Sensor

In a closed loop topology, the output of the Hall element drives a secondary coil that will generate a magnetic field to cancel the primary current field. The secondary current, scaled proportional to the primary current by the secondary coil ratio, can then be measured as voltage across a sense resistor.

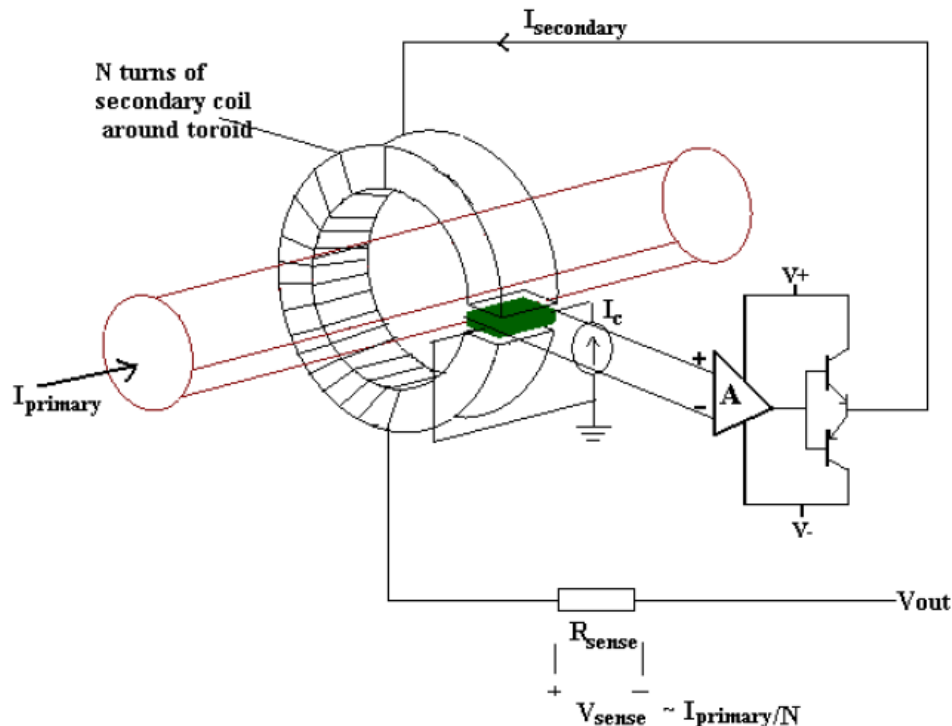


Figure 6-5 Basic Topology of Close Loop Hall Effect Current Sensor

By keeping the resultant field at zero, the errors associated with offset drift, sensitivity drift and saturation of the magnetic core will also be effectively canceled. Closed-loop Hall effect current sensors also provide the fastest response times. However, with a secondary coil that may be needed to drive up to several milli-amps of current, power consumption is much higher in closed loop Hall effect devices than open loop topologies. The closed loop configuration also limits the magnitude of the current that can be sensed since the device may only drive a finite amount of compensation current.

Thus for this application HT300M (Figure 6-6) is used to measure the tank current as its bandwidth is DC to 115kHz at -3dB and the frequency of operation is 7-8kHz.



Figure 6-6 Hall Effect Current Sensor Panel Mounting Type HT300M

The whole scheme of Figure 6-1 is divided into two boards:

1. Micro-controller Board (AT89C51ED2).
2. Embedded controller (Arm-7) Board.

These two cards interact with each other through MOD-BUS communication protocol.

6.4 Micro-controller Board (AT89C51ED2)

The self controlling is accomplished by micro-controller card, which takes the tank current as input (through hall-effect current sensor) & with load tuning circuit as shown in Figure 6-7 controls the on cycle duty of IGBT firing pulses. The Tank current is compared with the preset voltage (0.1V) to generate a falling edge as shown in Figure 6-8 on CUR-SEN1 pin which is connected to INT0_. This automatically compensates for the changes in load inductance. The second comparator compares for the over current and informs micro-controller about it.

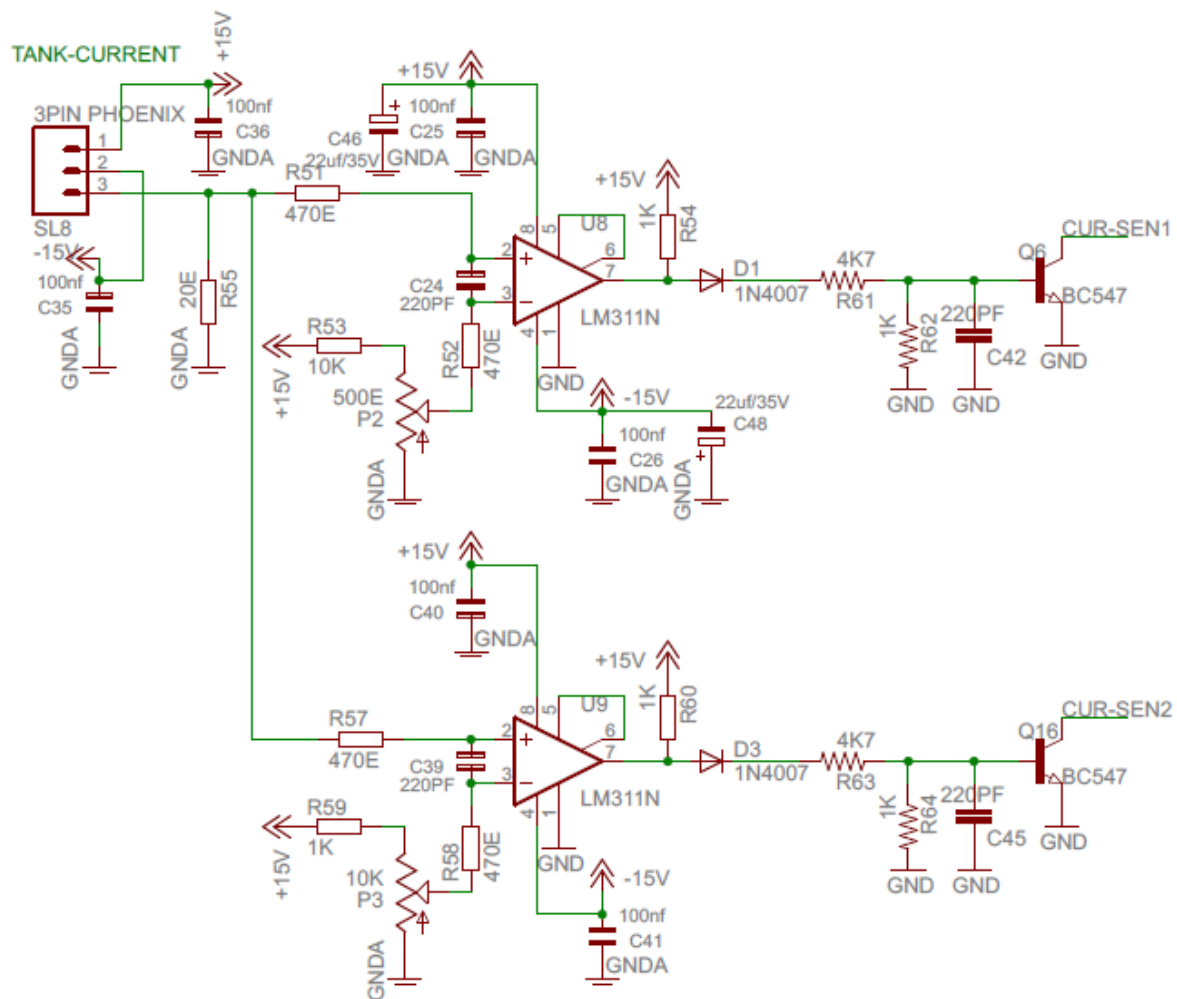


Figure 6-7 Load Tuning and Over Current Protection Circuit

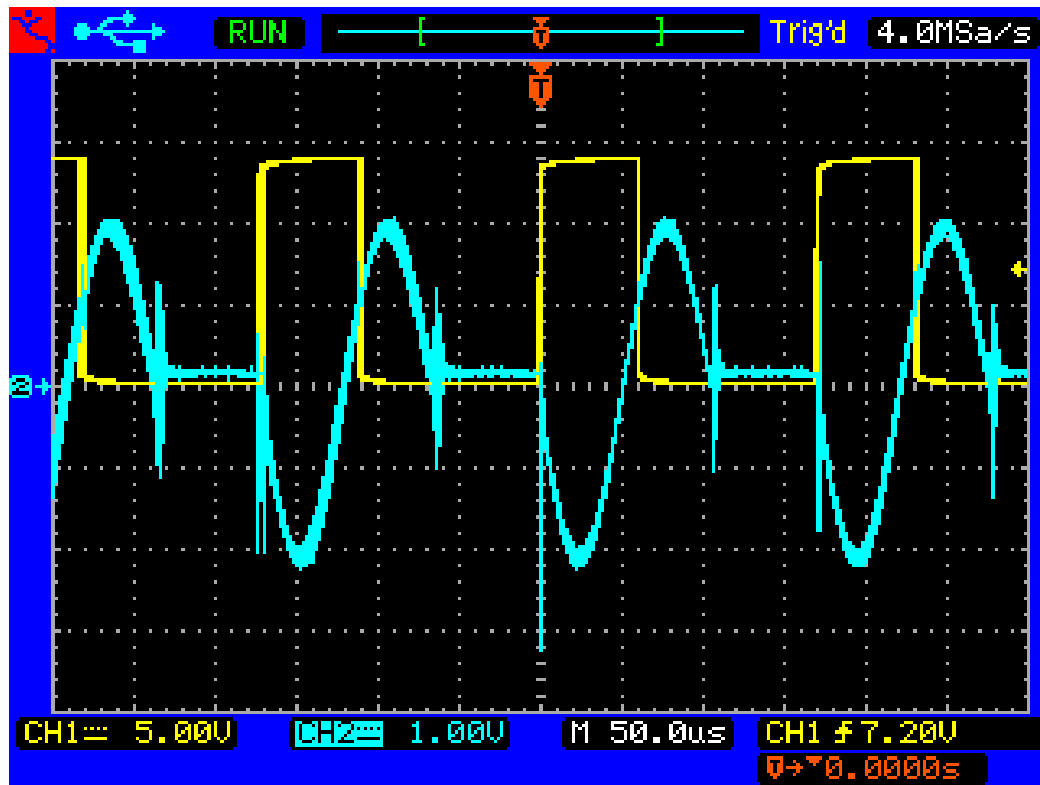


Figure 6-8 Waveform of Load Tuning Circuit
(Cyan: Tank Current Yellow: CUR-SEN1)

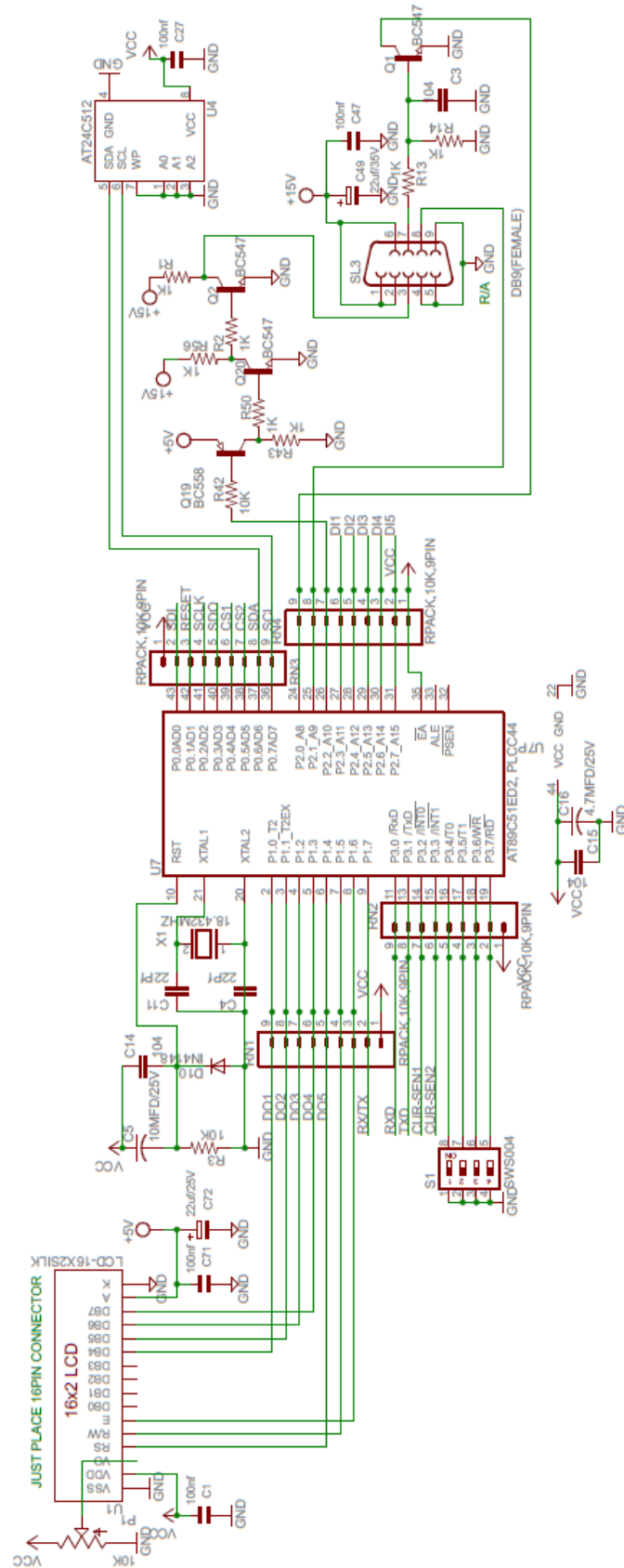


Figure 6-9 Micro-controller Circuit

Besides above function the microcontroller card digitizes the DC-Link Voltage & Current using a Sigma-Delta ADC and calculates DC-Link Power as shown in Figure 6-10.

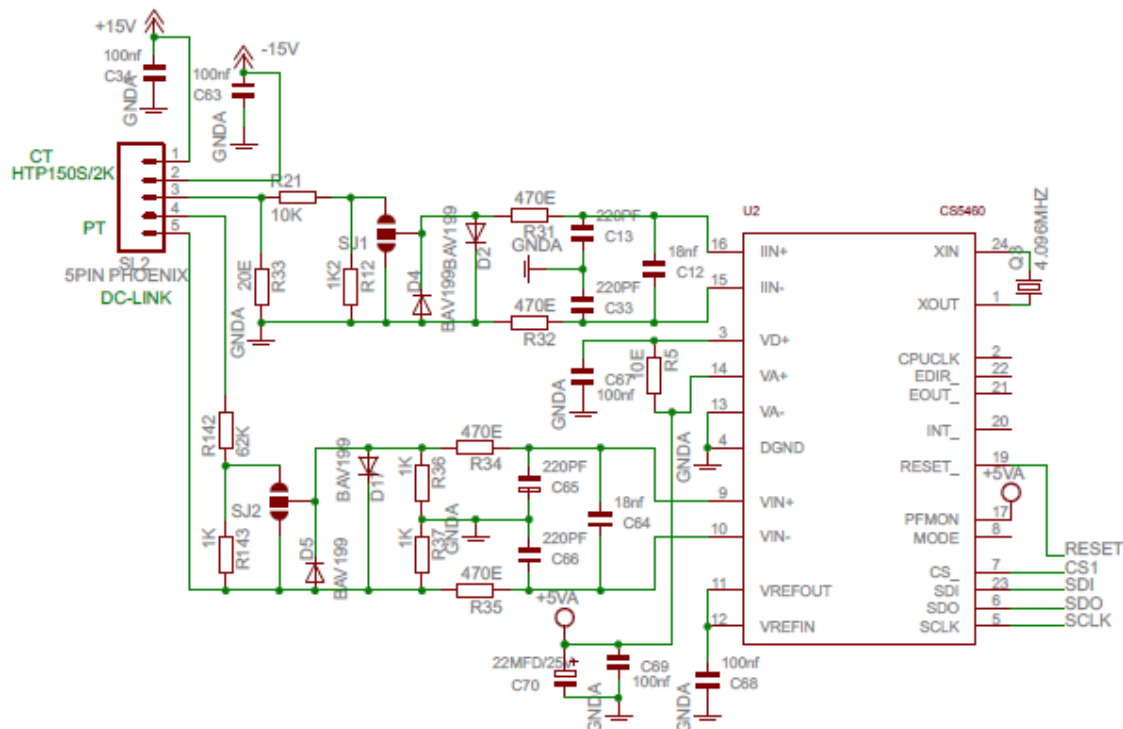


Figure 6-10 Measurement of DC-Link Voltage & Current

Using second Sigma-Delta ADC it measures the temperate of crucible through thermocouple & does cold junction compensation as shown in Figure 6-11.

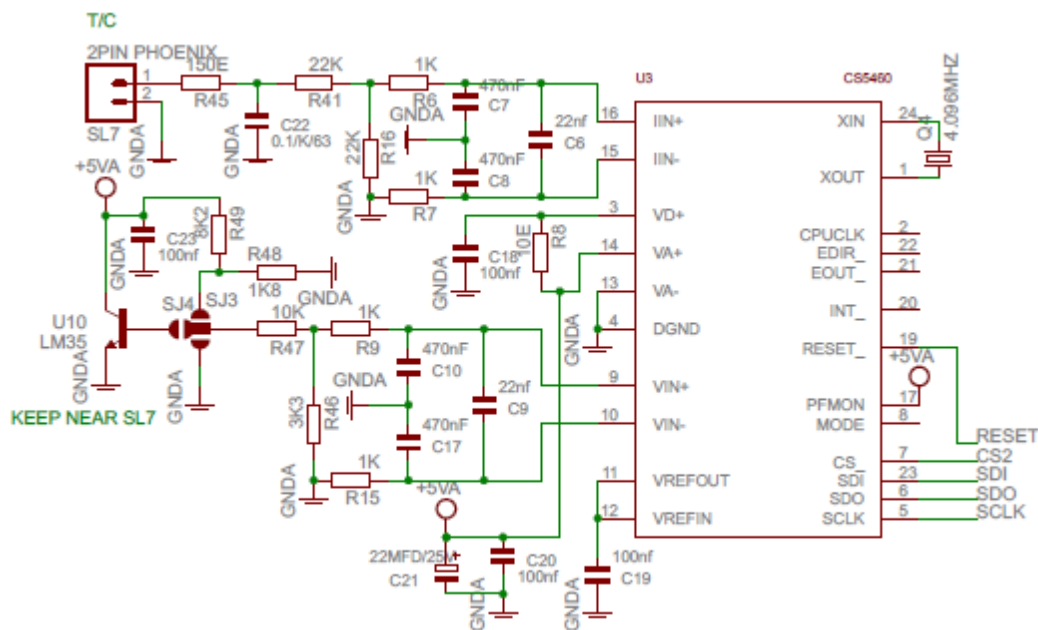


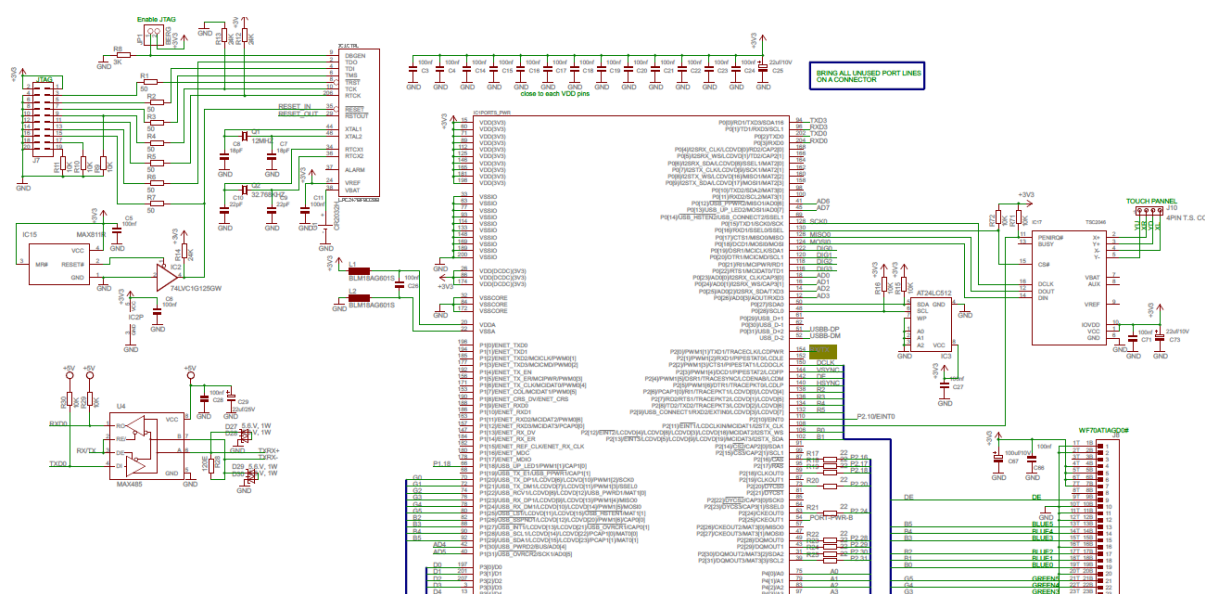
Figure 6-11 Measurement of Crucible Temperature

Finally these two quantities are sent to the ARM-7 card through RS-485 for further processing. After processing on these data the ARM-7 card decides about operating frequency and the frequency bursts which are then sent out to micro-controller card through RS-485. The micro-controller card taking these commands finally controls the converter.

6.5 Embedded controller (ARM-7) Board (LPC2478)

Figure 6-12 depicts the Arm-7 controller board. The core part of the design is the NXP LPC2478 microcontroller. NXP Semiconductors designed the LPC2478 microcontroller, powered by the ARM7TDMI-S core, to be a highly integrated microcontroller for a wide range of applications that require high-speed calculations, advanced communications and high quality graphic displays. The LPC2478 microcontroller has 512 kB of on-chip high-speed flash memory. This flash memory includes a special 128-bit wide memory interface and accelerator architecture that enables the CPU to execute sequential instructions from flash memory at the maximum 72 MHz system clock rate. The on-chip UART peripheral includes a fractional baud rate generator that allows standard baud rates to be generated with low frequency error. There is a 32.768 kHz crystal clock for the on-chip real-time clock peripheral unit or RTC for short. Power for the RTC (during these low power modes) comes from the VBAT input pin.

As the major function of ARM-7 board is to do processing on data received from Micro-controller card and to interface TFT with touch screen the LPC2478 becomes to ultimate choice with respect to price & performance. As seen in Figure 12-6a TSC2046 is used to interface touch screen while the bottom part shows the interfacing of TFT display (800x640). In Figure 12-6a the interfacing of SDRAM (MT48LC8M32B2) and NOR FLASH (SST39VF6401-70) is shown. The SDRAM is used as the display RAM while NOR-FLASH is used to store constant images.



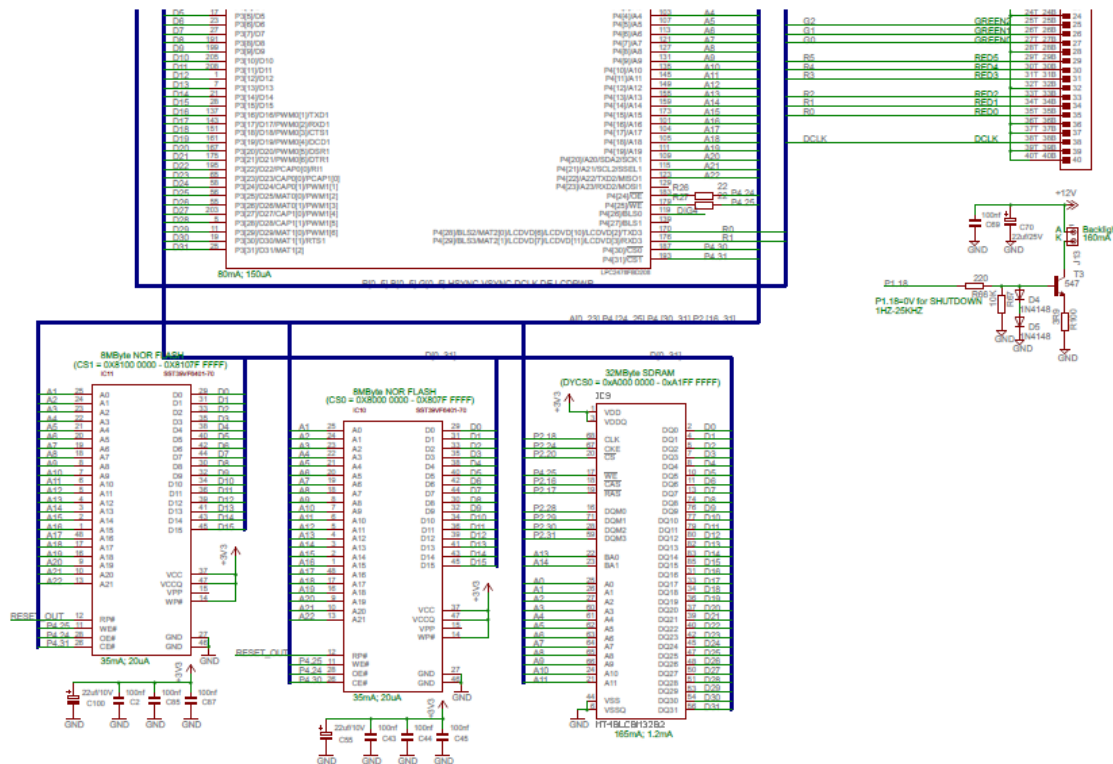


Figure 6-12b ARM-7 control board

6.6 Coreless IGBT Gate Driver

The design of IGBT driver circuit is very important for the satisfactory performance of IGBT.

The gate drive circuit as shown in Figure 6-13 is built around a primary and a secondary ASIC (application specific integrated circuit). The ASICs contain all integrated circuitry necessary for implementing the two main functions of a gate driver: First, to transmit signals between primary and secondary side, and second, to provide insulation and power supply for the secondary side.

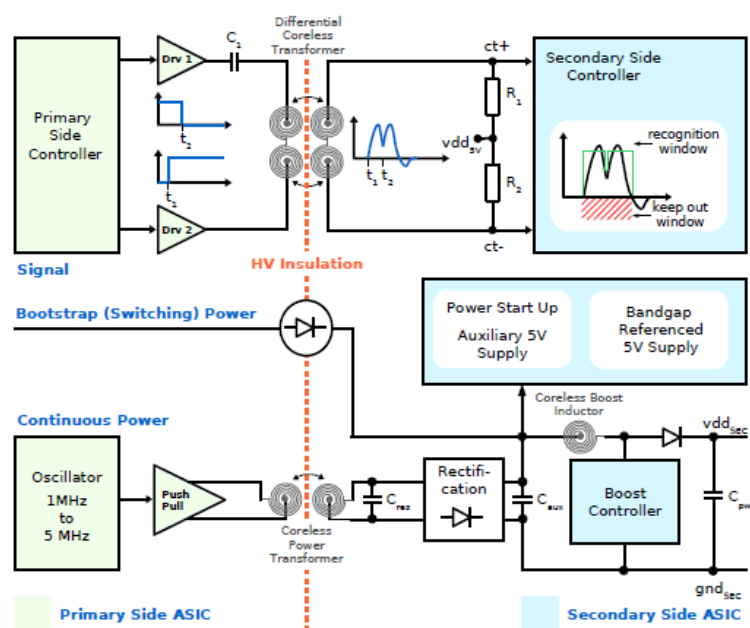


Figure 6-13 Block diagram of the coreless gate drive system

There are chip external coreless transformers on the PCB between primary and secondary side. These coreless transformers consist of spiral windings that are stacked on top of each other and that are separated by the PCB insulation material. No magnetic flux guidance, such as a ferrite core, is used.

6.7 New Generation Scale-2 IGBT-Driver Circuits

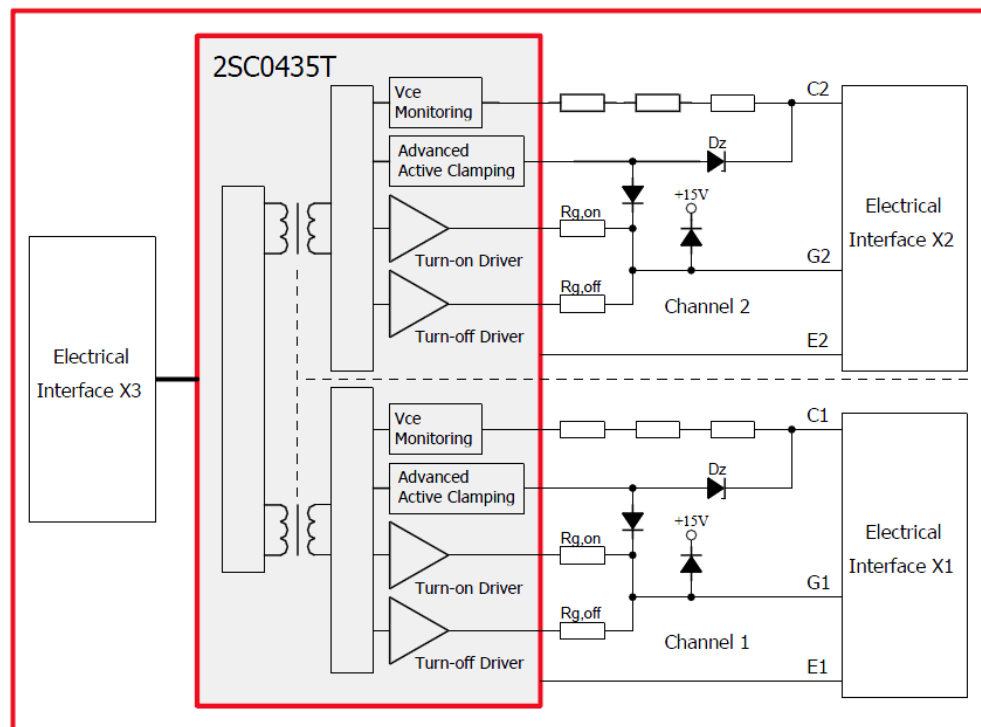


Figure 6-14 Basic Schematic of the gate drive board with 2SC0435T driver

The Scale-2 driver board contains all necessary components for optimal and safe driving of IGBT modules: gate clamping, active-clamping diodes (overvoltage protection at turn-off), Vce monitoring (short-circuit protection) as well as the input electrical connector and both output electrical connectors to connect both the power switch. It is equipped with usual protection functions such as Vce monitoring for short-circuit protection, operation inhibit after fault, supply under voltage shutdown and status feedback. It also features advanced active-clamping function and very low propagation delay time.

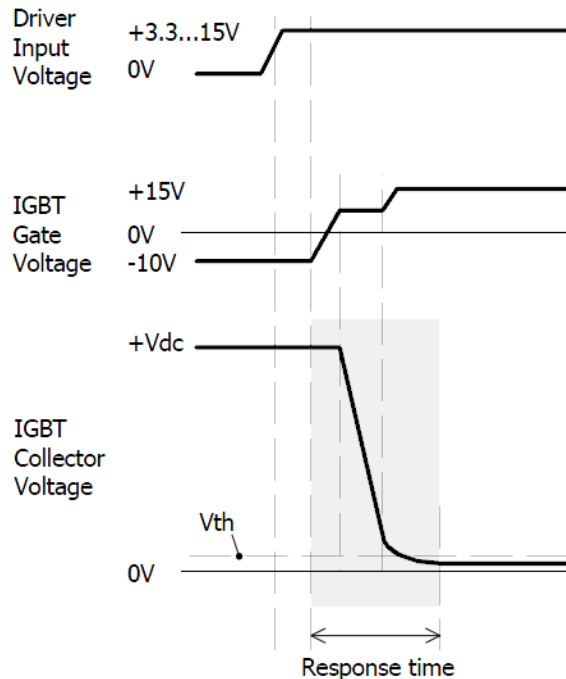
The 2SC0435T is the most compact driver core in its power range with a footprint of only 57.2 x 51.6mm and an insertion height of max. 20mm. It combines a complete two-channel driver core with all components required for driving, such as an isolated DC/DC converter, short-circuit protection, advanced active clamping as well as supply voltage monitoring. Each of the two output channels is electrically isolated from the primary side and the other secondary channel.

An output current of 35A and 4W drive power is available per channel, making the 2SC0435T an ideal driver platform for universal usage in medium and high-power applications. The driver provides

a gate voltage swing of +15V/-10V. The turn-on voltage is regulated to maintain a stable 15V regardless of the output power level.

Its outstanding EMC allows safe and reliable operation in even hard industrial applications.

Vce monitoring/short-circuit protection



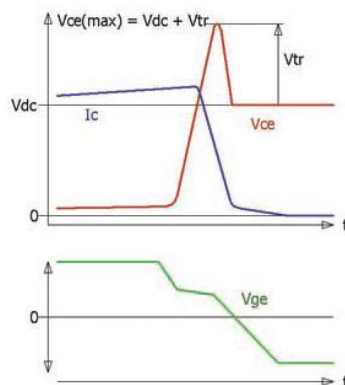
The basic Vce monitoring circuit of Scale-2 board is illustrated in Figure 6-14. Both IGBT collector-emitter voltages are measured with a resistor network. Vce is checked after the response time (as shown in Figure 6-15) at turn-on to detect a short circuit. If this voltage is higher than the programmed threshold V_{th} , the driver detects a short circuit at the IGBT and signals it immediately to the corresponding SOx output. The corresponding IGBT is immediately switched off. The IGBT is kept off and the fault is shown at pin SOx as long as the blocking time is active.

Figure 6-15 Turn-on characteristic of an IGBT

The blocking time is applied independently to each channel. It starts when Vce exceeds the threshold of the Vce monitoring circuit. This de-saturation function is for short circuit detection only and cannot provide over current protection. Hence over current protection is directly provided through micro-controller as seen in Figure 6-7.

Active clamping

Parasitic inductances in IGBT modules and converter circuits cannot be completely eliminated for

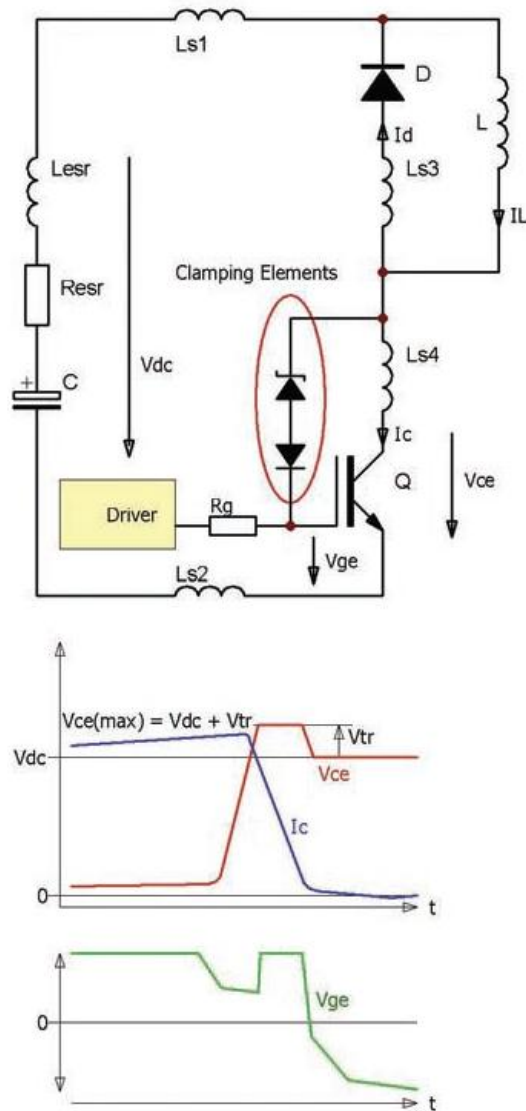


physical reasons, and their influence on the system behavior cannot be neglected. The current change caused by turning off the IGBT produces voltage transients at its collector, as shown in the upper part of Figure 6-16.

The commutation speed and thus, the turn-off over-voltage at an IGBT can, in principle, be affected by the turn-off gate resistance $R_{g(off)}$. This technique is used particularly at lower powers.

Figure 6-16 Typical characteristic at IGBT turn-off

However, $R_{g(off)}$ must then be dimensioned for overload conditions such as turn-off of the double rated current, short circuit and a temporarily increased link circuit voltage. In normal operation this results in increased switching losses and turn-off delays, which reduces the usability of the modules. So this simple method is unsuitable for modern high-power modules.



Simple Active Clamping has already been used for some time to protect IGBTs. Active clamping means the direct feedback of the collector potential to the gate via an element with an avalanche characteristic. Figure 6-17 (upper part) shows the principle on the basis of an IGBT switch.

The feedback branch consists of a clamping element, as a rule comprising a series of transient voltage suppressors (TVS). If the collector-emitter voltage exceeds the approximate breakdown voltage of the clamping element, a current flows via the feedback to the gate of the IGBT and raises its potential, so that the rate of change of the collector current is reduced and a stable condition results. The voltage across the IGBT is then determined by the design of the clamping element. The IGBT operates in the active range of its output characteristic and converts the energy stored in the stray inductance into heat. The clamping process continues until the stray inductances have been demagnetized. The fundamental relationships involved here on the basis of typical curves are illustrated in the lower part of Figure 6-17.

Figure 6-17 Principle of an IGBT driver with Active Clamping

Advanced active clamping

Simple Active Clamping is traditionally used only to protect the semiconductor in the event of overload. Consequently, the clamping elements are never subjected to recurrent pulse operation.

The problem of repetitive operation takes the following form: modern high power IGBTs are optimally driven with gate resistors in the range from 0.1 to several ohms. For turn-off, the driver supplies an output voltage of $-10V$. However, the Active Clamping Circuit must raise the gate voltage temporarily to about $+15V$, in order to reduce the rate of current change. This produces a voltage drop of $25V$ across the gate resistor. A high current is absorbed by the driver, which flows through the

Active Clamping circuit, where it produces high losses and additional voltage drops. The simple Active Clamping circuit is consequently unsuitable for repetitive operation.

An improved Active Clamping circuit has been presented in Figure 6-18. Here, the base of the chain of clamping diodes is, as usual, connected to the gate of the IGBT, but additionally to the input of a booster stage. The driver voltage is consequently raised as soon as a current flows through the clamping element. The driver stage now no longer draws any current from the clamping element, and the current flowing through the latter is then available exclusively for charging the gate. The voltage drop and power loss in the clamping diodes can thus be dramatically reduced.

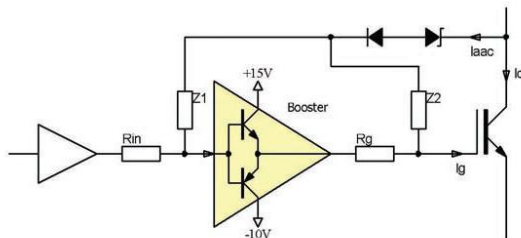


Figure 6-18 Principle of an IGBT driver with Advanced Active Clamping

The final board shown in Figure 6-22 supports the advanced active clamping based on this principle: when active clamping is activated, the turn-off MOSFET of the driver is switched off in order to improve the effectiveness of the active clamping and to reduce the losses in the TVS.

Intelligent paralleling

Parallel-connected IGBTs are conventionally driven by a common driver, with individual gate and emitter resistors for each IGBT. However, modules of the Prime PACK power class require more extensive circuitry: they cannot, for instance, dispense with active clamping [25], which results in solutions such as that proposed in Figure 6-19.

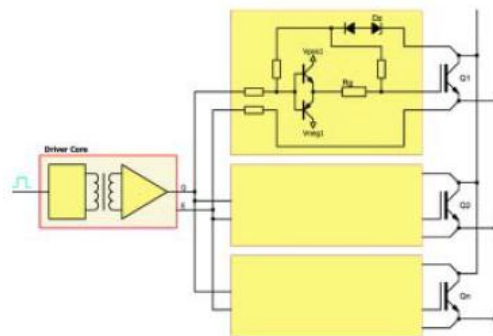


Figure 6-19 Principle of a central driver

An alternative approach to driving parallel-connected IGBT modules is to use an individual driver for each module, as shown in Figure 6-20. However, this attractively simple approach was hardly practical in the past because the drivers previously available on the market had excessive runtime differences and jitter, which would have led to an

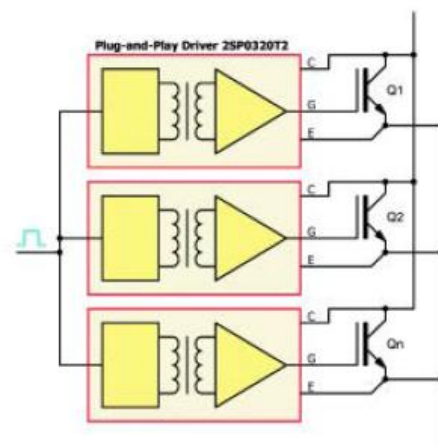


Figure 6-20 Principle of driving parallel connected IGBTs with individual drivers

asymmetrical distribution of the collector currents and losses in the parallel-connected modules. Moreover, previous drivers also failed to offer any scenario for the behavior of parallel-connected drivers in the event of a fault.

A solution is now available with the SCALE-2 driver chipset from CONCEPT [26] [27]. With a runtime of just below 80ns, as shown in Figure 6-21, it is about five times as fast as the preceding generation and 8 to 20 times faster than typical competitor solutions. In addition, the small deviations in the runtimes of the various drivers of $\leq \pm 4\text{ns}$ and the extremely low jitter of $\leq \pm 2\text{ns}$ make it ideal for use in the parallel circuit. The low tolerance of these parameters ensures that the parallel-driven IGBTs switch almost simultaneously. As every IGBT module has its own driver, the power of a single driver does not need to be distributed over several IGBTs. So this concept also allows high clock frequencies with parallel circuits.

Power supply	Remarks	Min	Typ	Max	Unit
Supply current I_{OC}	Without load		32		mA
Supply current I_{CC}	$F = 0\text{Hz}$		26		mA
Supply current I_{CC}	$F = 100\text{kHz}$		38		mA
Coupling capacitance C_{io}	Primary to output, total		20		pF
Power Supply Monitoring	Remarks	Min	Typ	Max	Unit
Supply threshold V_{CC}	Primary side, clear fault	11.9	12.6	13.3	V
	Primary side, set fault (Note 12)	11.3	12.0	12.7	V
Monitoring hysteresis	Primary side, set/clear fault	0.35			V
Supply threshold $V_{ISOx}-V_{Ex}$	Secondary side, clear fault	12.1	12.6	13.1	V
	Secondary side, set fault (Note 13)	11.5	12.0	12.5	V
Monitoring hysteresis	Secondary side, set/clear fault	0.35			V
Supply threshold $V_{Ex}-V_{COMx}$	Secondary side, clear fault	5	5.15	5.3	V
	Secondary side, set fault (Note 13)	4.7	4.85	5	V
Monitoring hysteresis	Secondary side, set/clear fault	0.15			V
Logic Inputs and Outputs	Remarks	Min	Typ	Max	Unit
Input bias current	$V(INx) > 3\text{V}$		190		μA
Turn-on threshold	$V(INx)$		2.6		V
Turn-off threshold	$V(INx)$		1.3		V
SOx output voltage	Failure condition, $I(SOx) < 20\text{mA}$			0.7	V
Short-Circuit Protection	Remarks	Min	Typ	Max	Unit
Current through pin REFx	$R(REFx, VEx) < 70\text{k}\Omega$		150		μA
Minimum response time	Note 9		1.2		μs
Minimum blocking time	Note 10		9		μs
Timing Characteristics	Remarks	Min	Typ	Max	Unit
Turn-on delay $t_{d(on)}$	Note 6		85		ns
Turn-off delay $t_{d(off)}$	Note 6		70		ns
Jitter of turn-on delay	Note 17		± 3		ns
Jitter of turn-off delay	Note 17		± 3		ns
Output rise time $t_{r(out)}$	Note 7		20		ns
Output fall time $t_{f(out)}$	Note 7		20		ns
Transmission delay of fault state	Note 14		400		ns

Figure 6-21 Electrical characteristics of 2SC0435T

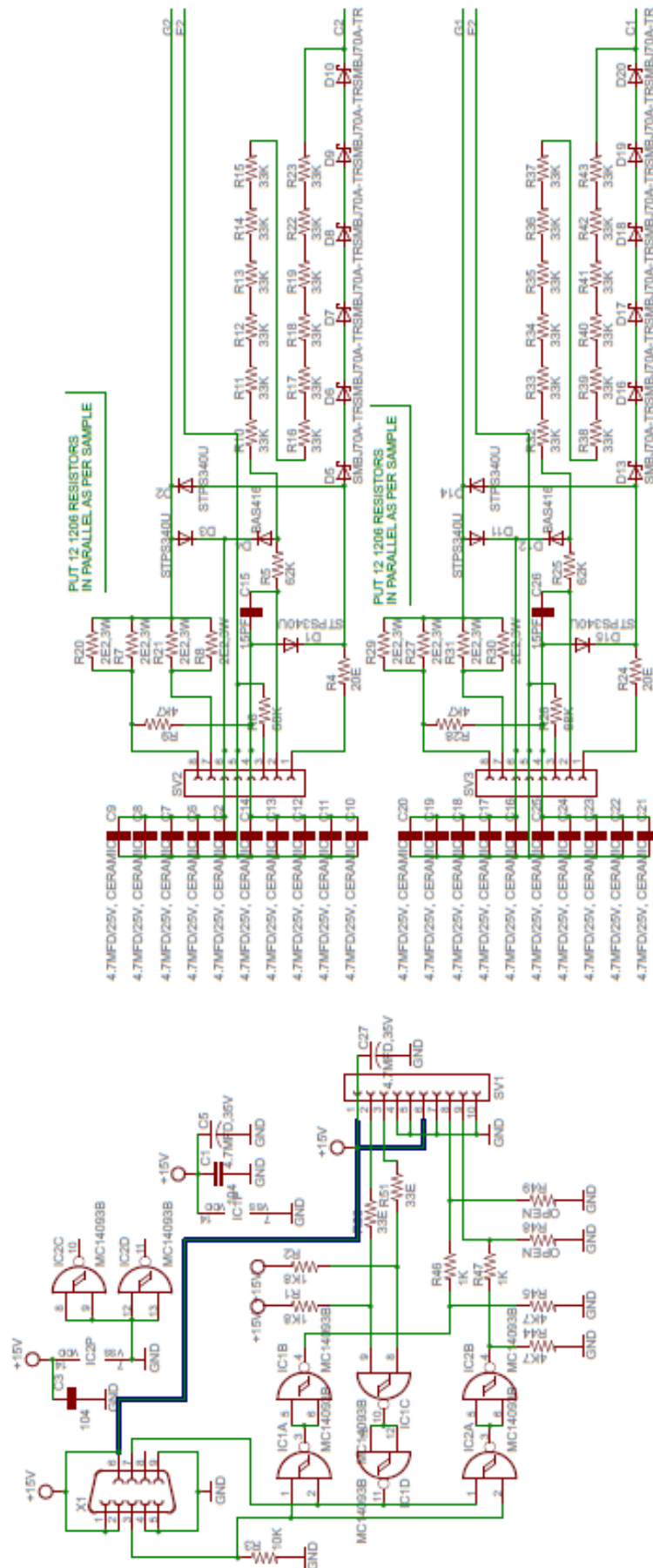


Figure 6-22 Final Schematic of the gate drive board with 2SC0435T driver

6.8 Summary

In this chapter the Micro-controller Board & Embedded controller board based on Arm-7 are developed and tested.

The different driving methods for IGBT are discussed & SCALE-2 driver is used to build the driver board.

The main finding of this discussion reveals following:

In comparison with other driving methods, active clamping allows enhanced utilization of the IGBT modules during normal operation by increasing the switching speed and therefore reducing switching losses. The overvoltage at fault-current turn-off is also managed by active clamping.

Chapter 7

SOFTWARE IMPLEMENTATION

7.1 Introduction

This chapter describes the implementation of microcontroller software to control the quasi resonant converter. It has to take care of load tuning, over current protection and mod-bus communication.

It also describes the implementation of Embedded software for implementation of GUI, a discrete Proportional-Integral-Derivative (*PID*) controller and autotuning.

There are two parts of the complete software.

1. Low-level (Assembly Language) software for Micro-controller Board.
2. High-level (C Language) software for ARM-7 Board.

7.2 Low-level software for Micro-controller Board

The micro-controller board has to perform following tasks.

1. Read Temperature of crucible through thermocouple using Sigma-Delta ADC and do linearization and cold junction compensation.
2. Reading of RMS value of DC-Link voltage & current using sigma-delta ADC and finding DC-Link power.
3. Sending calibrated DC-Link power & linearized temperature to ARM-7 board through MOD-BUS communication.
4. Taking commands of frequency & frequency bursts from ARM-7 board.
5. Generating gate pulses for IGBT using these commands & to automatically tune the on duty cycle of gate pulses according to changes in load inductance.
6. To switch off IGBT gate firing in case of over current in tank circuit, DC-Link over current, DC-Link under voltage, over temperature (sensed through thermostat), driver card fault, etc.

To implement all above tasks the whole software is divided into 5 parts.

7.2.1 Main program

Following is the listing of Main program which initializes the SFR's to set the modes of timers & serial port and enables interrupts. It checks calibration data stored in Eeprom and validates them & informs ARM-7 board for any error. After which it enables timer & external interrupts as well as serial port interrupt. And finally remains in a loop where it checks for any error & informs ARM-7 board as per error generated.

MAIN:

```

MOV SP,#BDH
MOV P0,#11111011B ;KEEP SCLK (CS5460) LOW
MOV P1,#00111111B ;KEEP ENABLE PIN(LCD) LOW, 485 IN RECV. MODE
MOV P2,#FFH
MOV AUXR,#00010001B ;XRAM SIZE 1792 BYTES, INT-XRAM SELECTED
MOV CKCON0,#7FH ;X2 SPEED (3.072 MIPS)
MOV CKCON1,#01H
MOV CKRL,#FFH
MOV PCON,#00H ;RESET POWER-OFF FLAG
MOV AUXR1,#00H ;BOOT ROM DISABLED & DPTR0 SELECTED
MOV WDTPRG,#05H ;TIMEOUT -> 170MS FOR X2 MODE
MOV IPH1,#00000000B
MOV IPL1,#00000000B ;SPI & KBD INTERRUPTS ARE NOT USED
MOV IPH0,#00001101B
MOV IPL0,#00010010B ;PRIORITY -> T1,INT0,INT1; SRL,T0; T2
MOV TCON,#00000101B ;INT0,1-FALLING EDGE
MOV TMOD,#00010001B ;TIMER-1,0 IN TIMER MODE-1
MOV TH0,#FAH ;COUNT FOR 1MS
MOV TL0,#07H ;(LESS BY 7 CYCLES TO GET EXACT 1MS TIME)
SETB TR0
MOV TH1,#FFH
MOV TL1,#66H ;COUNT FOR ON CYCLE TIME = 100uS
SETB TR1
SETB ET1
MOV T2CON,#00000000B ;T2 -> 16BIT AUTORELOAD MODE
MOV RCAP2H,#10H
MOV TH2,#10H
MOV RCAP2L,#00H
MOV TL2,#00H ;COUNT FOR 40MS
SETB TR2
ORL PCON,#00000000B ;SMOD1 = 0
CLR TI
MOV BRL,#246 ;9600 BAUD (X2-SPEED)
MOV BDRCON,#00011100B ;START BRG, USE BRG FOR TX,RX BOTH
MOV SCON,#60H ;SERIAL MODE-1, WITH SM2=1
;
MOV 0FH,#FDH
MOV 0EH,#04H ;COUNT FOR OFF CYCLE TIME FOR 1.67KHZ
MOV 31H,#250 ;CS5460-1 TIMEOUT = 10 SEC
MOV 35H,#250 ;CS5460-2 TIMEOUT = 10 SEC
MOV 38H,#30
MOV 39H,#00H
MOV 3AH,#00H ;INIT ROOM TEMP. AS 30 DEG
MOV 3BH,#01H ;RESET KEY-DEBOUNCE COUNTER
MOV 3FH,#00H ;INIT PRESENT POWER O/P = 0KW
MOV 40H,#00H ;MAKE PRESENT O/P FREQ. = 1.67KHZ
MOV 59H,#10 ;COUNT FOR 1 SEC

```

```

MOV    5AH,#03H    ;COUNT FOR 0.12 SEC
MOV    5BH,#25     ;COUNT FOR 1 SEC
MOV    5CH,#00H    ;RESET ERROR BYTE
MOV    5EH,#00H    ;RESET OPERATION MODE BYTE TO POWER OFF MODE
MOV    67H,#A8H    ;INIT RECV_BUF POINTER
MOV    6AH,#10     ;TO GIVE DEBOUNCE TO CJ-ERR (10 SECONDS)
MOV    6BH,#06H    ;TO DELAY XMISSION ATLEAST BY 6MS
MOV    70H,#10     ;COUNT FOR 10MS
MOV    71H,#03H    ;RESET UNDER VOLTAGE FAULT CHECK TRIAL CNTR
    LCALL DLY_20MS
;RESET CS5460-1,2 SERIAL PORT
CLR    P0.1
NOP
NOP
NOP
NOP
NOP
SETB   P0.1        ;APPLY H/W RESET
MOV    30H,#00H    ;TO CALL INIT5460-1 FOR 1ST TIME
MOV    34H,#00H    ;TO CALL INIT5460-2 FOR 1ST TIME
MOV    WDTRST,#1EH
MOV    WDTRST,#E1H ;RESET WATCH-DOG TIMER TO ENABLE IT
SETB   ET2
SETB   EA
CLR    P2.1        ;REMOVE RESET SIGNAL OF IGBT-DRIVER
LCALL  RDY_EE      ;WAIT TILL EEPROM IS READY
JC     ERR1
LCALL  BYTE_FIL
JC     ERR1
LCALL  VERFY
JNC    OK24512
ERR1:
    LCALL ERR2
OK24512:
    MOV    32H,#00H    ;RELOAD COUNT FOR 10SEC
    SETB   05H        ;START KBD TIMER (IF OFF)
    LCALL  VALID1      ;CHECK FOR VALIDITY OF DATA IN EEPROM
    JNC    A2
    MOV    5CH,#03H    ;FLAG THAT DATA IS INVALID
    LCALL  W_KBD       ;WAIT FOR A KEY STROKE
    LCALL  DEFLT1      ;LOAD DEFAULT VALUES IN EEPROM
    LCALL  DLY_0.5
    MOV    5CH,#00H    ;RESET ERROR BYTE
A2:
    LCALL  VALID11     ;CHECK IMP. DATA IN EEPROM
    JNC    AA2
    MOV    5CH,#03H    ;FLAG THAT DATA IS INVALID
    LCALL  W_KBD       ;WAIT FOR A KEY STROKE

```

```

    LCALL DEFLT11      ;LOAD DEFAULT VALUES IN EEPROM
    LCALL DLY_0.5
    MOV  5CH,#00H      ;RESET ERROR BYTE
AA2:
    LCALL VALID2       ;CHECK FOR VALIDITY OF DATA IN EEPROM
    JNC  A4
    MOV  5CH,#03H      ;FLAG THAT DATA IS INVALID
    LCALL W_KBD        ;WAIT FOR A KEY STROKE
    LCALL DEFLT2       ;LOAD DEFAULT VALUES IN DS12887
    LCALL DLY_0.5
    MOV  5CH,#00H      ;RESET ERROR BYTE
A4:
    LCALL LD_VARS      ;LOAD VARIABLES FROM EEPROM INTO INT.XRAM
    CLR  0BH           ;RESET CS5460-1 FAULT BIT TO START ACCESSING
    CLR  0CH           ;RESET CS5460-2 FAULT BIT TO START ACCESSING
;
    SETB ET0
    CLR  RI            ;DISCARD RI (DUE TO ANY REFLECTIONS)
    SETB REN
    SETB ES           ;ENABLE RECEPTION (FOR MODBUS COMMUNICATION)
    SETB 10H          ;ALLOW ACCESS TO I2C LINE IN INT.
    LCALL DELAY_1S
    CLR  P2.7         ;SW.ON CONTACTOR TO ACTIVATE POWER
    LCALL DELAY_1S     ;ALLOW CS5460 TO START
    SETB 41H          ;ACTIVATE DC-LINK UNDER-VOLT FAULT CHECKING
ST0:
    JBC  42H,UNDERV1   ;CHECK UNDER-VOLTAGE FAULT
    JB   59H,EMG1      ;CHECK EMERGENCY SWITCH
    JBC  53H,OCERR1    ;CHECK OVER-CURRENT FAULT
    JBC  55H,IEXCEED1  ;CHECK I/P-CURRENT EXCEED FAULT
    JB   4EH,DRVER1
    JB   0BH,ER54601
    JB   0CH,ER54601
    JBC  1EH,ERR22
    JBC  02H,CRCERR
    JBC  06H,CJTERR
    SJMP ST0

```

Table-7.1 Main program listing (Micro-controller board)

7.2.2 Timer-0 Interrupt at 1ms

In this subroutine the MOD-BUS timings are taken care off. If Melter power is on then it generates IGBT on/off commands as per required frequency bursts.

```

T0_OVF:
    MOV  TH0,#FAH      ;COUNT FOR 1MS
    MOV  TL0,#07H      ;(LESS BY 7 CYCLES TO GET EXACT 1MS TIME)
    JNB  2AH,I60

```

```

    DJNZ  6BH,I60
    MOV   6BH,#06H    ;TO DELAY XMISSION ATLEAST BY 6MS
    CLR   2AH
    SETB  TI          ;START TRANSMISSION
I60:
    JNB   2BH,I61
    DJNZ  6CH,I61
    MOV   6CH,#50      ;COUNT FOR 50MS
    MOV   67H,#A8H     ;RE-INIT RECV_BUF POINTER FOR RE-SYNCHRONISM
    CLR   2BH
I61:
    JNB   2CH,I62
    DJNZ  6DH,I62
    CLR   2CH
    CLR   RI           ;DISCARD RI (DUE TO ANY REFLECTIONS)
    SETB  REN
    MOV   67H,#A8H     ;RE-INIT RECV_BUF POINTER FOR RE-SYNCHRONISM
I62:
    DJNZ  70H,RET30
    MOV   70H,#10      ;RELOAD COUNT FOR 10MS
;10MS
    PUSH  PSW
    PUSH  A
        CLR  RS1
        SETB RS0      ;R.B - 1
    JNB   52H,P_OFF    ;CHECK POWER ON/OFF BIT
;SWITCH IGBT ON/OFF BIT ACCORDING TO ITS ON/OFF TIMER
    MOV   R0,#B1H
    MOV   A,@R0
    DEC   R0
    DEC   @R0
    CJNE  @R0,#00H,I64 ;CHECK FOR CT
    MOV   @R0,A        ;RESET CYCLE TIME TIMER (HEAT)
;
    MOV   R0,#BAH
    MOV   A,@R0
    INC   R0
    INC   R0
    ORL   A,@R0
    JNZ   ON1
    INC   R0
    MOV   A,@R0
    DEC   R0
    MOV   @R0,A        ;RELOAD PRECALCULATED OFF CYCLE COUNT
    DEC   R0
    MOV   A,@R0
    DEC   R0
    MOV   @R0,A        ;RELOAD PRECALCULATED ON CYCLE COUNT

```

```

ON1:
    MOV    R0,#BAH
    MOV    A,@R0
    JZ     OFF1      ;CHECK FOR ON CYCLE COUNT
    DEC    @R0
    SETB   50H       ;START SWITCHING IGBT
    SJMP   I64
OFF1:
    INC    R0
    INC    R0
    MOV    A,@R0
    JZ     I64       ;CHECK FOR OFF CYCLE COUNT
    DEC    @R0
P_OFF:
    CLR    50H       ;STOP SWITCHING IGBT
I64:
    POP    A
    POP    PSW
RET30:
    RETI

```

Table-7.2 Timer-0 Interrupt service subroutine listing

7.2.3 Timer-1 Interrupt for maximum on-cycle time

This subroutine takes care of maximum on-cycle time and generates firing signals for IGBT.

```

T1_OVF:
    JBC    51H,I104
    MOV    TH1,#FFH
    MOV    TL1,#66H    ;COUNT FOR ON CYCLE TIME = 100uS
    JNB    50H,RET12   ;CHECK IGBT ON/OFF COMMAND
    SETB   51H         ;FLAG THAT GATE IS ON
    CLR    P2.2        ;SW.ON THE GATE
    CLR    IE0         ;DISCARD PREVIOUS EDGES
    SETB   EX0         ;ENABLE INT0
RET12:
    RETI
I104:
    SETB   P2.2        ;SW.OFF GATE
    JBC    EX0,I105
    RETI
I105:
    PUSH   PSW
    CLR    RS1
    SETB   RS0         ;R.B - 1
    CJNE   R7,#FFH,I107
    CJNE   R6,#B5H,I107
I107:

```

```

JC    I108
MOV   TL1,#B5H
MOV   TH1,#FFH    ;LIMIT COUNT FOR OFF CYCLE TIME = 48uS
POP   PSW
RETI
I108:
MOV   TL1,R6
MOV   TH1,R7      ;COUNT FOR OFF CYCLE TIME
POP   PSW
RETI

```

Table-7.3 Timer-1 Interrupt service subroutine listing

7.2.4 Timer-2 Interrupt at 40ms

It reads DC-Link voltage and current from CS5460 and then calculates DC-Link power. Then it reads temperature and does linearization and cold junction compensation. In the later portion of this subroutine it applies accelerating/decelerating slope to the frequency of IGBT gate pulses as per start/stop command.

```

T2_OVF:
CLR   TF2
PUSH  PSW
PUSH  A
PUSH  B
PUSH  DPH
PUSH  DPL
ORL   PSW,#00011000B ;R.B.- 3
MOV   WDTRST,#1EH
MOV   WDTRST,#E1H
;READING CS5460-1 STARTS...
JB    0BH,I132      ;IF 5460-1 IS FAULTY THEN SKIP READING
CLR   P0.4          ;SELECT 5460-1
MOV   A,30H
JNZ   NORST1        ;IF RESET IS NOT IN PROGRESS
MOV   R2,#00H       ;CURRENT GAIN = 10
LCALL INIT5460
MOV   36H,#06H      ;DISCARD 5 SAMPLES AFTER INITIALIZATION
MOV   30H,#12        ;REINIT TRIAL COUNTER
LJMP  I31
NORST1:
MOV   A,#00011110B  ;READ STATUS REG. COMMAND
LCALL W_5460
LCALL R_5460        ;DUMMY READ OF STATUS REGISTER
MOV   R7,A
LCALL R_5460        ;DUMMY READ A BYTE FROM CS5460
LCALL R_5460        ;DUMMY READ A BYTE FROM CS5460
MOV   A,R7
JNB   ACC.7,I30     ;IF DRDY IS NOT ACTIVE

```

```

MOV  A,#00011000B  ;READ V-RMS REG. COMMAND
LCALL W_5460
LCALL R_5460      ;READ A BYTE FROM CS5460
MOV  79H,A
LCALL R_5460      ;READ A BYTE FROM CS5460
MOV  78H,A      ;SAVE 16BIT V-RMS DATA
LCALL R_5460      ;DUMMY READ A BYTE FROM CS5460
MOV  A,#00010110B  ;READ I-RMS REG. COMMAND
LCALL W_5460
LCALL R_5460      ;READ A BYTE FROM CS5460
MOV  77H,A
LCALL R_5460      ;READ A BYTE FROM CS5460
MOV  76H,A      ;SAVE 16BIT I-RMS DATA
LCALL R_5460      ;DUMMY READ A BYTE FROM CS5460
MOV  A,#01011110B  ;WRITE STATUS REG. COMMAND
LCALL W_5460
MOV  A,#80H
LCALL W_5460
MOV  A,#00H
LCALL W_5460
MOV  A,#00H      ;RESET DRDY INT.STATUS BIT
LCALL W_5460
SETB P0.4      ;DISABLE 5460-1
MOV  30H,#12      ;REINIT TRIAL COUNTER
MOV  31H,#250      ;RELOAD CS5460 TIMEOUT = 10 SEC
DJNZ 36H,I32      ;DISCARD 5 SAMPLES AFTER INITIALIZATION
MOV  36H,#01H      ;NOW DON'T DISCARD ANY SAMPLE
SETB 09H      ;FLAG THAT VRMS,IRMS DATA IS AVAILABLE
LCALL CAL_VI
LCALL CH_VRMS      ;CHECK V_RMS FOR UNDER VOLTAGE FAULT
LCALL CH_IRMS      ;COMPARE I_RMS WITH I/P CURRENT MAX. LIMIT
LCALL CAL_PWR      ;CALCULATE POWER FROM V_RMS & I_RMS
II32:
    SJMP I32
I30:
    DJNZ 31H,II30
    MOV  31H,#250      ;CS5460 TIMEOUT = 10 SEC
    SETB 0BH      ;FLAG THAT CS5460-1 IS FAULTY
II30:
    DJNZ 30H,I31      ;CHECK FOR 12 TRIALS (0.48SEC)
;RESET CS5460 SERIAL PORT
    CLR  P0.1
    NOP
    NOP
    NOP
    NOP
    NOP
    SETB P0.1      ;APPLY H/W RESET

```

```

    MOV    34H,#00H    ;ALSO CALL INIT5460-2
    SETB   P0.4        ;DISABLE 5460-1
    LJMP   I10          ;SKIP 5460-2 & ALL ITS CALCULATIONS
I31:
    SETB   P0.4        ;DISABLE 5460-1
I32:
;READING CS5460-2 STARTS...
    JB     0CH,III10    ;IF 5460-2 IS FAULTY THEN SKIP READING
    CLR    P0.5        ;SELECT 5460-2
    MOV    A,34H
    JNZ    NORST2      ;IF RESET IS NOT IN PROGRESS
    MOV    R2,#01H     ;CURRENT GAIN = 50
    LCALL  INIT5460
    MOV    37H,#06H    ;DISCARD 5 SAMPLES AFTER INITIALIZATION
    MOV    34H,#12     ;REINIT TRIAL COUNTER
    LJMP   I34
NORST2:
    MOV    A,#00011110B ;READ STATUS REG. COMMAND
    LCALL  W_5460
    LCALL  R_5460      ;DUMMY READ OF STATUS REGISTER
    MOV    R7,A
    LCALL  R_5460      ;DUMMY READ A BYTE FROM CS5460
    LCALL  R_5460      ;DUMMY READ A BYTE FROM CS5460
    MOV    A,R7
    JB     ACC.7,I33    ;IF DRDY IS ACTIVE
    DJNZ   35H,I34
    MOV    35H,#250     ;CS5460 TIMEOUT = 10 SEC
    SETB   0CH         ;FLAG THAT CS5460-2 IS FAULTY
    LCALL  RESTMR      ;RESET ON/OFF CYCLE TIMERS
    LCALL  HT_OFF      ;SW.OFF MELTER POWER
    LCALL  STP_TMR     ;STOP O/P ON/OFF CHECK TIMER
    LCALL  SW_OFF      ;SW. OFF ALARM RELAYS
I34:
    DJNZ   34H,I34     ;CHECK FOR 12 TRIALS (0.48SEC)
;RESET CS5460 SERIAL PORT
    CLR    P0.1
    NOP
    NOP
    NOP
    NOP
    NOP
    SETB   P0.1        ;APPLY H/W RESET
    MOV    30H,#00H    ;ALSO CALL INIT5460-1
I34:
    SETB   P0.5        ;DISABLE 5460-2
III10:
    LJMP   I10         ;SKIP ALL CALCULATIONS
I33:

```


;0.1SEC

```

MOV  A,#00011000B  ;READ V-RMS REG. COMMAND
LCALL W_5460
LCALL R_5460      ;READ A BYTE FROM CS5460
MOV  R7,A
LCALL R_5460      ;READ A BYTE FROM CS5460
MOV  R6,A        ;SAVE 16BIT C.J.TEMP. DATA
LCALL R_5460      ;DUMMY READ A BYTE FROM CS5460
MOV  A,#00010110B  ;READ I-RMS REG. COMMAND
LCALL W_5460
LCALL R_5460      ;READ A BYTE FROM CS5460
MOV  R2,A
LCALL R_5460      ;READ A BYTE FROM CS5460
MOV  R5,A
LCALL R_5460      ;READ A BYTE FROM CS5460
MOV  R4,A
MOV  A,#01011110B  ;WRITE STATUS REG. COMMAND
LCALL W_5460
MOV  A,#80H
LCALL W_5460
MOV  A,#00H
LCALL W_5460
MOV  A,#00H      ;RESET DRDY INT.STATUS BIT
LCALL W_5460
SETB P0.5        ;DISABLE 5460-2
MOV  34H,#12      ;REINIT TRIAL COUNTER
MOV  35H,#250     ;RELOAD CS5460 TIMEOUT = 10 SEC
DJNZ 37H,III10    ;DISCARD 5 SAMPLES AFTER INITIALIZATION
MOV  37H,#01H     ;NOW DON'T DISCARD ANY SAMPLE
LCALL HALF
LCALL HALF        ;CONVERT INTO 14BIT FOR COLD-JUNCTION TEMP.
MOV  7FH,R7
MOV  7EH,R6      ;SAVE 14BIT C.J.TEMP. DATA
LCALL SH_LFT
MOV  A,#00H
RLC  A
MOV  B,A
LCALL SH_LFT
MOV  A,B
RLC  A          ;CONVERT 24BITS TO 18BITS
MOV  R0,#80H
MOV  @R0,1DH
INC  R0
MOV  @R0,1AH
INC  R0
MOV  @R0,A      ;SAVE 18BITS DATA IN INT. RAM
SETB 00H        ;FLAG THAT ADC DATA IS AVAILABLE
LCALL C_CJTMP   ;CALCULATE COLD JUNCTION TEMP.

```

```

    LCALL  LINEAR      ;CALIBRATE & LINEARIZE TEMPERATURE
;
;ACC. SLOPE OF IGBT FIRING FREQUENCY AS PER SET O/P POWER (0-10KW -> 10SEC)
    JB     52H,I92      ;IF POWER IS ON THEN GO FOR ACC/DEC SLOPE
    CLR    EA
    MOV    0FH,#FDH
    MOV    0EH,#04H      ;COUNT FOR OFF CYCLE TIME FOR 1.67KHZ
    SETB   EA
    MOV    40H,#00H      ;MAKE PRESENT O/P FREQ. = 1.67KHZ
    SJMP   I99
I92:
    JNB    54H,I99      ;IF SLOPE IS NOT REQUIRED
    MOV    A,42H        ;TAKE ONLINE REQD. O/P POWER
    JZ     DECSL        ;IF POWER IS TO BE SWITCHED OFF
    DJNZ   5AH,I99
    MOV    5AH,#03H      ;COUNT FOR 0.12 SEC
;0.12SEC
    CJNE   A,3FH,I93    ;COMPARE WITH PRESENT O/P POWER
    SJMP   I95
I93:
    JC     DECSL
    MOV    A,40H
    CJNE   A,#100,I94
I94:
    JNC    I96
    INC    40H
    MOV    A,40H
    SJMP   I96
DECSL:
    DJNZ   40H,I95
    CLR    EX1          ;DISABLE INT1 (TO MONITOR OVER-CURRENT FAULT)
    CLR    52H          ;SW. OFF THE MELTER POWER
I95:
    MOV    A,40H
I96:
    ADD    A,A
    MOV    B,A
    MOV    DPTR,#CNTTBL
    MOVC   A,@A+DPTR     ;AS MAX. PWR IS 100 THIS WILL WORK OK
    CLR    EA
    MOV    0FH,A
    INC    DPTR
    MOV    A,B
    MOVC   A,@A+DPTR
    MOV    0EH,A        ;UPDATE COUNT FOR OFF CYCLE TIME
    SETB   EA
I99:
    POP    DPL

```

```

POP   DPH
POP   B
POP   A
POP   PSW
RETI

```

Table-7.4 Timer-2 Interrupt service subroutine listing

7.2.5 Interrupt on external falling edge (generated by Load Tuning Circuit of Figure 6-7)

INT0_ISS:

```

SETB  P2.2      ;SW.OFF GATE
RETI

```

Table-7.5 External Interrupt service subroutine listing

7.2.6 Serial port Interrupt

Here the serial transmission & reception is implemented using MODBUS protocols. It acts as the slave and responds to the commands received from ARM-7 board. It sends DC-Link power & linearized temperature to ARM-7 and receives the frequency of operation as well as frequency bursts parameters from ARM-7 board.

SRL_ISS:

```

JBC   RI,RECV
CLR   TI
DJNZ  69H,M51      ;69H = NO.OF CH. IN XMIT BUF. + 1
SETB  04H          ;FLAG THAT COMPLETE TRANSMISSION IS OVER
CLR   P1.7         ;CONVERT INTO RECV MODE
MOV   6DH,#04H     ;TIME BETWEEN SENDING & RECEIVING = 4MS
SETB  2CH          ;ENABLE RECEPTION AFTER ATLEAST 4MS
RETI

```

M51:

```

PUSH   PSW
CLR   RS1
SETB  RS0          ;R.B - 1
CLR   04H          ;TRANSMISSION IS GOING ON
MOV   R0,68H
MOV   SBUF,@R0
INC   68H
POP   PSW

```

RET2:

```

RETI

```

RECV:

```

JNB   REN,RET2     ;AS PER 89C51ED2-ERRATA WORK AROUND
PUSH   A
MOV   A,SBUF

```

```

    PUSH    PSW
    PUSH    B
    PUSH    DPH
    PUSH    DPL
    CLR     RS1
    SETB    RS0          ;R.B - 1
    MOV     6CH,#50      ;COUNT FOR 50MS
    SETB    2BH          ;START 50MS RECEPTION-TIMEOUT TIMER
    MOV     R0,67H
    MOV     @R0,A
    INC     67H
    MOV     A,67H
    CJNE    A,#B0H,RET01
    MOV     67H,#A8H
    LCALL   C_CRC_R      ;CALCULATE CRC FROM RECV.BUFFER(DPH,DPL)
    MOV     R0,#AEH
    MOV     A,@R0
    CJNE    A,DPL,M55
    INC     R0
    MOV     A,@R0
    CJNE    A,DPH,M55
    CLR     02H          ;IF NO CRC ERROR THEN RESET COMM. ERROR BIT
    SJMP    M56
M55:
    SETB    02H          ;IF CRC ERROR THEN SET COMM. ERROR BIT
RET01:
    LJMP    RET0
M56:
    MOV     DPTR,#00D8H
    MOVX    A,@DPTR      ;GET M/C ID. NO.
;    MOV     B,A
    MOV     B,#01H        ;FIX M/C ID. NO.=01
    MOV     R0,#A8H
    MOV     A,@R0
    JZ      M57           ;IF GLOBLE ADDRESS
    CJNE    A,B,RET00     ;CHECK 1ST DIGIT WITH M/C ID NO.
M57:
;CHECK & ANALYZE THE COMMAND
    MOV     R0,#A9H
    CJNE    @R0,#03H,M65  ;CHECK FOR READ HOLDING REGISTER CMD
    INC     R0
    CJNE    @R0,#00H,ADRER1 ;IF ADDR. DOESNT MATCH THEN SEND EXCPN RESP.
    INC     R0
    MOV     A,@R0
    CJNE    A,#12H,M58
M58:
    JNC     ADRER1        ;IF ADDR. DOESNT MATCH THEN SEND EXCPN RESP.
    ACALL   RDHREG        ;PROCESS READ HOLDING REGISTER COMMAND

```

AJMP RET0

M65:

```
CJNE  @R0,#06H,M72  ;CHECK FOR PRESET SINGLE REGISTER CMD
INC   R0
CJNE  @R0,#00H,ADRER1 ;IF ADDR. DOESNT MATCH THEN SEND EXCPN RESP.
INC   R0
MOV   A,@R0
CJNE  A,#12H,M67
```

M67:

```
JNC   ADRER1        ;IF ADDR. DOESNT MATCH THEN SEND EXCPN RESP.
ACALL PRSREG        ;PROCESS PRESET SINGLE REGISTER COMMAND
SJMP  RET0
```

ADRER:

```
MOV   R0,#A8H
MOV   A,@R0
JZ    RET0          ;DONT SEND RESPONSE FOR BROAD CAST MESSAGE
JNB   04H,$         ;WAIT TILL PREVIOUS TRANSMISSION IS OVER
MOV   R0,#99H
MOV   @R0,B
MOV   R0,#A9H
MOV   A,@R0        ;TAKE FUNCTION CODE
SETB  ACC.7
MOV   R0,#9AH
MOV   @R0,A
INC   R0
MOV   @R0,#02H     ;ILLEGAL DATA ADDRESS
SJMP  M79
```

VALER:

```
MOV   R0,#99H
MOV   @R0,B
MOV   R0,#A9H
MOV   A,@R0        ;TAKE FUNCTION CODE
SETB  ACC.7
MOV   R0,#9AH
MOV   @R0,A
INC   R0
MOV   @R0,#03H     ;ILLEGAL DATA VALUE
```

M79:

```
MOV   R2,#03H
LCALL CALCRC
INC   R0
MOV   @R0,DPL
INC   R0
MOV   @R0,DPH
MOV   69H,#06H     ;5 NO.OF CH. IN XMIT BUFFER
LCALL XMIT
```

RET0:

```
POP   DPL
```

POP	DPH
POP	B
POP	PSW
POP	A
RETI	

Table-7.6 Serial Port Interrupt service subroutine listing

7.3 High-level software for Embedded controller (ARM-7) Board

The Embedded controller (ARM-7) board has to perform following tasks.

1. Interfacing TFT display & touch screen.
2. To implement graphical user interface for displaying & modifying machine parameters.
3. Reading calibrated DC-Link power & linearized temperature from micro-controller board through MOD-BUS communication.
4. Implement PID on temperature & DC-Link power to determine frequency of operation & frequency bursts and send them to micro-controller board.
5. Implement Auto-tune for PID loop to optimize the control.

7.3.1 Graphical User Interface

As the monitoring quantities are Crucible temperature, DC-Link Voltage & DC-Link Current they are displayed as shown in Figure 7.1. From this figure it is also seen that three buttons are kept in the bottom part of GUI. The first START button is used to start the Melter power, the second STOP button is used to stop the Melter power and the third Right Arrow button is used to go to next page to change different parameters.

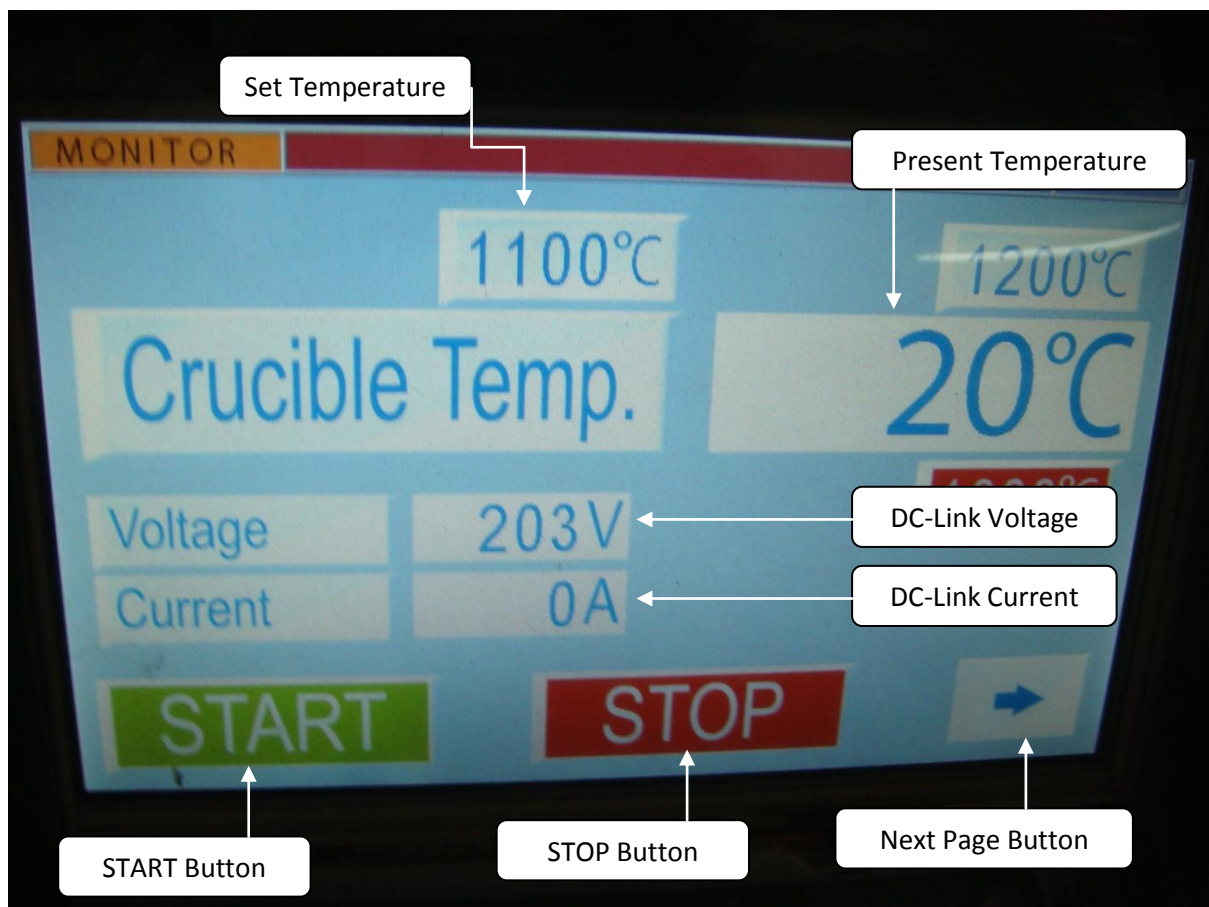


Figure 7-1 Monitor Page of GUI

By pressing the right arrow the parameter setup page as shown in Figure 7.2 is opened. Here it is possible to set required output power, Alarm set point, Unit of temperature displayed, date & time.

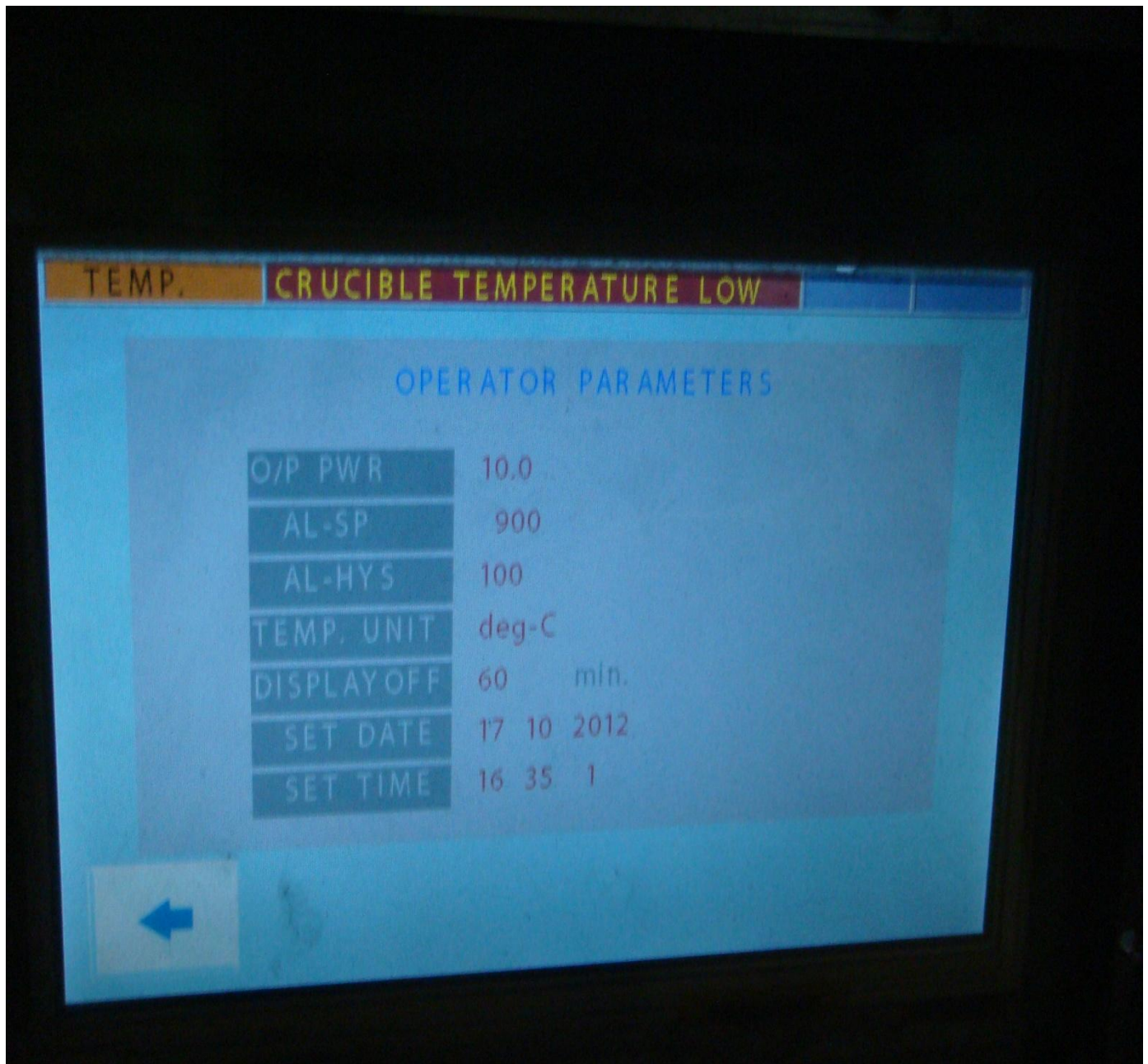


Figure 7-2 Setup Page of GUI

To implement the required tasks the whole software is divided into 5 parts. The program is written in C-Language using Keil-Real-View as shown in Figure 7-3.

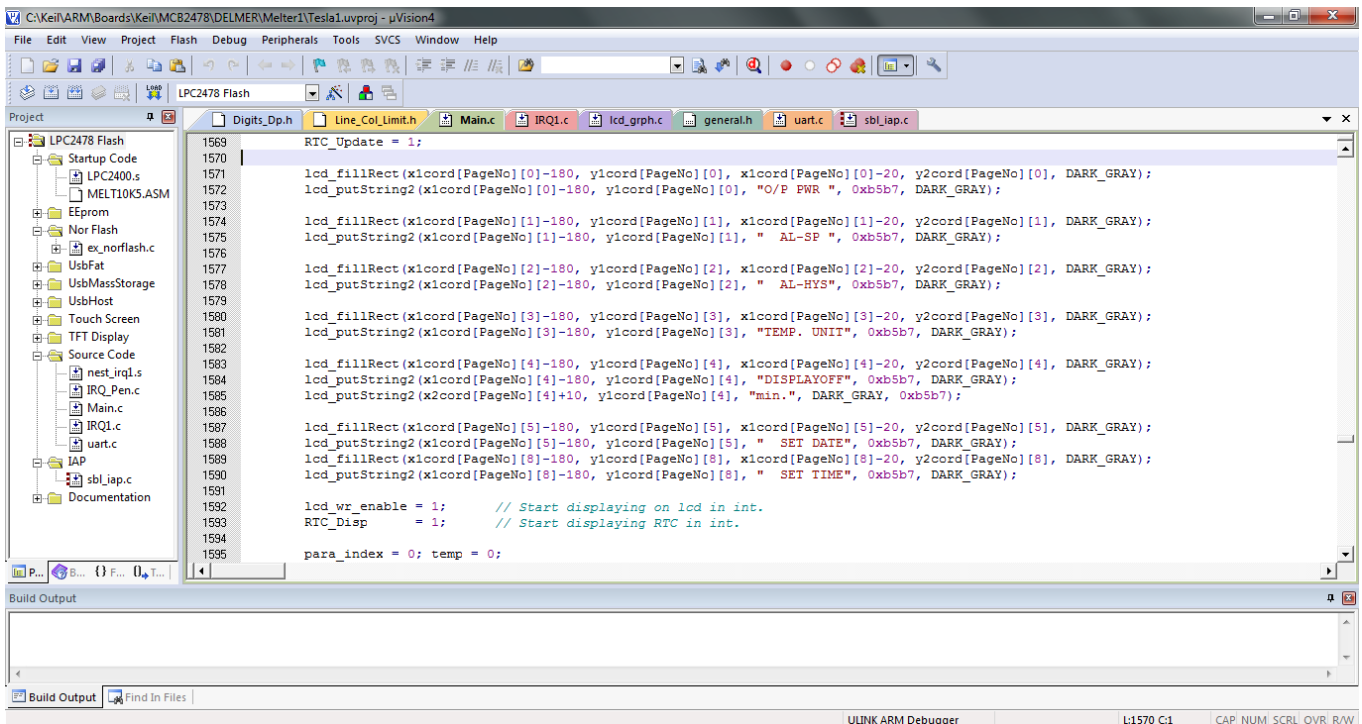


Figure 7-3 Snapshot of Melter Project in Keil Real View

As seen from Figure 7.3 the whole project is distributed in different groups.

1. **Startup Code:** Here stack configuration is defined and system as well as peripheral clocks are configured and started. It also initializes the external dynamic memory interface & external static memory interface.
2. **Eeprom:** Contains driver routines for AT24C512 Eeprom which is used to store non-volatile data.
3. **Nor Flash:** Contains driver routines for reading & writing from & to the nor flash which is used to store the still images (Initial title pages).
4. **Touch Screen:** Contains driver routines for interfacing TSC2046 touch screen controller as well as 4-point calibration routines for touch screen.
5. **TFT display:** Contains driver routines that initialize peripheral for TFT display. It also includes all low level graphics functions to create images.
6. **Source Code:** The most important part of the whole project is source code which includes MAIN.C, IRQ1.C & UART.C

7.3.2 Main program (MAIN.C)

Following is the listing of Main program which initializes the ports for input/output configuration. And then sets the modes of timers & serial port and enables interrupts.

Finally enters into a loop where it continuously display the Set & Present temperature as well as DC-Link voltage & current. It also checks for touch screen for any key pressed and sends commands to micro-controller card (through MOD-BUS) to start/stop the Melter power.

```

0933 int main(void)
0934 {
0935     tU8   ee_buf[128], temp;
0936     tS32  x, y, z = 0;
0937     tU32  i, j;
0938
0939     SCS |= 0x01; // High speed GPIO on Port 0 & 1
0940
0941     PCONP &= 0x00000B86; // Switch off power to unused blocks
0942
0943     // Set P0.29-P0.30 for Output (TO CHECK INTERRUPT TIMINGS)
0944     PINSEL1 &= 0xC3FFFFFF;
0945     FIO0DIR |= 0x60000000;
0946
0947     // Set for PORT-PWR-B Output, SET dir & output ON P2.25
0948     PINSEL5 &= 0xFFFF3FFFF;
0949     FIO2DIR |= 0x1<<25;
0950     FIO2CLR  = 0x1<<25; // KEEP USB-POWER OFF
0951
0952     // Set P0.4-P0.11 for Output ROW0-ROW7
0953     PINSEL0 &= 0xFF0000FF;
0954     FIO0DIR |= 0x00000FF0;
0955     FIO0CLR  = 0x00000FF0;
0956     // Set P1.6-P1.13 for Input COL0-COL7
0957     PINSEL2 &= 0xF0000FFF;
0958     FIO1DIR &= 0xFFFFC03F;
0959
0960     // Set P0.19-P0.22, P4.26 for Output DIG0-DIG4
0961     PINSEL1 &= 0xFFFFC03F;
0962     PINSEL9 &= 0xFFCFFFFFF;
0963     FIO0DIR |= 0x00780000;
0964     FIO0SET  = 0x00780000;
0965     FIO4DIR |= 0x04000000;
0966     FIO4SET  = 0x04000000;
0967
0968     // Set P2.10 for Input
0969     PINSEL4 &= 0xFFCFFFFFF;
0970     FIO2DIR &= ~(0x1<<10);
0971
0972     // Set P1.0-P1.5 for Output SEG0-SEG5
0973     PINSEL2 &= 0xFFFFF000;
0974     FIO1DIR |= 0x0000003F;
0975     FIO1SET  = 0x0000003F;
0976
0977     // Set P1.14,P1.15 for Digital Input DI1-DI2

```

Table-7.7 MAIN.C Part-1 listing

```

0987 /* Enable and setup timer-0 interrupt, start timer */
0988 PCONP |= (1 << 1); /* Enable power to TIM block */
0989 T0MR0 = 576000; /* 40msec at 14.4 MHz */
0990 T0MCR = 3; /* Interrupt and Reset on MRO */
0991 T0TCR = 1; /* Timer0 Enable */
0992 VICVectAddr4 = (unsigned long)T0_IRQHandler; /* Set Interrupt Vector */
0993 VICVectCntl4 = 15; /* Lowest Priority for Timer0 Interrupt */
0994 VICIntEnable = (1 << 4); /* Enable Timer0 Interrupt */
0995
0996 /* Enable and setup timer-1 interrupt, start timer */
0997 // PCONP |= (1 << 2); /* Enable power to TIM block */
0998 // T1MR0 = 7200; /* 1khz at 14.4 MHz */
0999 // T1MCR = 3; /* Interrupt and Reset on MRO */
1000 // T1TCR = 1; /* Timer1 Enable */
1001 // VICVectAddr5 = (unsigned long)T1_IRQHandler; /* Set Interrupt Vector */
1002 // VICVectCntl5 = 0; /* Highest Priority than any other Interrupt */
1003 // VICIntEnable = (1 << 5); /* Enable Timer1 Interrupt */
1004
1005 /* Enable and setup timer-2 interrupt, start timer */
1006 PCONP |= (1 << 22); /* Enable power to TIM block */
1007 T2MR0 = 28800; /* 2msec at 14.4 MHz */
1008 T2MCR = 3; /* Interrupt and Reset on MRO */
1009 T2TCR = 1; /* Timer2 Enable */
1010 // VICIntSelect = (1 << 26); /* Timer2 as FIQ Interrupt */
1011 VICVectAddr26 = (unsigned long)T2_IRQHandler; /* Set Interrupt Vector */
1012 VICVectCntl26 = 14; /* More Priority than Timer0 Interrupt */
1013 VICIntEnable = (1 << 26); /* Enable Timer2 Interrupt */
1014
1015 //initialize LCD
1016 lcdInit(&ftt_para);
1017 lcdTurnOn();
1018
1019 I2C_Init();
1020
1021 touch_init();
1022
1023 UARTInit(0); /* Init & Enable UART-0 */
1024 // UARTInit(3); /* Init & Enable UART-3 */
1025
1026 lcdTurnOn();
1027 lcdSetBacklight(100);
1028
1029 Startup = 0;
1030 TouchIntChk = 1;
1031

```

Table-7.8 MAIN.C Part-2 listing

```

1074 case MONITOR1:
1075     RTC_Disp = 0; /* Stop displaying RTC in int. */
1076     lcd_wr_enable = 0; /* Stop displaying on lcd in int. */
1077
1078     load_picture1(0,0,800,480);
1079     save_picture2(0,0,800,480,MON2_NORADR); /* Save MONITOR2 picture into 2nd temp. memory */
1080
1081     P_Fv=P_Sp=P_ALSp=P_ALHys=P_I_rms=P_V_rms=P_Unit=-1000; /* To display fresh value in int. */
1082     P_PWRStatus=P_IGBTONOFF=P_Warning18=P_Warning19=0xff;
1083
1084     lcd_wr_enable = 1; /* Start displaying on lcd in int. */
1085     RTC_Disp = 1; /* Start displaying RTC in int. */
1086
1087     para_index = temp = 0;
1088     while(1)
1089     {
1090         if (temp == 1)
1091             SaveNORFLASH1(); /* Save receipt data in Nor-Flash */
1092
1093         Var[MONITOR1][0] = 0;
1094         if ((temp=KBD_Loop()) == 0)
1095             break;
1096         else if (para_index == 2)
1097         {
1098             // if (ERStatus==0)
1099             // {
1100                 while(WrCmd0); /* Wait untill previous write command is over */
1101                 Pid_ID = 0x01;
1102                 WrAddr0 = 0x000f; /* Address of Operation Mode Byte */
1103                 WrData0 = 0x01; /* Sv.On Melter Power */
1104                 WrCmd0 = 1; /* Write specified variable into PID-card */
1105             // }
1106             while(UpYet);
1107         }
1108         else if (para_index == 3)
1109         {
1110             while(WrCmd0); /* Wait untill previous write command is over */
1111             Pid_ID = 0x01;
1112             WrAddr0 = 0x000f; /* Address of Operation Mode Byte */
1113             WrData0 = 0x00; /* Sv.Off Melter Power */
1114             WrCmd0 = 1; /* Write specified variable into PID-card */
1115             while(UpYet);
1116         }
1117     }

```

Table-7.9 MAIN.C Part-3 listing

7.3.3 Interrupt Routines (IRQ1.C)

The temperature of crucible is to be controlled through PID control loop, which is implemented as follows:

Discrete-time PID Algorithm

In Figure 7-4 a schematic of a system with a *PID* controller is shown. The *PID* controller compares the measured process value (crucible temperature) with a reference set point temperature. The difference or error is then processed to calculate a frequency burst.

This frequency burst will try to adjust the measured process value back to the desired set point.

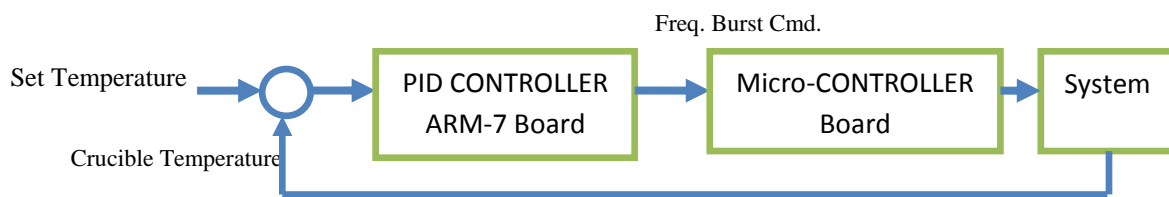


Figure 7-4 Closed Loop System with *PID* controller

Unlike simple control algorithms, the *PID* controller is capable of manipulating the process inputs based on the history and rate of change of the signal. This gives a more accurate and stable control method. The basic idea is that the controller reads the system state by a sensor. Then it subtracts the measurement from a desired reference to generate the error value. The error will be managed in three ways, to handle the present, through the proportional term, recover from the past, using the integral term, and to anticipate the future, through the derivate term.

Figure 7-5 shows the *PID* controller schematics, where K_p , T_i , and T_d denote the constants of the proportional, integral, and derivative terms respectively.

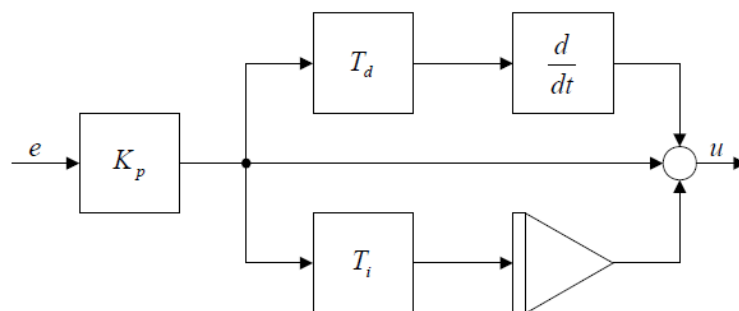


Figure 7.5 *PID* controller schematic

Table 7.10 shows how this algorithm is coded in C.

```
int Pid_Algorithm(int sv, int pv)
{
    int temp, retval, Error, p_term, i_term, d_term;
    // Proportionate
    Error = sv - pv;
    if(Error > Max_Error)
        p_term = MAX_INT;
    else if(Error < -Max_Error)
        p_term = -MAX_INT;
    else
        p_term = (Error * 256000)/P_Band ;
    // Integral
    temp = PID_sum_error + Error;
    if(temp > Max_Sum_Error)
    {
        PID_sum_error = Max_Sum_Error;
        i_term = MAX_INT;
    }
    else if(temp < -Max_Sum_Error)
    {
        PID_sum_error = -Max_Sum_Error;
        i_term = -MAX_INT;
    }
    else
    {
        PID_sum_error = temp;
        i_term = (((PID_sum_error*2000)/I_Time)*128)/P_Band;
    }
    // Derivative
    d_term = (((PID_Last_pv-pv)*2000*D_Time)/P_Band)*128;
    if (d_term > MAX_INT)
        d_term = MAX_INT;
    else if (d_term < -MAX_INT)
        d_term = -MAX_INT;
    PID_Last_pv = pv;

    retval = (p_term+i_term+d_term)/128;

    if(retval > MAX_INT)
        retval = MAX_INT;
    else if(retval < -MAX_INT)
        retval = -MAX_INT;

    return (retval);
}
```

Table-7.10 C code for PID algorithm

Autotuning Implementation

To transform the Ziegler-Nichols Frequency Domain (ZNFD) method to C code, the components needed are a relay, and a function to read the magnitude and frequency of oscillation. As the output of PID required to be generated is frequency bursts it can be considered as the relay operation. Following is the C code for functions to detect a and T_u and compute magnitude and frequency of oscillation, which are then utilized to compute K_p , T_i & T_d .

```

532
533
534
535 /****** Global Variables *****/
536 /*These two variables are what we want to find */
537 double p; // magnitude of P
538 double w; // frequency of P
539 double tu; // oscillation period (w = 1/tu)
540 double d; // relay amplitude. This is constant for a particular relay
541 double a; // peak process output amplitude.
542 double yold; // keep previous process output
543 double ts; //sampling period
544 int i=0; // a counter to keep the number of iterations between two peaks
545 /******
546 void detect_a_tu(void) / this must be a timer ISR running each ts seconds
547 {
548     double y; // use to keep process output each sampling period
549     y = read_input( ); // read input from specified channel
550     if (y>a) a = y; // compare new input with a, if greater keep it as new a
551     if (yold<0 && y>=0)
552     { // detect zero crossing
553         tu=i*ts;
554         i=0;
555     }
556     yold=y;
557     i++;
558 }
559 void compute_pw(void) // run this after we get values for a and tu
560 {
561     double Na;
562     Na = (4*d)/(pi*a);
563     p = -1/Na; // gain of P(jw) at point of intersection
564     w = 2*pi/tu; // frequency in rad/s
565 }

```

Table-7.11 C code for computing a & T_u for Autotuning.

7.3.4 Serial Port Routines (UART.C)

The MOD-BUS communication & reading & writing of machine parameters from & to micro-controller board is carried out in this section as listed in Table 7.12.

```

if (RdAddr0 == 0x0000)
{
    Sp = (int)((UART0Buffer[3]<<8) + UART0Buffer[4]);
    ALSp = (int)((UART0Buffer[5]<<8) + UART0Buffer[6]);
    ALHys = (int) UART0Buffer[8];
}
else if (RdAddr0 == 0x0003)
{
    Var[PIDPAGE][1] = (int)((UART0Buffer[3]<<8) + UART0Buffer[4]);
    Var[PIDPAGE][2] = (int)((UART0Buffer[5]<<8) + UART0Buffer[6]);
    Var[PIDPAGE][3] = (int)((UART0Buffer[7]<<8) + UART0Buffer[8]);
    ReadPBITID = 0;
}
else
{
    if (UART0Buffer[4] != 3)
        AutoTuneON = 0;
}
else if (UART0Buffer[1] == 4)
{
    switch(RdAddr0)
    {
        case 0x0003:
            OPStatus = UART0Buffer[3];
            ERStatus = UART0Buffer[4];
            break;

        case 0x0004:
            ALStatus = UART0Buffer[4];
            break;

        default:
            if (UART0Buffer[3]&0x80)
                Pv = 0;
            else
                Pv = (int)((UART0Buffer[3]<<8) + UART0Buffer[4]);
            if (UART0Buffer[5]&0x80)
                I_rms=0;
            else
                I_rms = (int)((UART0Buffer[5]<<8) + UART0Buffer[6]);
            if (UART0Buffer[7]&0x80)
                V_rms=0;
            else
                V_rms = (int)((UART0Buffer[7]<<8) + UART0Buffer[8]);
    }
}

```

Table-7.12 UART.C subroutines listing

7.4 Summary

In this chapter the software implementation for micro-controller board as well as ARM-7 board is described. The micro-controller board software automatically tunes the gate firing of IGBT according to the changes in load inductance. ARM-7 board software takes care of graphical user interface to view/insert machine parameters. The PID & Autotuning is explained with respect to ARM-7 controller.

Chapter 8

EXPERIMENTAL VERIFICATION

8.1 Introduction

The objective of the conducted experiment is to assess the versatility of Induction melting technology using Quasi-Resonant converter which melts gold/silver/copper material.

In this chapter first the proposed modified quasi-resonant converter system has been described and the experimental parameter has been defined and then follows the experimental results.

8.2 Experimental System

Induction melting takes power from the 3phase mains, rectifies it & converts into dc. The power components are designed in such a way that DC-Link voltage is 200v. This is then converted into high frequency which is used to generate heat in conducting material.

The Figure 8-1 shows the micro-controller board duly assembled. The LCD placed on this board is just to display the parameters locally.

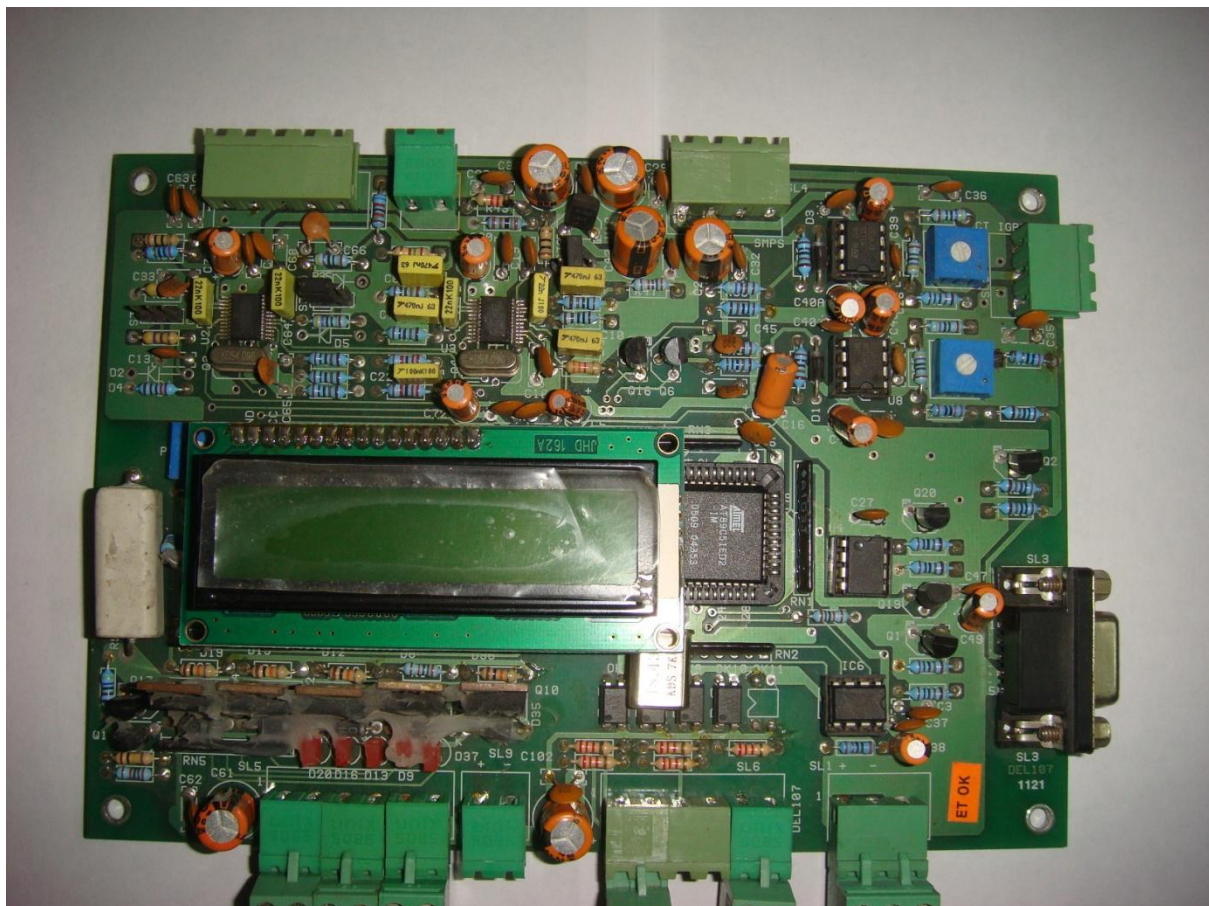


Figure 8-1 Micro-controller (AT89C51ED2) Board

The micro-controller board is divided into following 3 sections.

1. The section generating IGBT gate pulses according to the frequency burst commands received from ARM-7 board is shown in Figure 8-2. The output pulses are converted into 15v pulses to avoid noise into cable layout from this board to IGBT driver board which is placed near IGBT as shown in Figure 8-3.

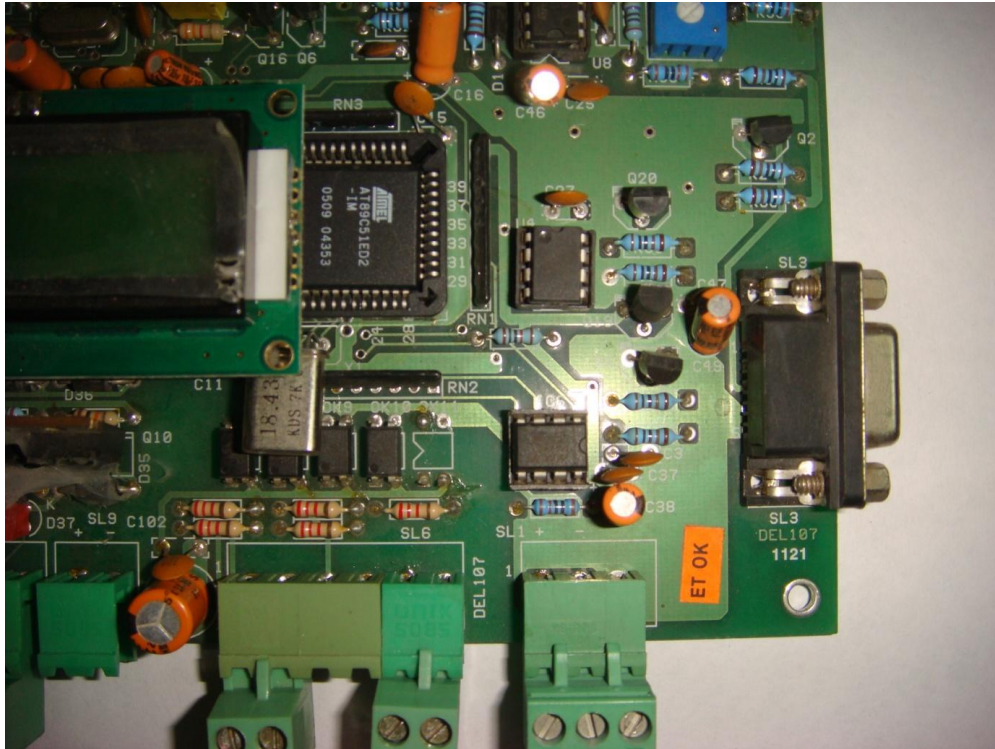


Figure 8-2 Gate firing section of Micro-controller Board

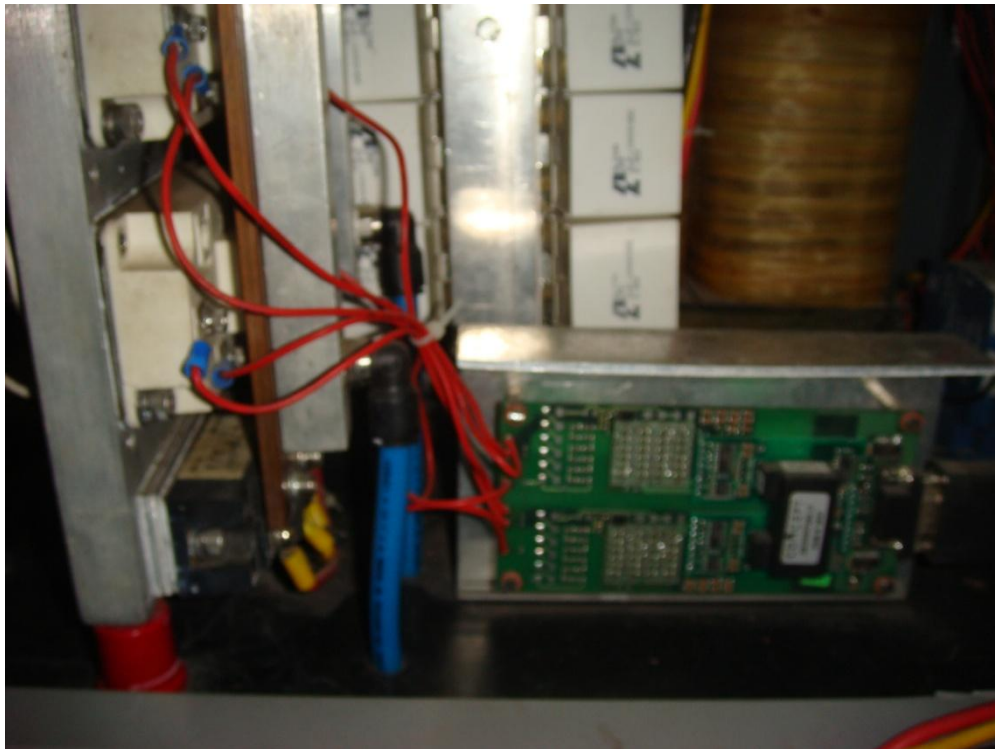


Figure 8-3 IGBT driver board placed near IGBT assy.

- This section tunes on duty of the IGBT gate pulses according to the load inductance changes.

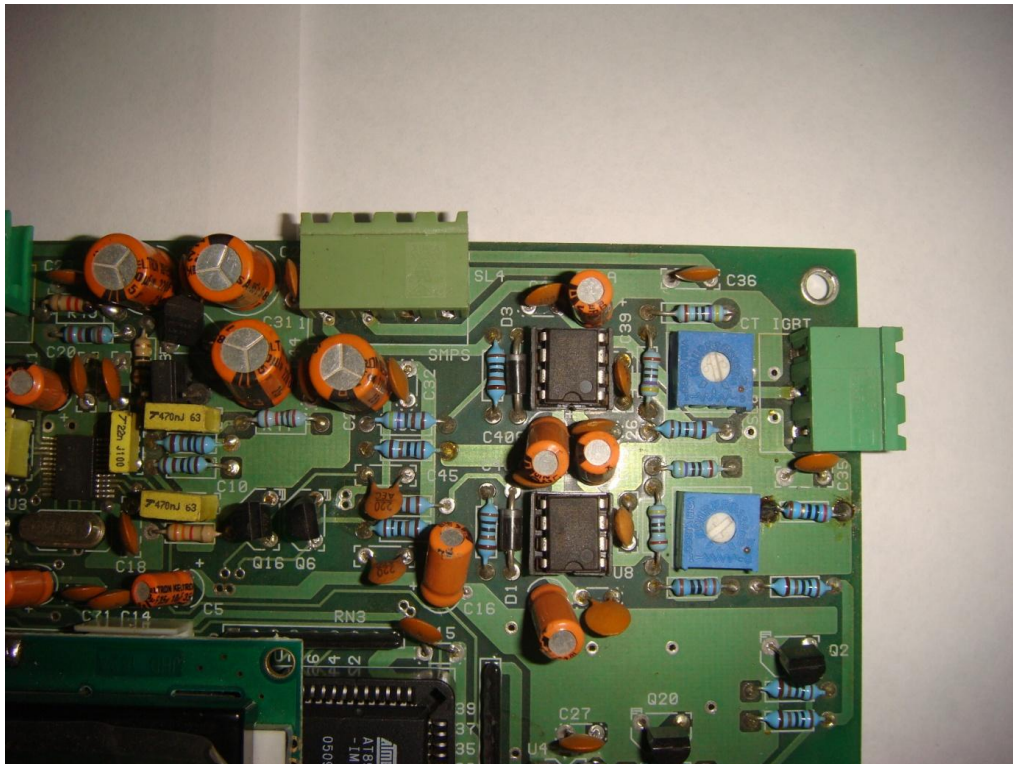


Figure 8-4 Comparator section of Micro-controller Board

- This section converts thermocouple output into digital value of temperature using CS5460 IC. Through another CS5460 IC it converts the DC-Link voltage & current into their RMS values.

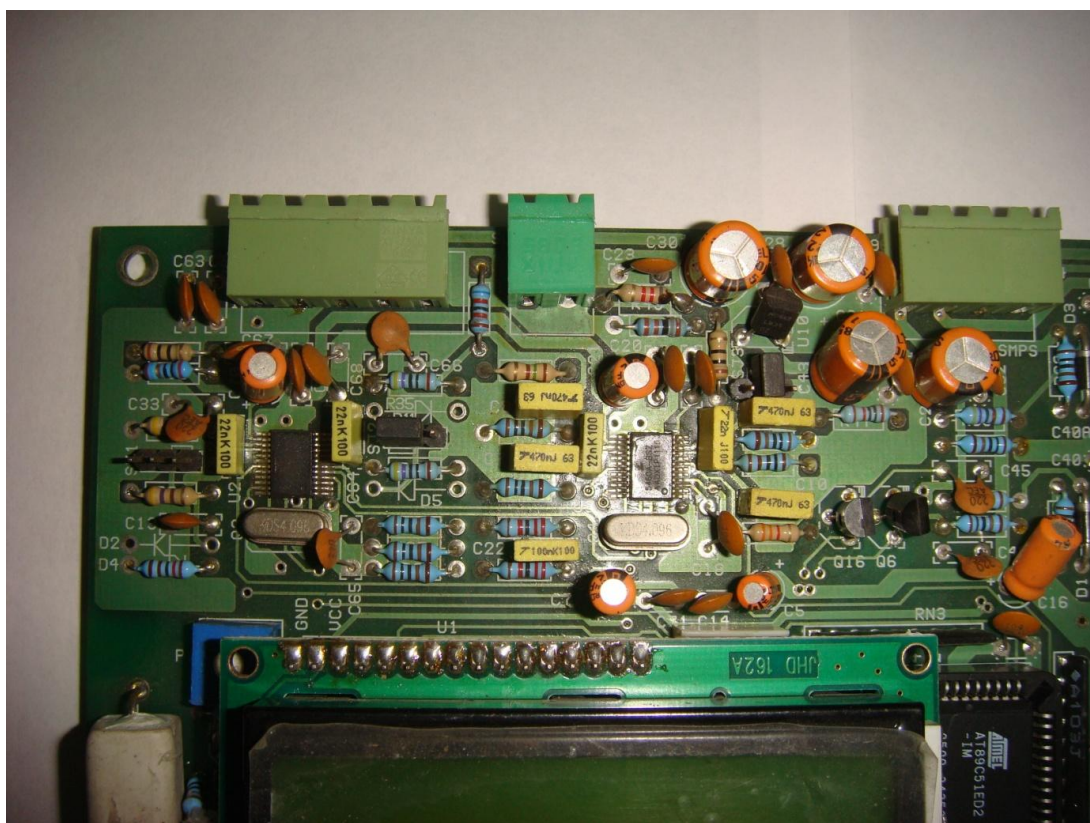


Figure 8-5 CS5460(ADC) section of Micro-controller Board

The Figure 8-6 shows the ARM-7 board duly assembled. This board is mounted on the back side of TFT & touch screen. It is connected to micro-controller board through RS485 cable.

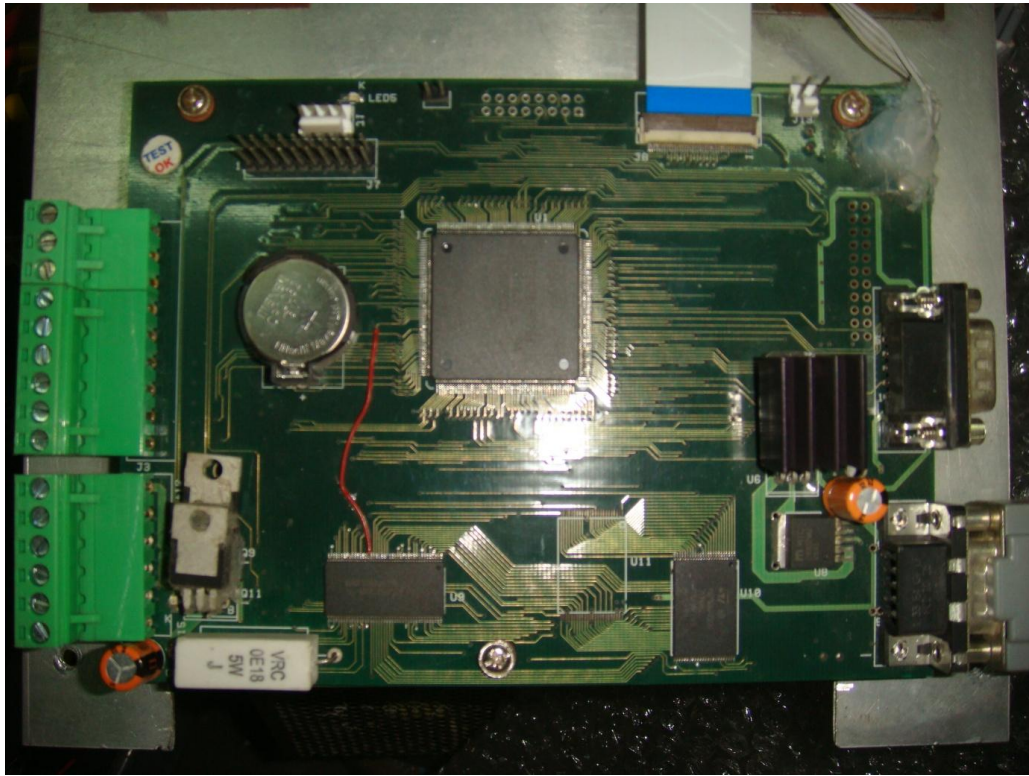


Figure 8-6 ARM-7 controller Board

The schematic of the gate drive board with 2SC0435T driver (Figure 6-22) is converted into pcb form as shown in Figure 8-7.

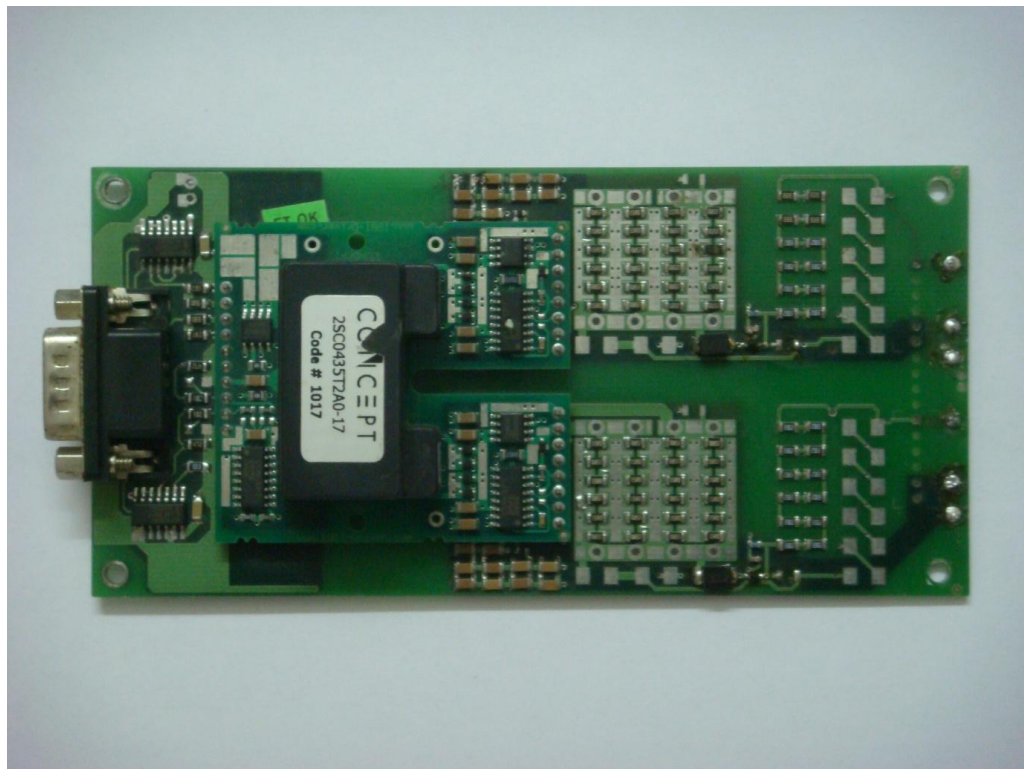


Figure 8-7 Gate drive board with 2SC0435T driver

8.3 Protection Considerations

The protection against under voltage is required, as when the voltage is less (if any one line of input 3phase supply is open creating single phasing) the converter starts malfunctioning. Thus the sensed DC-Link voltage is compared with the lower threshold and the Melter power is switched off when a under voltage condition is sensed. The over current protection is provided in three different ways.

1. Vce monitoring in IGBT gate driver circuit
2. Protection against over current in Tank circuit is accomplished by micro-controller card using comparator circuit.
3. Protection against over current in DC-Link is achieved by micro-controller card through software.

The temperature of coil as well as switching devices is controlled by flowing chilled water through them. Any leakage or breakage in the cooling system is detected by thermostat mounted on coil as well as heat sink of IGBT. The micro-controller card senses the o/p of thermostat & switches off the Melter power in case of over temperature.

8.4 Experimental Results

The experiment is carried out with the pieces of copper placed in crucible as shown in Figure 8-8.

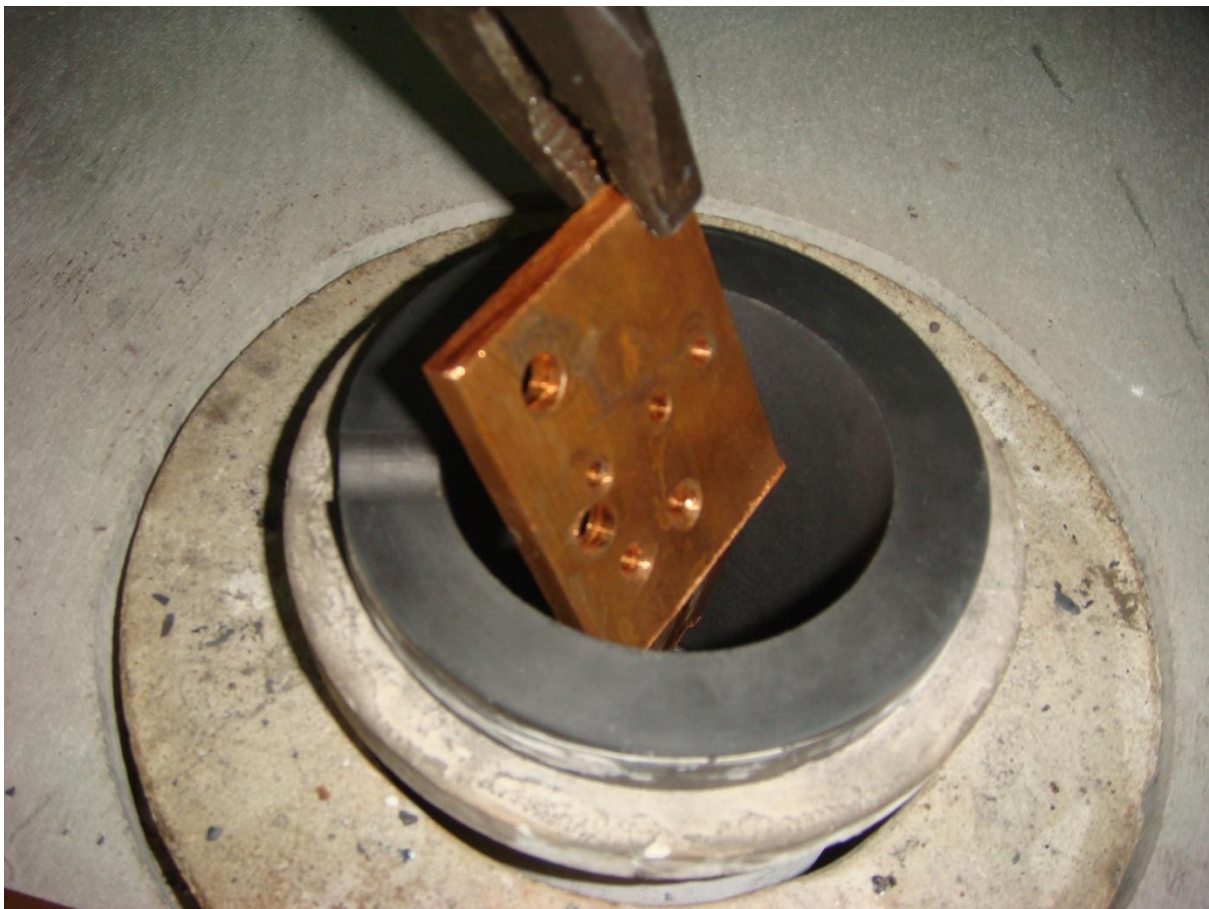


Figure 8-8 Copper work pieces kept into crucible

Experimental circuit parameters are given in Table 8.1. The Figure 8-9 shows the waveform of IGBT gate pulses & the tank circuit current. It is clear that the tank current is pure sinusoidal. The Figure 8-10 and Figure 8-11 show the waveforms of IGBT gate pulses & the DC-Link current and DC-Link voltage. The waveforms are directly stored on pen-drive by digital storage oscilloscope.

Figure 8-12 & Figure 8-13 shows the waveform of DC-Link current & the power factor meter reading. The experimental sample result is shown in Figure 8-14.

WEIGHT OF WORK PIECE	2 KG	4 KG
V _{ab}	410 V	411 V
I _{ab}	13.4 A	6.2 A
V _{DC-LINK}	177 V	185 V
I _{DC-LINK}	46 A	24 A
Power Factor	0.999	0.999

Table 8.1 Experimental Verification Summaries

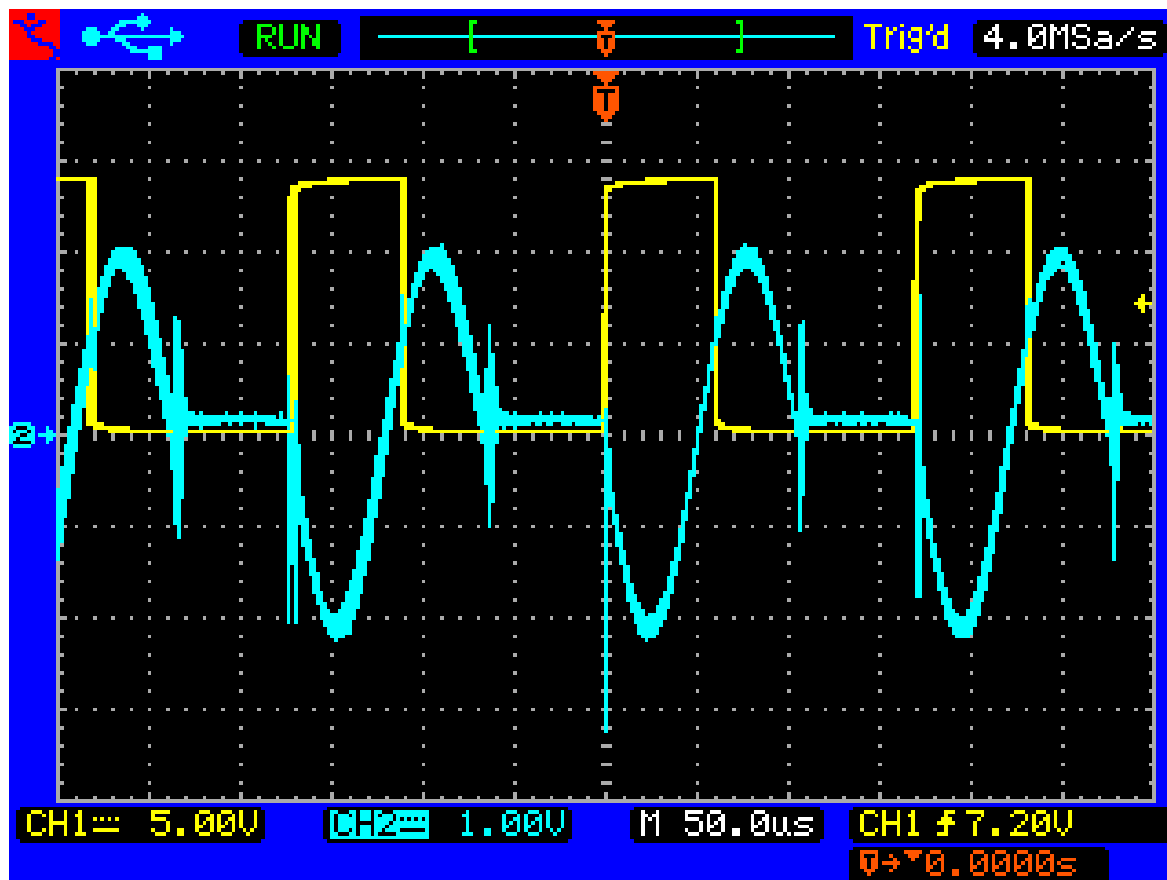


Figure 8-9 Gate Pulse v/s Tank current

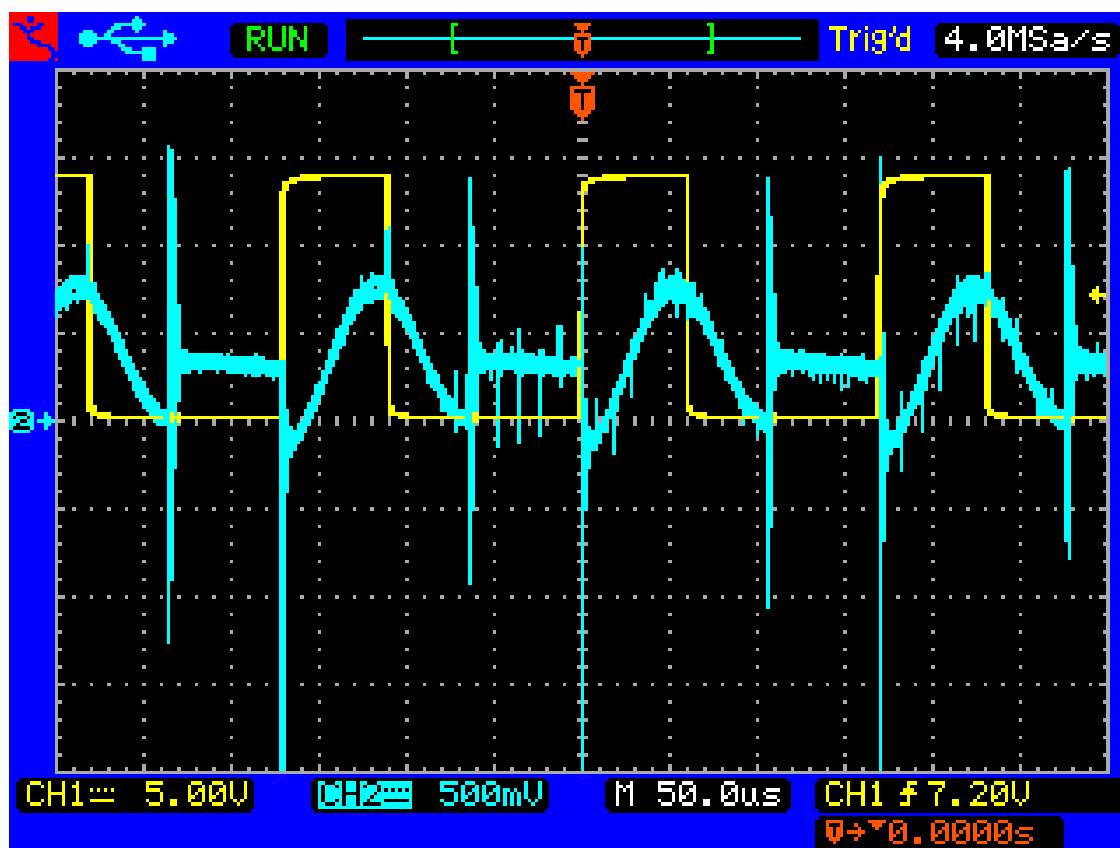


Figure 8-10 Gate Pulse v/s DC-Link current

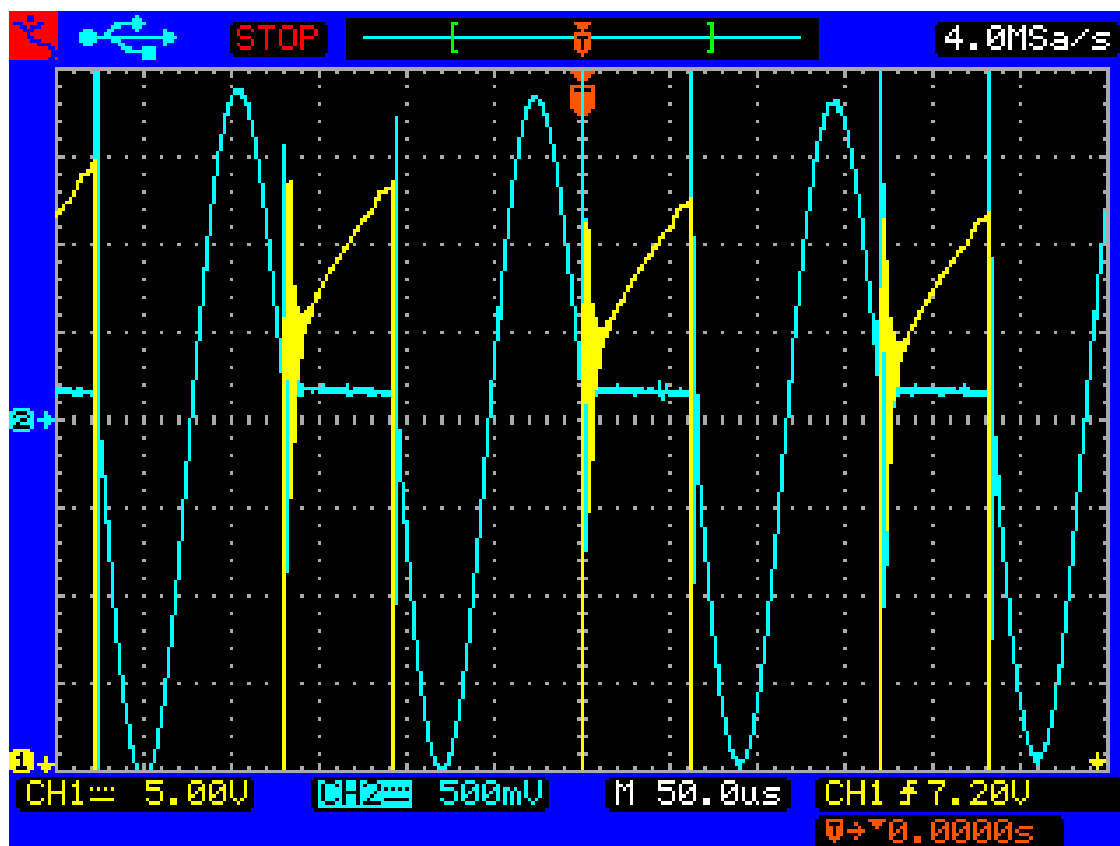


Figure 8-11 Gate Pulse v/s DC-Link voltage

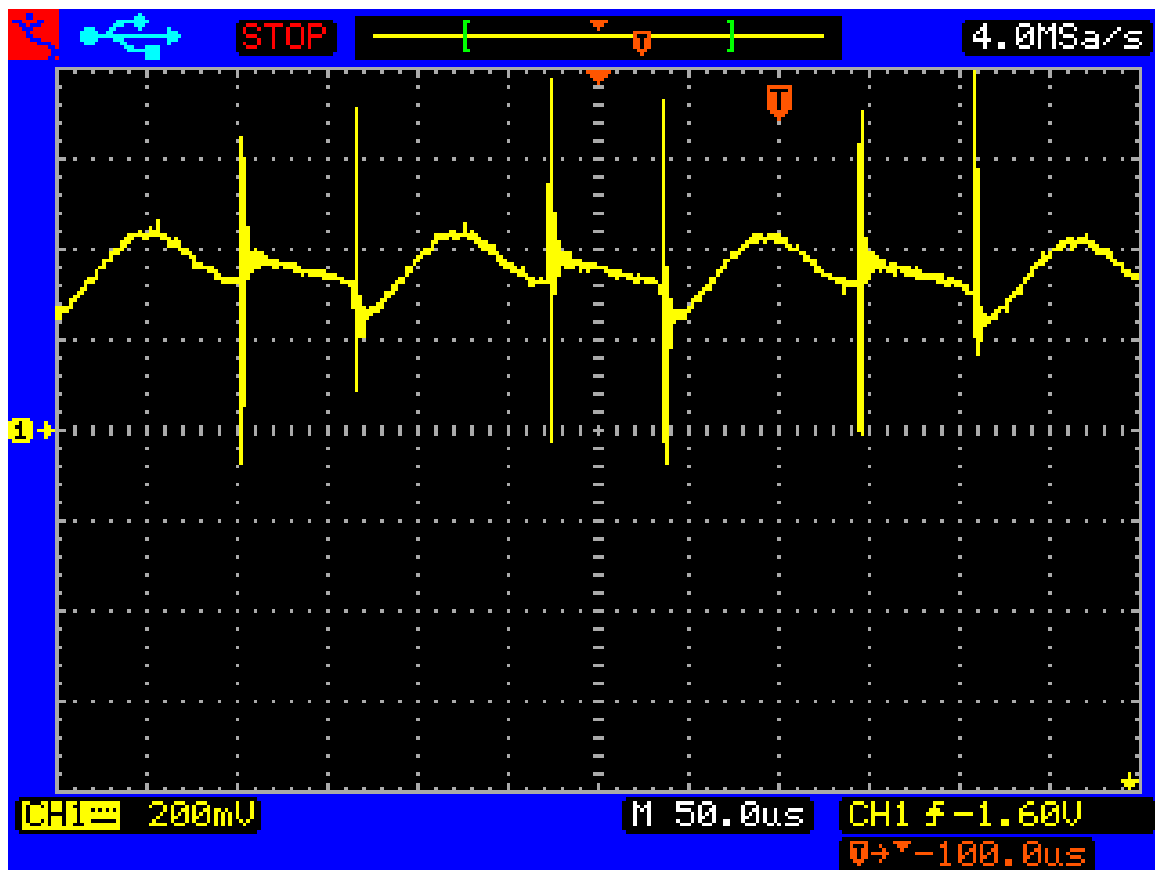


Figure 8-12 DC-Link Current

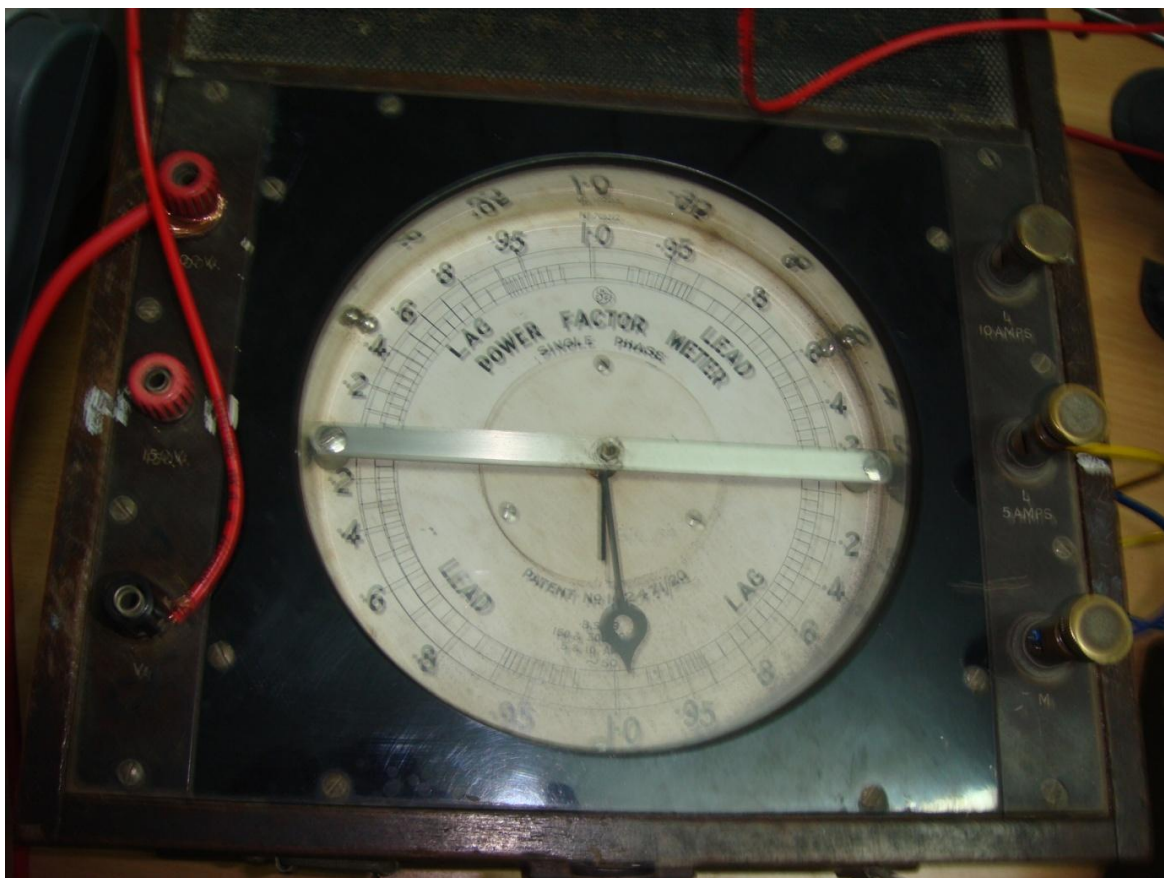


Figure 8-13 Power Factor Reading 0.999

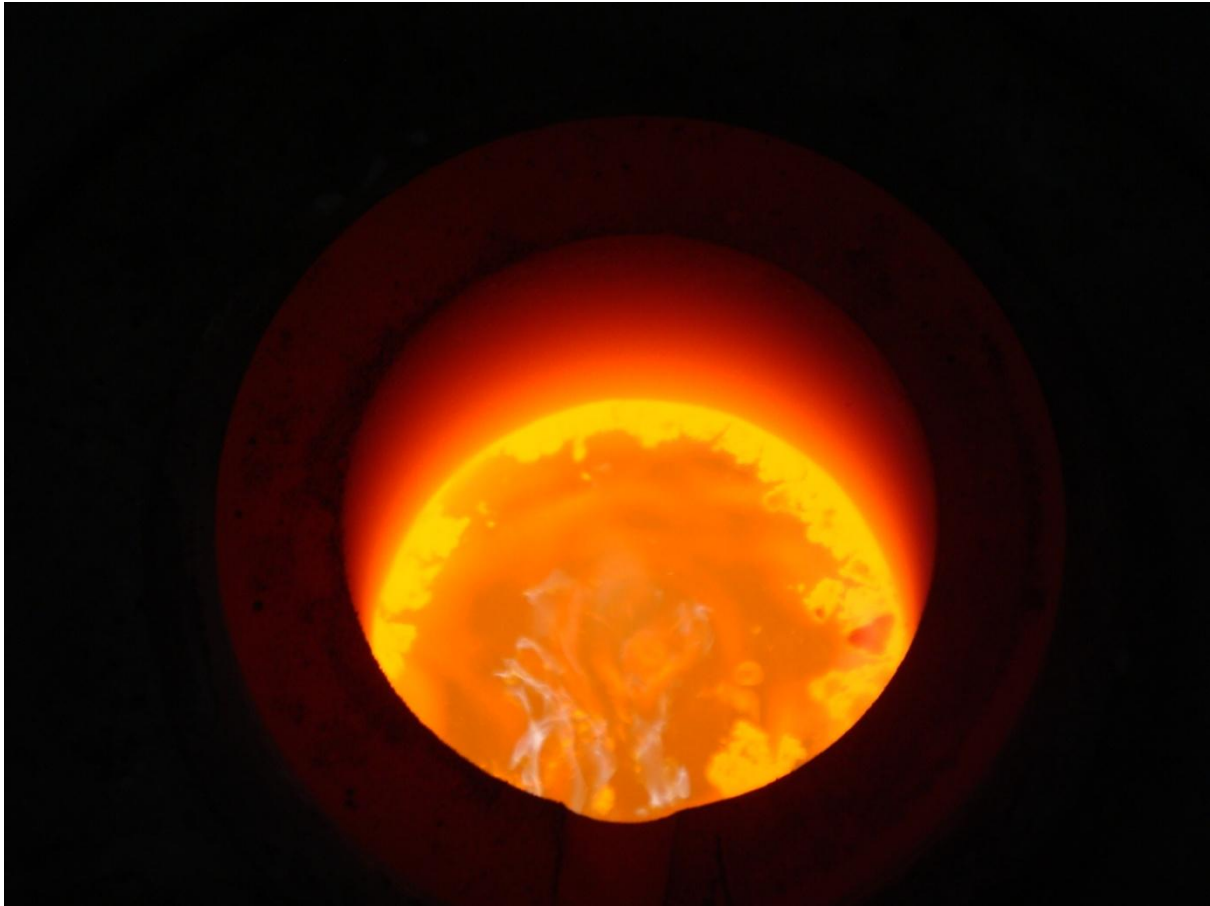


Figure 8-14 Melted work pieces

8.5 Summary

This chapter has described an induction melting experimental control structure and following are the findings:

1. The experiment demonstrated the ability of controlling temperature of crucible at desired set power.
2. As work pieces are added the inductance changes & the converter automatically tunes itself to match the resonance frequency.
3. The frequency of operation can be valued by changing the set value of power.
4. The switching strategy minimizes the distortion in input current which improves power factor.
5. It also provides excellent output performance optimized efficiency and high reliability compared to similar conventional converters.
6. It leads to several advantages such as nearly unity power factor without any reactive elements, symmetric loading from utility point of view and almost uniform temperature. It is proved by experimental setup.

Chapter 9

CONCLUSION & FUTURE SCOPE

This chapter describes the conclusions about the results and remarks about it. Also some future scope suggested here to extend the project for further real time implementations.

9.1 General

This thesis has addressed the modified Quasi-resonant converter system, simulation results and experimental verification for induction melting system. The main contribution of the thesis includes following:

- Principle of induction melting is explained & different power topologies & different tuning methods for pid are elaborated in chapter 2.
- Design of a quasi-resonant converter is described in chapter 3. Simulation study of the quasi-resonant convert is carried out & waveforms are generated.
- Chapter 4 proposes modified quasi-resonant converter and gives detailed study of the same. Simulation study is carried out.
- Development of power circuit for quasi-resonant converter is included in chapter 5.
- The micro-controller board, ARM-7 controller board, driver board developments are presented in chapter 6 & 7.
- The chapter 8 describes an induction melting experimental control structure.

The objective of this concluding chapter is to highlight the main finding of the work carried out in this thesis and provide suggestions for further research work in this area.

Some of the main findings are given below.

9.2 Summary of Important Findings

Chapter 2 describes induction melting principle and different power topologies. The main finding of this chapter reveals following:

1. As a resonant converter provides most of the energy conversion efficiency in a power system by minimizing switching loss, they are best suited for DC-AC converters as compared to PWM converters.
2. Due to skin effect the high frequency switching creates heat on the surface of the load, hence medium switching frequency is used for melting applications.
3. Zero-voltage switching refers to eliminating the turn-on switching loss by having the voltage of the switching circuit set to zero right before the circuit is turned on.

4. Zero-current switching is to avoid the turn-off switching loss by allowing no current to flow through the circuit right before turning it.
5. Different Tuning methods for PID loop are surveyed. It is found that the Ziegler and Nichols method for tuning is simple, accurate and can be easily implemented in digital PID control.

In chapter 3 a quasi-resonant converter has been proposed, to reduce total switching loss. The design and implementations of a quasi-resonant converter for melting at a high temperature has been carried out.

The main findings of this chapter reveals following:

1. The half-bridge series resonant converter is having stable switching & low cost. As the voltage of the circuit is limited to the level of the input voltage, the switching circuit can have low internal pressure, which helps reduce the cost.
2. As the half-bridge method requires two switching circuits, the overall working process becomes more complicated and the size of heat sink and PCB should be also bigger. In addition, the gate operating circuits must be insulated.
3. As compared to half-bridge series resonant converter the quasi-resonant converter needs only one switching circuit inside. This enables a relatively smaller design for the heat sink and PCB, making the working process far simpler. Another strong point is the fact that the system ground can be shared.
4. In case of quasi-resonant converter the high internal pressure of the switching circuit, caused by the resonant voltage administered to both sides of the circuit, pushes the cost of the circuit higher. But as mentioned earlier, technological development in high frequency semiconductor switching devices has lead to an innovation in terms of low price, high performance, and reliability. Quasi-resonant converters are now more generally used because of the smaller heat sink and PCB size and simpler operation process.

In chapter 4 a modified quasi-resonant converter is proposed to eliminate large amount of filter capacitors. It also includes the simulation study of control strategy using MATLAB/SIMULINK.

The main findings of this chapter reveals following:

1. The modified quasi resonant converter is low cost as the filter capacitor is eliminated as compared to quasi resonant converter. This new scheme also requires one switching device which maintains the advantage of a relatively smaller design for the heat sink and PCB.
2. This new scheme is more advantageous as the positive & negative current flows through the same resonant path resulting into a pure sine wave of current.
3. This system has advantages like low switching losses, reduced stress and increased power density.

4. The variation in power can easily be obtained by changing the operating frequency of IGBT gate pulses.
5. The simulation results are in line with the predictions.

Chapter 5 discusses Design, Analysis and Simulation of power circuit for the proposed topology. The chapter includes the implementation of Power circuit.

The calculations are shown & how to prepare inductor & capacitor are explained. The IGBT's are introduced & their types are explained. The new generation Trench/Fieldstop IGBT4 is selected and it is described how to connect two IGBT's in parallel. The need and details of RCD snubber is explained.

Chapter 6 describes the development of the control circuit for quasi-resonant converter. It also contains the development and design of main generator card with new generation SCALE-2 IGBT-driver circuits.

The Micro-controller Board & Arm-7 controller board are developed and tested.

In comparison with other driving methods, active clamping allows enhanced utilization of the IGBT modules during normal operation by increasing the switching speed and therefore reducing switching losses. The overvoltage at fault-current turn-off is also managed by active clamping.

Chapter 7 discusses the software implementation for micro-controller board & ARM-7 board. As well as development and design of MMI with TFT, touch screen and all modern facilities are presented.

The micro-controller board software automatically tunes the gate firing of IGBT according to the changes in load inductance. ARM-7 board software takes care of graphical user interface to view/insert machine parameters. The PID & Autotuning is explained with respect to ARM-7 controller.

Chapter 8 deals with the experimental verification of proposed induction Melter. The auto-tuning algorithm, the temperature accuracy and efficiency is verified.

This chapter has described an induction melting experimental control structure and following are the findings:

1. The experiment demonstrated the ability of controlling temperature of crucible at desired set power.
2. As work pieces are added the inductance changes & the converter automatically tunes itself to match the resonance frequency.
3. The frequency of operation can be valued by changing the set value of power.
4. The switching strategy minimizes the distortion in input current which improves power factor.

5. It also provides excellent output performance optimized efficiency and high reliability compared to similar conventional converters.
6. It leads to several advantages such as nearly unity power factor without any reactive elements, symmetric loading from utility point of view and almost uniform temperature. It is proved by experimental setup.

9.3 Scope for Further Research

Consequent to investigations carried out in thesis, the following aspects are being suggested as future work to be carried out.

1. By using new techniques the 3 phase input transformer can be removed to reduce size of Melter so as to design as a table top model as well as providing Ethernet connectivity to the machine to monitor as well as service the machine from remote.
2. Though the PID controller is developed for temperature as a parameter of performance, the second PID loop can be incorporated to control the power of Melter. This can be made possible by interposing suitable software with slight modification as per parametric requirement.
3. More optimization techniques can be used to carry out autotuning of the PID to get better accuracy.

Chapter 10

BIBLIOGRAPHY

This chapter contains the list of papers referred throughout the thesis.

1. K.H.Liu and F.C.Lee, “*Resonant switches-A unified approach to improve performances of switching converters*”, IEEE INTELEC Conference Record, pp.344~351, 1984.
2. K.H.Liu and F.C.Lee, “*Zero-voltage switching technique in DC-DC converters*”, IEEE Power Electronics Specialists Conference Record, pp.58~70, 1986.
3. K.H.Liu, R.Oruganti and F.C.Lee, “*Resonant switches-Topologies and characteristics*”, IEEE Power Electronics Specialists Conference Record, pp.106~116, 1985.
4. H.Ogiwara , A.Okuno and M.Nakaoka, “*High frequency Induction heating load resonant inverter with voltage-clamped quasi-resonant switched using newly improved static induction transistors/thyristors and their phase shifted controlled scheme*” IEEE [Industry Applications Society Annual Meeting, 1992., Conference Record of the 1992 IEEE](#)
Digital Object Identifier: [10.1109/IAS.1992.244445](#). Page(s): 941 - 948 vol.1
5. “*Practical Evaluations Of Single-Ended Load-Resonant Inverter Using Application specific Igbt & Driver Ic For Induction-Heating Appliance*” By Izuo Hirota, Hideki Omori, Kundu Arun Chandra and Mutsuo Nakaoka, [Power Electronics and Drive Systems, 1995., Proceedings of 1995 International Conference on](#) Digital Object Identifier.
6. “*A New half-bridge Inverter Topology with Active Auxiliary Resonant Circuit Using IGBT for Induction Heating Applications*” By Ryoung-Kuk Lee, Jin-Woo Jung, Bum-Seok Suh and Dong-Seck Syun. IEEE [Power Electronics Specialists Conference, 1997. PESC '97 Record., 28th Annual IEEE](#).
7. “*Induction-Heated Cooking Appliance Using New Quasi-Resonant ZVS-PWM Inverter With Power Factor Correction*” By Shengpei Wang, Kiyoshi Izaki, Izuo Hirota, Hidekazu Yamashita, Hideki Omori, and Mutsuo Nakaoka, IEEE Transactions on Industry Applications, Vol. 34, No, 4, JULY/AUGUST 1998 705
8. H.Omori, M.Nakaoka, H.Yamashita and T.Marubishi, “*A novel type induction-heating single ended resonant inverter using new bipolar darlington transistor*”, IEEE PESC Proc., pp.590~599, 1985.
9. G.Zaiser, G.Fischer, M.Bruckmann and H.Doht, “*ZVS driver for voltage-controlled switches in resonant converters*”, Power Conversion, June 1995 Proceedings, pp.481~489.
10. H.W.Koertzen, J.D.van Wyk and J.A.Ferreira, “*Design of the half-bridge series resonant converter for induction heating*”, IEEE PESC Record, vol.2, pp.729~735, 1995.
11. A. Petterteig, J. Lode, and T. M. Undeland, “IGBT turn-off losses for hard switching and with capacitive snubbers,” in *Proc. Conf. Rec. Ind. Appl. Soc. Annu. Meet.*, 1991, pp. 1042–1049.

12. V. K. Khanna, *IGBT Theory and Design*. Piscataway, NJ: IEEE Press, 2003.
13. T.Laska, F.Pfirsch, F.Hirler, J.Niedermeyer, C.Schäffer, T.Schmidt “1200V-Trench- IGBT Study with Square Short Circuit SOA” ISPSD 1998-Kyoto
14. P.Kanschat, T.Stolze, T.Passe, H.Rüthing, F.Umbach, O.Hellmund “600V IGBT³- Technology in New Low Cost Modules for Consumer Drives Applications” PCIM 2003- Nürnberg
15. P.Kanschat, H.Rüthing, F. Umbach, F. Hille „600V-IGBT³: A detailed Analysis of Outstanding Stativ and Dynamic Properties“ PCIM 2004-Nürnberg
16. P.Jain and S.B.Dewan, “*Starting problems associated with a transformer coupled load in a series inverter*”, IEEE Transactions on Magnetics, vol.24, no.6, pp.2895~2897, 1988.
17. G.Zaiser, G.Fischer, M.Bruckmann and H.Doht, “*ZVS driver for voltage-controlled switches in resonant converters*”, Power Conversion, June 1995 Proceedings, pp.481~489.
18. S.Hinchliffe and L.Hobson, *Review of solid state devices and circuits for HF electric process heating applications:Part_ devices*, Int'l Journal of Electronics, vol.61,no.2,pp.143~167, 1986.
19. S.Hinchliffe and L.Hobson, *Review of solid state devices and circuits for HF electric process heating applications:Part_ circuit*, Int'l Journal of Electronics, vol.61,no.3,pp.261~279, 1986.
20. M.Orfeuil & A.Robin, *Electric Process Heating*, Battelle Press, 1987
21. J.Davies, *Induction Heating Handbook*, McGraw-Hill, 1979
22. M.G.Loizinskii, *Industrial Applications of Induction Heating*, Pergamon Press, 1969
23. N.Mohan, T.M.Undeland & W.P.Robbins, *Power Electronics: Converters, Applications, and Design*, John Wiley & Sons, 1989
24. Review of Project at Purdue University... “*Fuzzy logic and Genetic Algorithm Synergism to Control & Identification of Dynamical System*” by Yonghan Lee & Prof. Stanislaw H. Zak. – Project sponsored by National Science Foundation
25. S. Brehaut, F. Costa, J. Casarin, B. Chauchat, “Gate driving of a 3.3kV IGBT chopper by an 8 bits encoded wireless(...)”, Proc. PCIM Europe, S3b2, May 2007
26. D. Vasic, F. Costa, E. Sarraute, “Piezoelectric transformer for integrated MOSFET (...)”, IEEE Trans. Power Electronics, Vol 21, No. 1, pp. 56ff., Jan. 2006
27. M. Münzer, W. Ademmer, B. Strzalkowski, K.T. Kaschani, “Insulated signal transfer in half bridge driver IC based on(...)”, Proc. PEDS, Vol. 1, pp. 93ff., 2003
28. S.Y. Hui, H.S. Chung, S.C. Tang, “Coreless printed circuit board (PCB) transformers (...)”, IEEE Trans. Power Electronics, Vol. 14, No. 3, pp. 422ff., 1999
29. B. Strzalkowski, U. Jansen, U. Schwarzer, “High Performance IGBT Driver in micro transformer technology (...)”, Proc. PCIM Europe, S3b4, May 2007
30. S.C. Tang, S. Y. Hui, H. S. Chung, “Coreless planar PCB transformers a fundamental Concept (...)”, IEEE Trans. Power Electronics, pp. 931ff., Sept. 2000

31. E. Dallago, M. Passoni, G. Venchi, "Design and Optimization of a high insulation voltage DC/DC power (...)", IEEE ICIT'04 Vol.2, pp.596ff., Dec. 2004
32. D.J. Lando, J.P. Mitchell, T.L. Welsher, „Conductive Anodic Filaments In Reinforced Polymeric Dielectrics“, Proc. 17th Annu. Rel. Phys., pp. 5163, 1979
33. P.J. Boddy, R.H. Delaney, J.N. Lahti, E.F. Landry, "Accelerated Life Testing in Flexible Printed Circuits", 14th. Annu. Proc. Rel. Phys, pp. 108ff., 1976
34. A. Brewin, L. Zou, C. Hunt, "Susceptibility of Glass Reinforced Epoxy Laminates to Conductive Anodic (...)", NPL Report MATC(A)155, Jan. 2004
35. K. Rogers, C. Hillman, M. Pecht, "Hollow Fibers Can Accelerate Conductive Filament Formation", ASM Int. Pract. Fail. Analysis, Vol. 1, No. 4, pp.57ff. 2001
36. E.J. Bergum, "CAF Resistance of NonDICY(...)" PCFAB, pp. 26ff. Sep 2002
37. H. Rüedi, P. Köhli, "SCALE Driver for High Voltage IGBTs" PCIM Europe Conference 1999
38. J. Thalheim, "Universal Chipset for IGBT and Power-MOSFET Gate Drivers", PCIM Europe Conference 2007
39. J. Thalheim, "Smart Power Chip Tuning", Bodo's Power Magazine 2007
40. S. Pawel, J. Thalheim, "Prime(PACK) Time for SCALE-2", Bodo's Power Magazine 2008
41. J. Thalheim, O. Garcia, "Optimized Utilization of IGBTs by Plug-and-Play Drivers", Power Electronics Europe 2008
42. B.D.O. Anderson and Y. Liu, "Controller reduction: concepts, and approaches," *IEEE Trans. Automatic Control*, vol. 34, pp. 802-812, Aug. 1989.
43. K.J. Wstrom and T. Hagglund, *PID Controllers: Theory, Design and Tuning, 2nd ed.*, North Carolina: Instrument Society of America, 1995.
44. K.J. Astrom and J. Nilsson, "Analysis of a scheme for iterated identification and control," *Proc. IFAC Symp. Identification*, pp, 171-176, 1994.
45. K.J. Wstrom and B. Wittenmark, *Adaptive Control*. Reading, Massachusetts: Addison-Wesley, 1989.
46. E De Bruyne, B.D.O. Anderson, M. Gevers, and N. Linard, "Iterative controller optimization for nonlinear systems," in *Proc. 36th IEEE Conf Decision and Control*, 1997, pp, 3749-3754.
47. E De Bruyne and P. Carrette, "Synthetic generation of the gradient for an iterative controller optimization method," *CD-ROM of the European Control Conference*, 1997, Paper THA-F2.
48. B. Ceysens and B. Godrons, "Synthèse itérative de contrôleurs sans identification," M.S. thesis, University Catholique de Louvain, 1995.
49. R.A. de Callafon and P.M.J. Van den Hof. "Suboptimal feedback control by a scheme of iterative identification and control design," *Mathematical Modelling of Systems*, vol. 3(1), pp. 77-101, 1997.
50. P.M.J. Van den Hof and R.J.P. Schrama, "Identification and control-- closed-loop issues," *Automatica*, vol. 31, pp. 1751-1770, Dec. 1995.

51. M. Gevers, "Towards a joint design of identification and control?" *Essays on Control: Perspectives in the Theory and its Applications*, eds. H. L. Trentelman and J. C. Willems, pp. 111-151, 1993.
52. C. C. Hang and K. J. Astrom, "Practical aspects of PID auto-tuners based on rely feedback," IFAC adaptive control of chemical process, pp. 153-158, Copenhagen, Denmark, 1988.
53. Ya-Gang Wang, "PI tuning for processes with large dead time," Proceeding of the ACC, pp. 4274-4278, Chicago Illinois, June 2000.
54. Eric Poulin and Andre Pomerleau, "PI setting for integrating processes based on ultimate cycle information," IEEE Trans. On control systems technology, Vol. 7, No. 4, July 1999.
55. K. Natarajan and A. F. Gilbert, "On direct PID controller tuning based on finite number of frequency response data," ISA Trans. Vol. 36, No. 2, pp. 139-149, 1977.
56. T. Hashimoto and Y. Ishida, "An adaptive I-PD controller based on frequency domain system identification," ISA Trans. Vol. 39, pp. 71-78, 2000.
57. Teng Fong-Chwee, "Self-tuning PID controllers for dead time process," IEEE Trans., Vol. 35, No. 1, pp. 119-125, 1988.
58. Kazuyuki Mori and Makoto Tsukiyama, "Immune algorithm with searching diversity and its application to resource allocation problem," Trans. JIEE, Vol. 113 - C, No. 10, '93.
59. A. Ishiguro, T. Kondo, Y. Watanabe and Y. Uchikawa, "Dynamic behavior arbitration of autonomous mobile robots using immune networks," In Proc. of ICEC' 95, vol.2, pp.722-727, 1995.
60. Ishiguro, Y. Watanabe and Y. Uchikawa, "An Immunological Approach to dynamic behavior control for autonomous mobile robots," In Proc. of IROS ' 95, Vol.1, pp.495-500, 1995.
61. Dong Hwa Kim, "Auto-tuning of reference model based PID controller using immune algorithm," IEEE international conference on evolutionary computation, Hawaii, May 12 - 17, 2002.
62. Reato A. Krohling and joost P.Rey, "Design of Optimal Disturbance Rejection PID Controllers Using Genetic Algorithms,"IEEE Trans. Evolutionary and computation. Vol. 5, No. 1, Feb. 2001.
63. Weng Khuen, Chang Chien Hang, and Liseng S. Cao, "Tuning of PID controllers based on gain and phase margin specifications," Automatica, Vol. 31, No. 3, pp. 497-502, 1995.
64. Dong Hwa Kim, Jae Hoon Cho, "Robust PID Controller Tuning Using Multiobjective Optimization Based on Clonal Selection of Immune Algorithm," Lecture Notes in Computer Science Proceeding of Springer (SCI) Sept 22-24, 2004.
65. M. Gevers, "Identification for cotltrol," *Proc. 5th IFAC Symposium Adaptive Control and Signal Processing*, pp. 1-12, 1995.
66. M. Gevers and L. Ljung, "Optimal experiment designs with respect to the intended model application," *Automatica*, vol. 22, pp. 543-554, 1986.

67. H. Hjalmarsson, "Model-free tuning of controllers: Experience with time-varying linear systems," *Proc. 3rd European Control Conference*, pages 2869-2874, 1995.
68. H. Hjalmarsson, "Control of nonlinear systems using iterative feedback tuning," *Proc. American Control Conf 98*, 1998.
69. H. Hjalmarsson, "Performance analysis of iterative feedback tuning," submitted to *Automatica*, 1998.
70. H. Hjalmarsson and T. Birkeland, "Iterative Feedback Tuning of linear time-invariant MIMO systems," submitted to *CDC 98*, 1998.
71. H. Hjalmarsson and M. Gevers, "Frequency domain expressions of the accuracy of a model-free control design scheme," *Proc. 11th IFAC Symp. On System Identification*, vol. 1, pp. 135-140, 1997.
72. H. Hjalmarsson, M. Gevers, and F. De Bruyne, "For model-based control design, closed-loop identification gives better performance," *Automatica*, vol. 32, pp. 1659-1673, 1996.
73. H. Hjalmarsson, S. Gunnarsson, and M. Gevers, "A convergent iterative restricted complexity control design scheme," *Proc. 33rd IEEE CDC*, pp. 1735-1740, 1994.
74. H. Hjalmarsson, S. Gunnarsson, and M. Gevers, "Model-free tuning of a robust controller for a flexible transmission system," *European J. Control*, vol. 1, pp. 148-156, 1995.
75. H. Hjalmarsson, S. Gunnarsson, and M. Gevers, "Optimality and sub-optimality of iterative identification and control design schemes," *Proc. American Control Conf*, vol. 4, pp. 2559-2563, 1995.
76. A.J. Isaksson and S.F. Graebe, "Model reduction for design of digital PID controllers," *Proc. 3rd European Control Conf*, vol. 3, pp. 2191-2196, 1995.
77. Y. Kawamura, "Direct synthesis of LQ controller from inner products of response signals," *Proc. 11th IFAC Symp. System Identification*, vol. 4, pp. 1717-1722, 1997.
78. W.S. Lee, B.D.O. Anderson, R. Kalman, and I.M. Y Mareels, "A new approach to adaptive robust control," *Int. J. Adaptive Control and Signal Processing*, vol. 7, pp. 183-211, 1993.
79. Lequin, "Optimal closed loop PID tuning in the process industry with the Iterative Feedback Tuning scheme," *CD-ROM of European Control Conference*, Paper TH-A-H6, 1997.
80. L. Ljung, *System Identification: Theory for the User*. Englewood Cliffs, NJ: Prentice-Hall, 1987.
81. L. Ljung and T. Soderstrom, *Theory and Practice of Recursive Identification*. Cambridge, Massachusetts: MIT Press, 1983.
82. D. Molenaar, "Model-free data-driven optimal tuning of controller parameters: A practical guide with application examples," Dep. Elec. Eng., Linkoping University, Sweden, Tech. Rep. LiTH-ISY-R-1722 1995.
83. K. S. Narendra and L.E. McBride, "Multiparameter self-optimizing systems using correlation techniques," *IEEE Trans. Automatic Control*, pp. 31-38, 1964.

84. K. S. Narendra and D.N. Streeter, "An adaptive procedure for controlling undefined linear processes," *IEEE Trans. Automatic Control*, pp, 545-548, Oct. 1964.
85. A.G. Partanen and R.R. Bitmead, "The application of an iterative identification and controller design to a sugar cane crushing mill," *Automatica*, vol. 31, pp. 1547-1563, 1995.
86. P. Persson and K.J. Astram, "Dominant pole design-a unified view of PID controller tuning," *Selected Papers from the 4th IFAC Symposium*, pp. 377-382, 1993.
87. H. Robbins and S. Monro, "A stochastic approximation method," *Ann. Math. Stat.*, vol. 22, pp. 400-407, 1951.
88. M.G. Safonov and T.C. Tsao, "The unfalsified control concept and ," *IEEE Trans. Automatic Control*, vol. 42(6), pp. 843-847, June 1997.
89. R.J.P. Schrama and P.M.J. Van den Hof, "Iterative identification and control design: A three step procedure with robustness analysis," *Proc. ECC*, pp. 237-241, 1993.
90. J. Sjöberg and M. Agarwal, "Model-free repetitive control design for nonlinear systems," *Proc. 35th Conference on Decision and Control*, pp. 2824-2829, Dec. 1996.
91. L. Triest, "Etude des paramètres de synthèse dans le réglage itératif optimal d'un régulateur PID," Tech. Rep., Final year undergraduate project, CESAME, Université Catholique de Louvain, Louvain La Neuve, Belgium, 1997.
92. E. Trueson and L. Ljung, "Adaptive control based on explicit criterion minimization," *Automatica*, vol. 21, pp. 385-399, 1985.
93. K. J. Åström, T. Hägglund, C. C. Hang, and W. K. Ho, "Automatic tuning and adaptation for PID controllers—a survey," *Control Eng. Pract.*, vol. 1, no. 4, pp. 699–714, 1993.
94. Control Arts Inc. (2004, May) Control Arts Inc: Process Control, Alarm Analysis, Abnormal Situation Management, Engineering Analysis and Operations Management Software. [Online] <http://www.controlartsinc.com/index.html>
95. Control & Optimization Specialists. (2004, May) COSpecialists—Control & Optimization Specialists. [Online] <http://www.cospecialists.com/index.html>
96. Control Soft Inc. (2004, May) Control Soft Inc.—The Company With Leading Control Technologies. [Online] <http://www.controlsoftinc.com/index.shtml>
97. Tune Plus-PID Tuning Product, Innovation Industries Inc. (2004, May). <http://www.innovin.com/tuneplus.htm> [Online]
98. IPCOS Netherlands/Belgium. (2004, May) IPCOS Creators in Control. [Online] <http://www.ipcos.be/welcome.htm>
99. W. H. Kwon and G. H. Cho, "Modified quantum and phase control of series resonant converter," in *ZEEWPESC Rec*, 1991, pp. 498-503.
100. L. Grajales, J. A. Sabat, K. R. Wang, W. A. Tabisz, and F. C. Lee, "Design of a 10 kW, 500 kHz phase-shift controlled series-resonant inverter for induction heating," in *IEEE/ZAS Annu. Meet.*, 1993, pp. 843-849

101. Zinn, S., Semiantin, S.L., "Elements of Induction Heating, Design, Control, and Applications," Electric Power Research Institute Inc, California, 1988, Chapter 7.
102. L. R. Egan and E. P. Furlani, "A computer simulation of an induction heating system," *IEEE Trans. Magn.*, vol. 27, pp. 4343–4354, Sept. 1991.
103. V. Vorperian and S. Cuk, "A complete analysis of the series resonant converter," in *Proc. IEEE Power Electron. Specialists Conf. Rec.*, 1982, pp. 85–100.
104. Y. Cheron, H. Foch, and J. Salesse, "Study of a resonant converter using power transistors in a 25 kW X-rays tube power supply," in *Proc. IEEE Power Electron. Specialists Conf. Rec.*, 1985, pp. 295–306.
105. H. Omori, T. Twai, M. Nakaoka, and T. Maruhashi, "Circuits topologies of self-controlled single-ended high frequency resonant inverters," in *Proc. Euro. Power Electron. Conf. Rec.*, vol. 1, 1987, pp. 205–211.
106. J. P. Ferrieux, J. P. Keradec, and Y. Baudon, "A high frequency seriesresonant converter using COMFET transistor-application to induction heating," in *Proc. IEEE Ind. Appl. Soc. Conf. Rec.*, 1987, pp. 717–723.
107. K. Isaki, I. Hirota, H. Yamashita, M. Kamli, H. Omori, and M. Nakaoka, "New constant-frequency variable powered quasi-resonant topology using soft-switched type IGBTs for induction-heated cooking appliance," in *Proc. Euro. Power Electron. Conf. Rec.*, vol. 2, 1995, pp. 129–134.
108. J. P. Ferrieux, M. C. Pera-Marion, J. P. Rognon, and J. Nuns, "Power control of two induction loads supplied by a single generator: Two solutions," in *Proc. Euro. Power Electron. Conf. Rec.*, vol. 2, 1995, pp. 379–384.
109. E. Labouré, F. Costa, C. Gautier, and W. Melhem, "Accurate simulation of conducted interferences in isolated DC-to-DC converters regarding to EMI standards," in *Proc. IEEE Power Electron. Specialists Conf. Rec.*, vol. II, 1996, pp. 1973–1978.
110. M. Kamli, S. Yamamoto, and M. Abe, "A 50 kHz–150 kHz half-bridge inverter for induction heating applications," *IEEE Trans. Ind. Electron.*, vol. 43, no. 1, pp. 163–172, 1996.
111. M. K. Kasimierczuk and D. Czarkowski, *Resonant Power Converter*. New York: Wiley, 1995.
112. L. Hobson and D. W. Tebb, "Transistorized power supply for induction heating," *Int. J. Electron.*, vol. 59, pp. 533–542, May 1985.
113. F. P. Dawson and P. Jain, "A comparison of load commutated inverter system for induction heating and melting applications," *IEEE Trans. Power Electron.*, vol. 6, no. 4, pp. 430–441, Jul. 1991.
114. L. Hobson, D. W. Tebb, and D. Turnbull, "Dual element induction cooking unit using power MOSFETs," *Int. J. Electron.*, vol. 59, pp. 747–757, Jun. 1985.

115. H. W. Koertzen, J. D. van Wyk, and J. A. Ferreira, "Design of the halfbridge series resonant converter for induction cooking," in *Proc. IEEE Power Electronics Specialists Conf. (PESC)*, 1995, pp. 729–735.
116. M. Kamli, S. Yamamoto, and M. Abe, "A 50–150 kHz half-bridge inverter for induction heating applications," *IEEE Trans. Ind. Electron.*, vol. 43, no. 1, pp. 163–172, Feb. 1996.
117. Irving Gottlieb; "Solid-state high-frequency power" Reston Publishing Company, Inc, Prentice-Hall Company, pp.31-41, 1989.
118. J.Pförr, L.Hobson, "Resonant-switched mode preconverters for hgh-frequency induction heaters" Proceedings of Power Conversion International Conference (PCIM), pp.245-259, June, 1991.
119. Rapoport, E., Pleshivtseva, Yu.: *Optimal Control of Induction Heating Processes*. DK6039, CRC Press/Taylor & Francis Group, 6000 Broken Sound Parkway, NW Suite, 300. Boca Raton, FL 33487 (USA), 2006, 349 pp.
120. P. P. Roy, S. R. Doradla, S. Deb: "Analysis of the Series Resonant Converter Using a Frequency Domain Model," *IEEE/PESC Rec.*, pp.482-489, 1991.
121. A. Dmowski, R. Bugyi, P. Szewczyk: "A Novel Series- Resonant DC/DC Converter with Full Control of Output Voltage at NeLoad Condition. Computer Simulation Based Design aspects," *IEEE/IAS Annual Meeting*, pp.924-928, 1992.
122. M. Nakaoka, Y. J. Kim, H. Ogiwara, H. Uemura: "Modern Digitally-Controlled Constant High- Frequency PWM Resonant DC-DC Converter Using Lumped Parastic Reactive Circuit Components of High-Voltage Transformer & Feeding Cable and its New Practical Application," *IEEE/IAS Annual Meeting*, pp.1088-1097, 1991.
123. W. H. Kwon, G. H. Cho: "Modified Quantum and Phase Control of Series Resonant Converter," [*EEE/PESC Rec.*, pp.498-503, 1991.
124. Paul Emerald, "'Non-Intrusive' Hall-Effect Current-Sensing Techniques Provide Safe, Reliable Detection and Protection for Power Electronics," Allegro Microsystems, Inc. Technical Paper STP 98-1, page 2.
125. Alex Goldman, *Handbook of Modern Ferromagnetic materials*, Boston: Kluwer Academic Publishers, 1999, 59.
126. "Using Current Monitoring for Load Analysis," Kele Technical Reference PM6, accessed 062802, <http://www.kele.com/Tech/Monitor/Power/TRefPM6.html>.
127. J. Thalheim, H. Ruedi, "Universal Chipset for IGBT and Power MOSFET Gate Drivers", *Proc. PCIM Europe Conference*, Nuremberg, 2007
128. H. Ruedi, P. Kohli: New drivers feature active clamping, *Power Electronics Europe* 1/2000, pp. 32-36.
129. J. Thalheim: *Control Strategies for Balancing of Series and Parallel Connected IGBT/Diode Modules*. Series in Microelectronics, volume 139, 2004.

APPENDIX-A

USING DEVELOPMENT TOOLS

A.1 Programming AT89C51ED2

Following steps should be executed in sequence to program AT89C51ED2 micro-controller.

1. Compile the whole project using Keil uv3 and generate hex file.
2. The hex file can be downloaded (programmed) into AT89C51ED2 using any third party programmer e.g. Crystal Programmer as shown in Figure A-1.
3. Run the P4MIC software and read the hex file into buffer.
4. Go to Device & select the ATMEL AT89C51ED2 controller.
5. Go to Function tab & then click on Auto, which will do all necessary steps automatically & the hex file will be downloaded into micro-controller.



Figure A-1 Crystal Programmer



Figure A-2 Programming window

A.2 Keil Real View Project Creation

Follow the steps to create embedded controller project.

1. Open Keil Real View/Keil uv4.
2. Click the New uvision project button to launch the New Project Wizard.
3. Provide name and location for the project as shown in Figure A-3.
4. Choose CPU as NXP LPC2478 and press ok.
5. The start-up file will be automatically loaded.

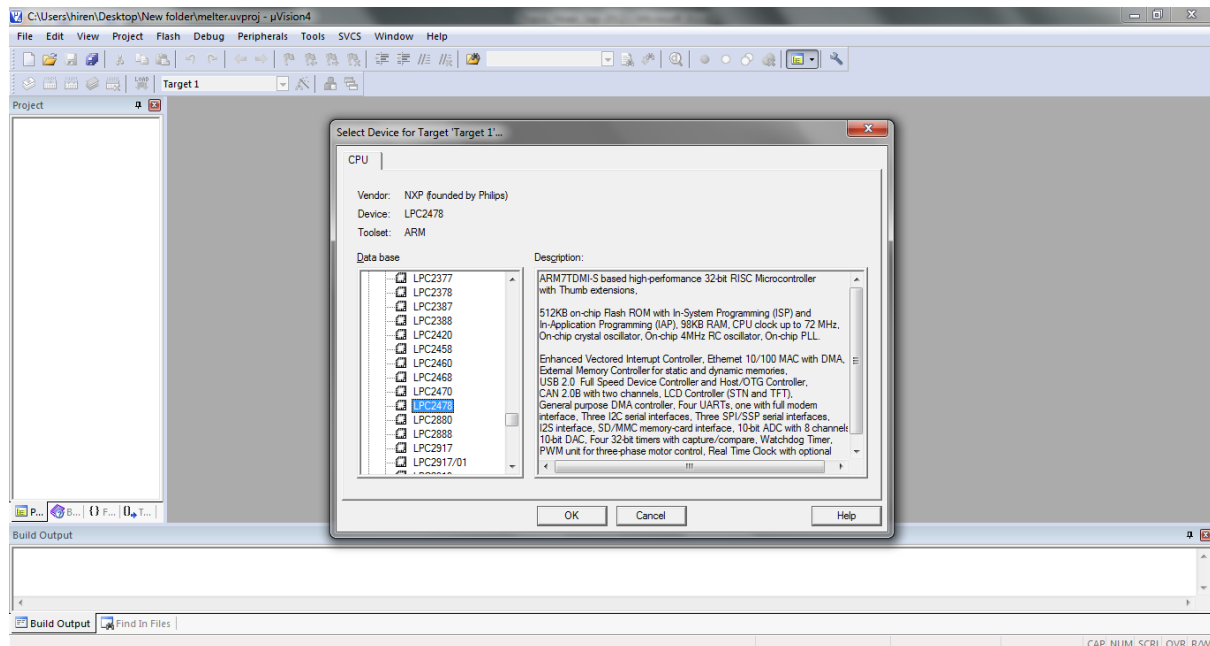


Figure A-3 New Project wizard

6. In Project window double click on LPC2400.S and configure external dynamic & static memory interface by entering into Configuration Wizard as shown in Figure A-4.

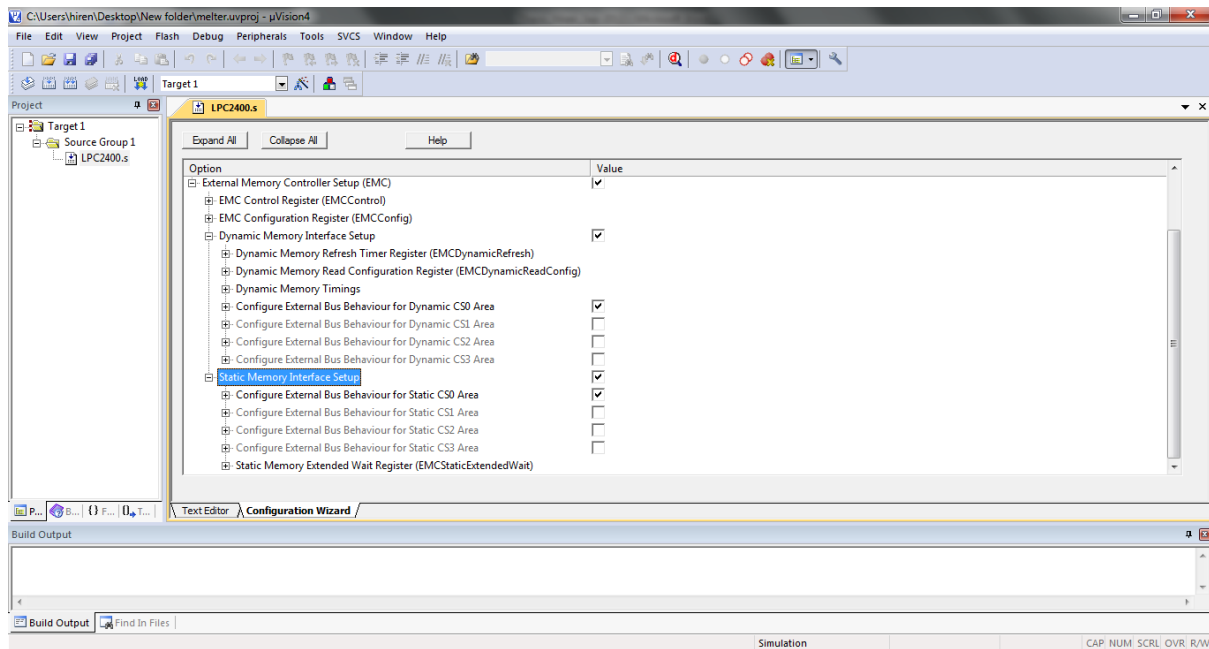


Figure A-4 Configuration wizard

7. Add groups as shown in the Figure A-5 and add c files and distribute whole program into different groups & files.

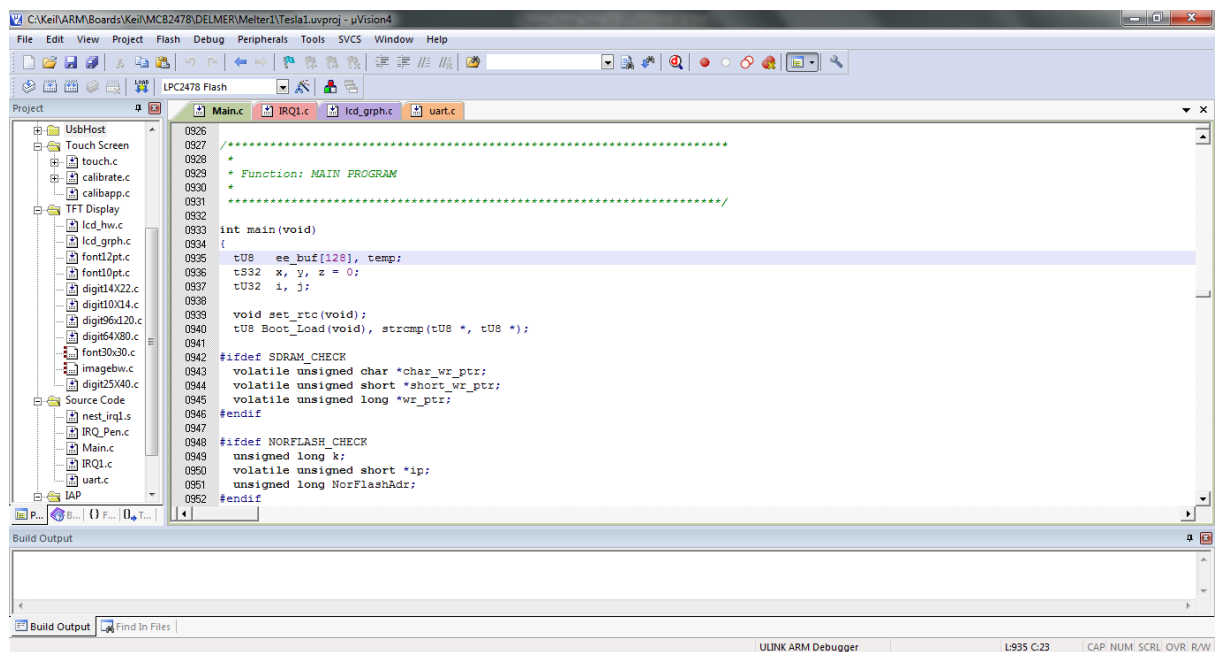


Figure A-5 Project Creation with Different groups

8. Once whole project is ready, click on Rebuild All target files button.
9. After successfully compiling the project, now it is ready to download and debug the project into actual hardware.
10. Connect a ULINK-2 converter between usb-port of PC and the Embedded hardware.
11. Press Debug button, the program will be downloaded into hardware & a debug window will open where the program can be executed step by step or the break points can be kept.

A.3 Eagle Schematic Design

Eagle 5.4 can be used to create schematic design & then to create artwork for manufacturing pcb.

Figure A-6 shows the schematic design created in Eagle 5.4.

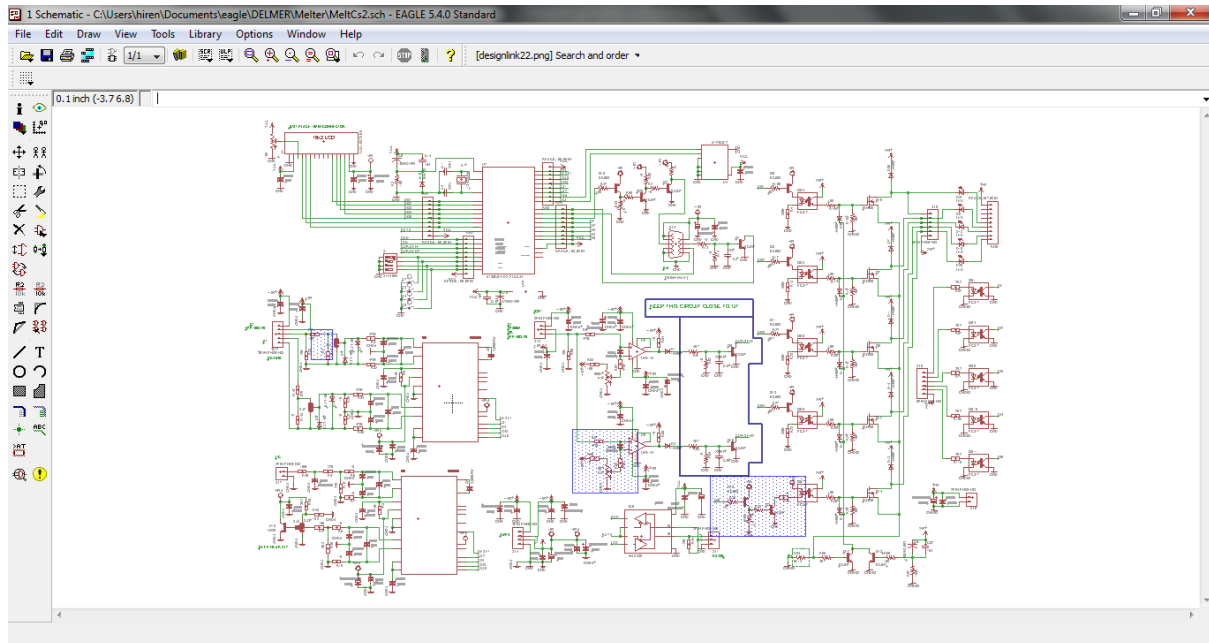


Figure A-6 Schematic Design in Eagle 5.4

A.3 Datasheet of IGBT



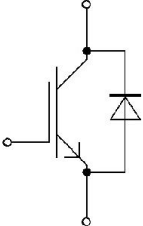


Technische Information / technical information															
IGBT-Module IGBT-modules <h1 style="text-align: center;">FZ600R12KE4</h1>															
62mm C-Serien Modul mit Trench/Fieldstopp IGBT4 und Emitter Controlled 4 Diode 62mm C-Series module with Trench/Fieldstop IGBT4 and Emitter Controlled 4 diode Vorläufige Daten / preliminary data															
 <p style="text-align: right;">Typical Appearance</p>		 <p> $V_{CES} = 1200V$ $I_{C\ nom} = 600A / I_{CRM} = 1200A$ </p>													
Typische Anwendungen <ul style="list-style-type: none"> • Hochleistungsumrichter • Motorantriebe • USV-Systeme • Windgeneratoren 		Typical Applications <ul style="list-style-type: none"> • High Power Converters • Motor Drives • UPS Systems • Wind Turbines 													
Elektrische Eigenschaften <ul style="list-style-type: none"> • Erweiterte Sperrschichttemperatur $T_{vj\ op}$ • Niedrige Schaltverluste • Sehr große Robustheit • V_{CEsat} mit positivem Temperaturkoeffizienten • niedriges V_{CEsat} 		Electrical Features <ul style="list-style-type: none"> • Extended Operation Temperature $T_{vj\ op}$ • Low Switching Losses • Unbeatable Robustness • V_{CEsat} with positive Temperature Coefficient • Low V_{CEsat} 													
Mechanische Eigenschaften <ul style="list-style-type: none"> • 4kV AC 1min Isolationsfestigkeit • Gehäuse mit CTI > 400 • Große Luft- und Kriechstrecken • Isolierte Bodenplatte • Standardgehäuse 		Mechanical Features <ul style="list-style-type: none"> • 4kV AC 1min Insulation • Package with CTI > 400 • High Creepage and Clearance Distances • Isolated Base Plate • Standard Housing 													
Module Label Code															
Barcode Code 128  <p>0000012345600000000000</p>		Content of the Code													
DMX - Code 		<table border="1"> <thead> <tr> <th></th> <th>Digit</th> </tr> </thead> <tbody> <tr> <td>Module Serial Number</td> <td>1 - 5</td> </tr> <tr> <td>Module Material Number</td> <td>6 - 11</td> </tr> <tr> <td>Production Order Number</td> <td>12 - 19</td> </tr> <tr> <td>Datecode (Production Year)</td> <td>20 - 21</td> </tr> <tr> <td>Datecode (Production Week)</td> <td>22 - 23</td> </tr> </tbody> </table>			Digit	Module Serial Number	1 - 5	Module Material Number	6 - 11	Production Order Number	12 - 19	Datecode (Production Year)	20 - 21	Datecode (Production Week)	22 - 23
	Digit														
Module Serial Number	1 - 5														
Module Material Number	6 - 11														
Production Order Number	12 - 19														
Datecode (Production Year)	20 - 21														
Datecode (Production Week)	22 - 23														
<table border="1"> <tr> <td>prepared by: MK</td> <td>date of publication: 2009-08-07</td> <td>material no: 31516</td> </tr> <tr> <td>approved by: WR</td> <td>revision: 2.1</td> <td>UL approved (E83335)</td> </tr> </table>		prepared by: MK	date of publication: 2009-08-07	material no: 31516	approved by: WR	revision: 2.1	UL approved (E83335)								
prepared by: MK	date of publication: 2009-08-07	material no: 31516													
approved by: WR	revision: 2.1	UL approved (E83335)													

Figure A-7a Datasheet of FZ600R12KE4 IGBT


Technische Information / technical information					
IGBT-Module IGBT-modules		FZ600R12KE4			
		Vorläufige Daten preliminary data			
IGBT-Wechselrichter / IGBT-inverter					
Höchstzulässige Werte / maximum rated values					
Kollektor-Emitter-Sperrspannung collector-emitter voltage	$T_{vj} = 25^{\circ}\text{C}$	V_{CES}	1200	V	
Kollektor-Dauergleichstrom DC-collector current	$T_C = 100^{\circ}\text{C}, T_{vj} = 175^{\circ}\text{C}$	$I_{C_{nom}}$	600	A	
Periodischer Kollektor Spitzenstrom repetitive peak collector current	$t_p = 1 \text{ ms}$	I_{CRM}	1200	A	
Gesamt-Verlustleistung total power dissipation	$T_C = 25^{\circ}\text{C}, T_{vj} = 175^{\circ}\text{C}$	P_{tot}	3000	W	
Gate-Emitter-Spitzenspannung gate-emitter peak voltage		V_{GES}	+/-20	V	
Charakteristische Werte / characteristic values					
			min.	typ.	max.
Kollektor-Emitter Sättigungsspannung collector-emitter saturation voltage	$I_C = 600 \text{ A}, V_{GE} = 15 \text{ V}$ $I_C = 600 \text{ A}, V_{GE} = 15 \text{ V}$ $I_C = 600 \text{ A}, V_{GE} = 15 \text{ V}$	$T_{vj} = 25^{\circ}\text{C}$ $T_{vj} = 125^{\circ}\text{C}$ $T_{vj} = 150^{\circ}\text{C}$	$V_{CE_{sat}}$	1,75 2,00 2,05	2,10 V V V
Gate-Schwellenspannung gate threshold voltage	$I_C = 23,0 \text{ mA}, V_{CE} = V_{GE}, T_{vj} = 25^{\circ}\text{C}$		$V_{GE_{th}}$	5,2	5,8 6,4 V
Gateladung gate charge	$V_{GE} = -15 \text{ V} \dots +15 \text{ V}$		Q_G	5,60	μC
Interner Gatewiderstand internal gate resistor	$T_{vj} = 25^{\circ}\text{C}$		R_{Gint}	1,3	Ω
Eingangskapazität input capacitance	$f = 1 \text{ MHz}, T_{vj} = 25^{\circ}\text{C}, V_{CE} = 25 \text{ V}, V_{GE} = 0 \text{ V}$		C_{iss}	42,0	nF
Rückwirkungskapazität reverse transfer capacitance	$f = 1 \text{ MHz}, T_{vj} = 25^{\circ}\text{C}, V_{CE} = 25 \text{ V}, V_{GE} = 0 \text{ V}$		C_{res}	1,70	nF
Kollektor-Emitter Reststrom collector-emitter cut-off current	$V_{CE} = 1200 \text{ V}, V_{GE} = 0 \text{ V}, T_{vj} = 25^{\circ}\text{C}$		I_{CES}		5,0 mA
Gate-Emitter Reststrom gate-emitter leakage current	$V_{CE} = 0 \text{ V}, V_{GE} = 20 \text{ V}, T_{vj} = 25^{\circ}\text{C}$		I_{GES}		400 nA
Einschaltverzögerungszeit (ind. Last) turn-on delay time (inductive load)	$I_C = 600 \text{ A}, V_{CE} = 600 \text{ V}$ $V_{GE} = \pm 15 \text{ V}$ $R_{Gon} = 1,2 \Omega$	$T_{vj} = 25^{\circ}\text{C}$ $T_{vj} = 125^{\circ}\text{C}$ $T_{vj} = 150^{\circ}\text{C}$	t_{don}	0,24 0,25 0,26	μs μs μs
Anstiegszeit (induktive Last) rise time (inductive load)	$I_C = 600 \text{ A}, V_{CE} = 600 \text{ V}$ $V_{GE} = \pm 15 \text{ V}$ $R_{Gon} = 1,2 \Omega$	$T_{vj} = 25^{\circ}\text{C}$ $T_{vj} = 125^{\circ}\text{C}$ $T_{vj} = 150^{\circ}\text{C}$	t_r	0,09 0,10 0,11	μs μs μs
Abschaltverzögerungszeit (ind. Last) turn-off delay time (inductive load)	$I_C = 600 \text{ A}, V_{CE} = 600 \text{ V}$ $V_{GE} = \pm 15 \text{ V}$ $R_{Goff} = 1,2 \Omega$	$T_{vj} = 25^{\circ}\text{C}$ $T_{vj} = 125^{\circ}\text{C}$ $T_{vj} = 150^{\circ}\text{C}$	t_{doff}	0,61 0,64 0,66	μs μs μs
Fallzeit (induktive Last) fall time (inductive load)	$I_C = 600 \text{ A}, V_{CE} = 600 \text{ V}$ $V_{GE} = \pm 15 \text{ V}$ $R_{Goff} = 1,2 \Omega$	$T_{vj} = 25^{\circ}\text{C}$ $T_{vj} = 125^{\circ}\text{C}$ $T_{vj} = 150^{\circ}\text{C}$	t_f	0,10 0,14 0,15	μs μs μs
Einschaltverlustenergie pro Puls turn-on energy loss per pulse	$I_C = 600 \text{ A}, V_{CE} = 600 \text{ V}, L_S = 60 \text{ nH}$ $V_{GE} = \pm 15 \text{ V}, di/dt = 5500 \text{ A}/\mu\text{s} (T_{vj}=150^{\circ}\text{C})$ $R_{Gon} = 1,2 \Omega$	$T_{vj} = 25^{\circ}\text{C}$ $T_{vj} = 125^{\circ}\text{C}$ $T_{vj} = 150^{\circ}\text{C}$	E_{on}	35,0 50,0 55,0	mJ mJ mJ
Abschaltverlustenergie pro Puls turn-off energy loss per pulse	$I_C = 600 \text{ A}, V_{CE} = 600 \text{ V}, L_S = 60 \text{ nH}$ $V_{GE} = \pm 15 \text{ V}, du/dt = 3500 \text{ V}/\mu\text{s} (T_{vj}=150^{\circ}\text{C})$ $R_{Goff} = 1,2 \Omega$	$T_{vj} = 25^{\circ}\text{C}$ $T_{vj} = 125^{\circ}\text{C}$ $T_{vj} = 150^{\circ}\text{C}$	E_{off}	50,0 75,0 80,0	mJ mJ mJ
Kurzschlussverhalten SC data	$V_{GE} \leq 15 \text{ V}, V_{CC} = 800 \text{ V}$ $V_{CE_{max}} = V_{CES} - L_{sCE} \cdot di/dt$	$t_p \leq 10 \mu\text{s}, T_{vj} = 150^{\circ}\text{C}$	I_{sc}	2400	A
Innerer Wärmewiderstand thermal resistance, junction to case	pro IGBT / per IGBT		R_{thJC}		0,05 K/W
Übergangs-Wärmewiderstand thermal resistance, case to heatsink	pro IGBT / per IGBT $\lambda_{Paste} = 1 \text{ W/(m}\cdot\text{K)} / \lambda_{grease} = 1 \text{ W/(m}\cdot\text{K)}$		R_{thCH}	0,017	K/W
prepared by: MK		date of publication: 2009-08-07			
approved by: WR		revision: 2.1			

Figure A-7b Datasheet of FZ600R12KE4 IGBT


Technische Information / technical information					
IGBT-Module IGBT-modules		FZ600R12KE4			
Vorläufige Daten preliminary data					
Diode-Wechselrichter / diode-inverter					
Höchstzulässige Werte / maximum rated values					
Periodische Spitzenspernung repetitive peak reverse voltage	$T_{vj} = 25^{\circ}\text{C}$	V_{RRM}	1200	V	
Dauergleichstrom DC forward current		I_F	600	A	
Periodischer Spitzenstrom repetitive peak forward current	$t_P = 1\text{ ms}$	I_{FRM}	1200	A	
Grenzlastintegral I^2t - value	$V_R = 0\text{ V}, t_P = 10\text{ ms}, T_{vj} = 125^{\circ}\text{C}$ $V_R = 0\text{ V}, t_P = 10\text{ ms}, T_{vj} = 150^{\circ}\text{C}$	I^2t	51000 49000	A ² s A ² s	
Charakteristische Werte / characteristic values					
			min.	typ.	max.
Durchlassspannung forward voltage	$I_F = 600\text{ A}, V_{GE} = 0\text{ V}$ $I_F = 600\text{ A}, V_{GE} = 0\text{ V}$ $I_F = 600\text{ A}, V_{GE} = 0\text{ V}$	$T_{vj} = 25^{\circ}\text{C}$ $T_{vj} = 125^{\circ}\text{C}$ $T_{vj} = 150^{\circ}\text{C}$	V_F	1,80 1,75 1,70	2,35 V V V
Rückstromspitze peak reverse recovery current	$I_F = 600\text{ A}, -di_F/dt = 5500\text{ A}/\mu\text{s} (T_{vj}=150^{\circ}\text{C})$ $V_R = 600\text{ V}$ $V_{GE} = -15\text{ V}$	$T_{vj} = 25^{\circ}\text{C}$ $T_{vj} = 125^{\circ}\text{C}$ $T_{vj} = 150^{\circ}\text{C}$	I_{RM}	440 560 590	A A A
Sperverzögerungsladung recovered charge	$I_F = 600\text{ A}, -di_F/dt = 5500\text{ A}/\mu\text{s} (T_{vj}=150^{\circ}\text{C})$ $V_R = 600\text{ V}$ $V_{GE} = -15\text{ V}$	$T_{vj} = 25^{\circ}\text{C}$ $T_{vj} = 125^{\circ}\text{C}$ $T_{vj} = 150^{\circ}\text{C}$	Q_r	55,0 100 115	μC μC μC
Abschaltenergie pro Puls reverse recovery energy	$I_F = 600\text{ A}, -di_F/dt = 5500\text{ A}/\mu\text{s} (T_{vj}=150^{\circ}\text{C})$ $V_R = 600\text{ V}$ $V_{GE} = -15\text{ V}$	$T_{vj} = 25^{\circ}\text{C}$ $T_{vj} = 125^{\circ}\text{C}$ $T_{vj} = 150^{\circ}\text{C}$	E_{rec}	27,0 52,0 60,0	mJ mJ mJ
Innerer Wärmewiderstand thermal resistance, junction to case	pro Diode / per diode		R_{thJC}		0,07 K/W
Übergangs-Wärmewiderstand thermal resistance, case to heatsink	pro Diode / per diode $\lambda_{Paste} = 1\text{ W}/(\text{m}\cdot\text{K}) \quad / \quad \lambda_{grease} = 1\text{ W}/(\text{m}\cdot\text{K})$		R_{thCH}	0,024	K/W
prepared by: MK date of publication: 2009-08-07					
approved by: WR revision: 2.1					

Figure A-7c Datasheet of FZ600R12KE4 IGBT

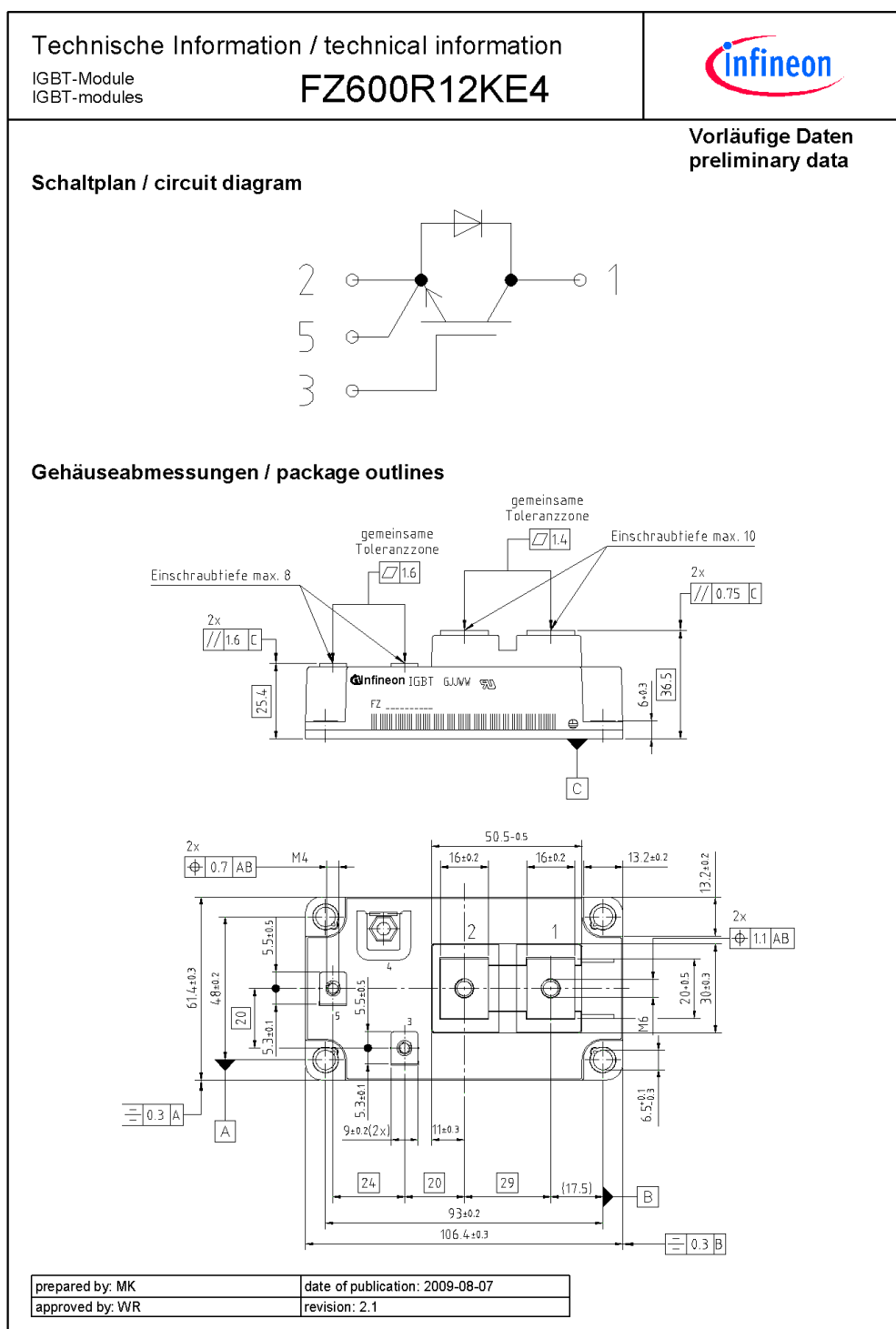


Figure A-7d Datasheet of FZ600R12KE4 IGBT

APPENDIX-B

PHOTO GALLERY

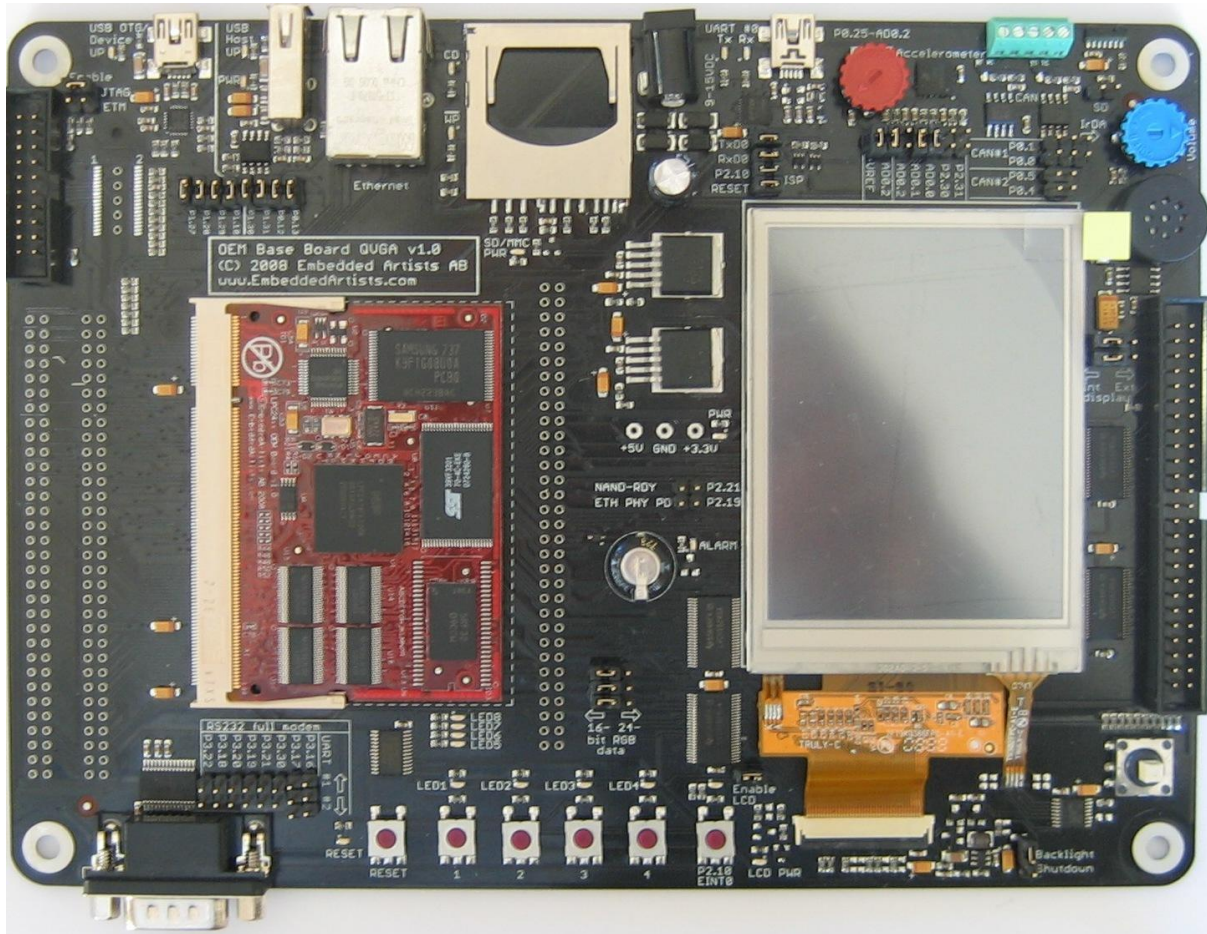


Figure B-1 LPC2478 OEM Board



Figure B-2 Thermocouple Mounting

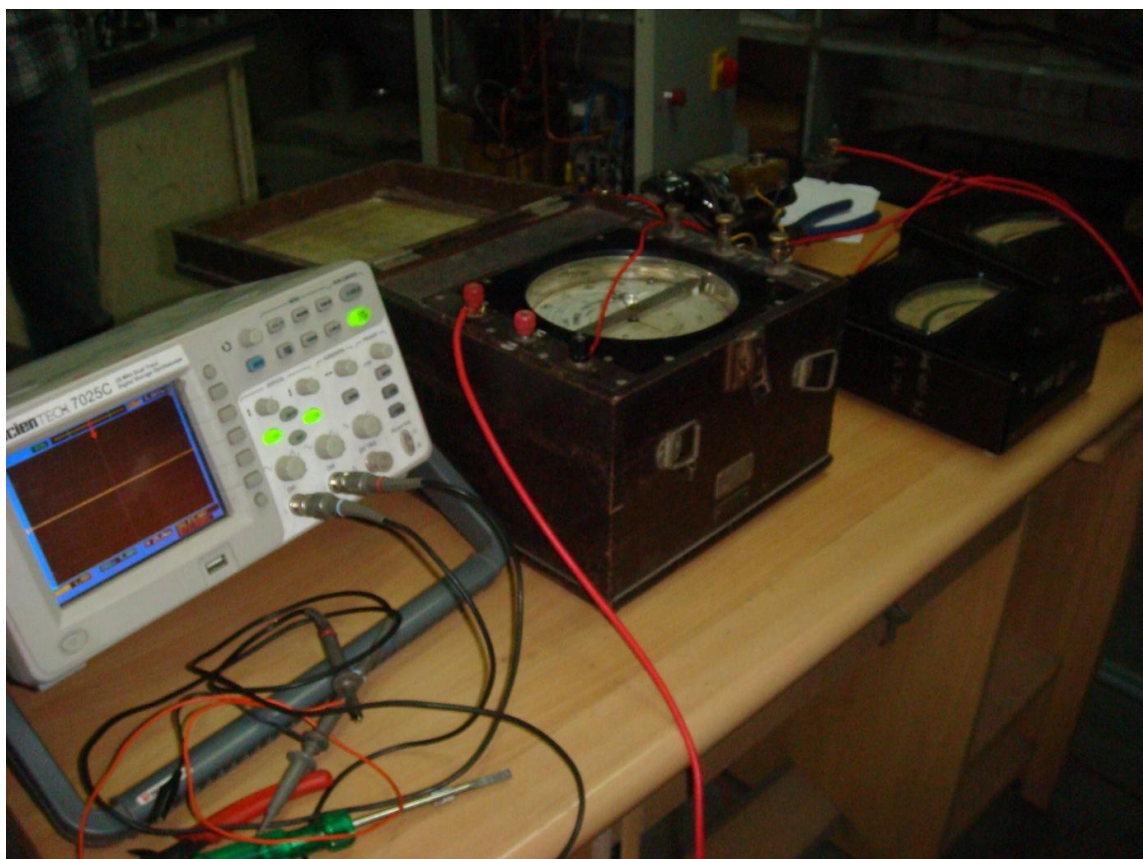


Figure B-3 Meters & DSO



Figure B-4 LCD display of Mirco-controller Board (POWER-OFF)

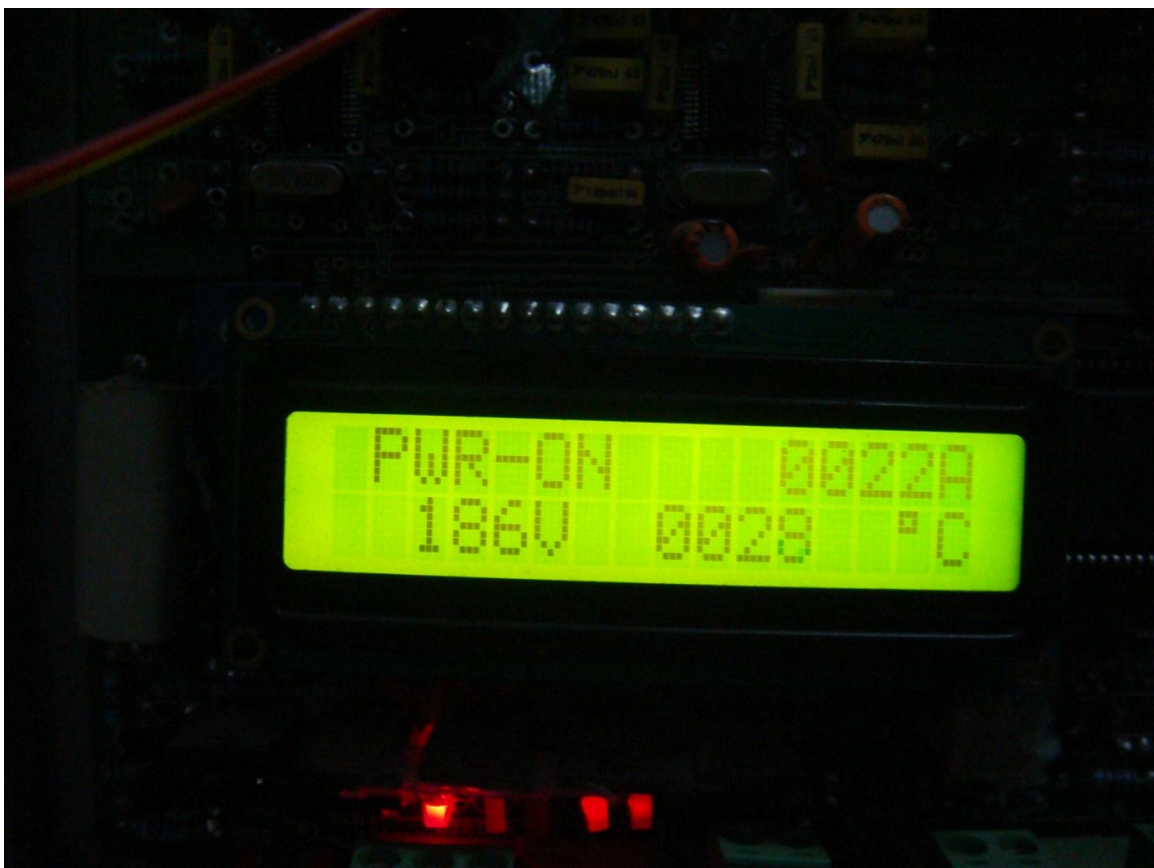


Figure B-5 LCD display of Mirco-controller Board (POWER-ON)

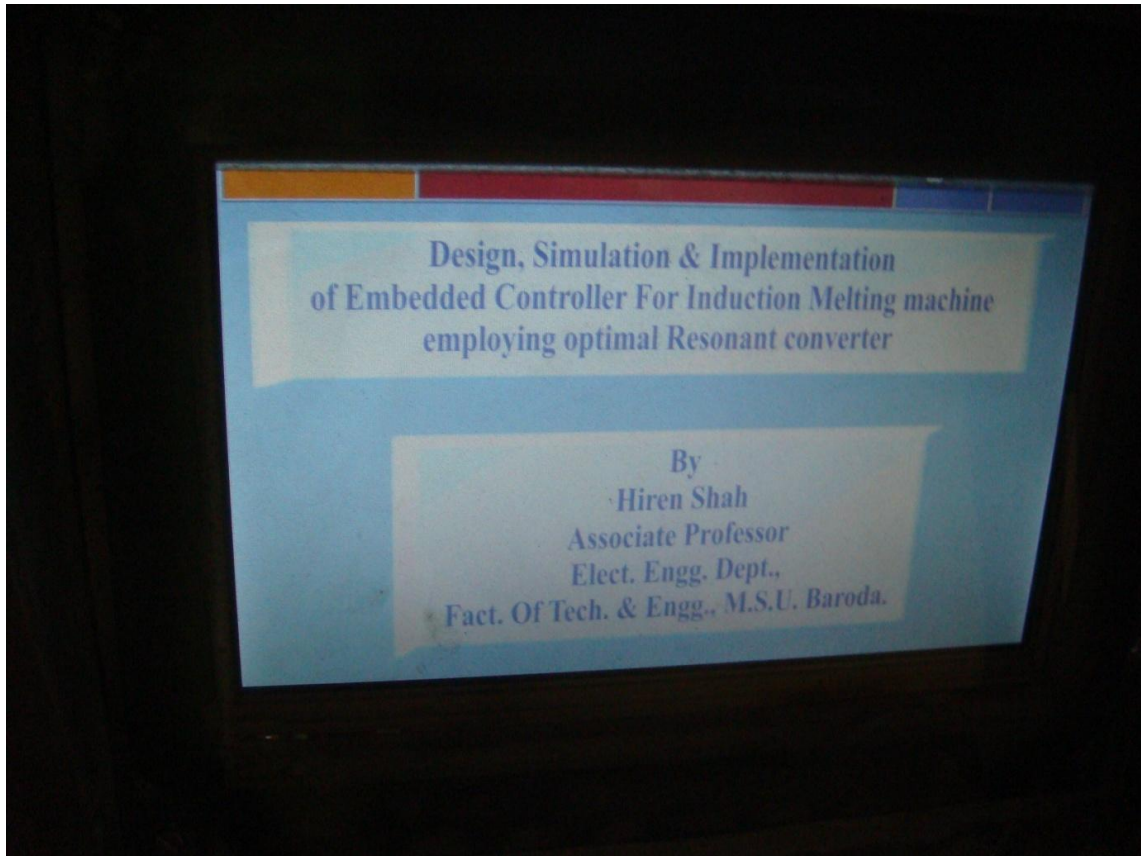


Figure B-6 Title Screen of Embedded Controller

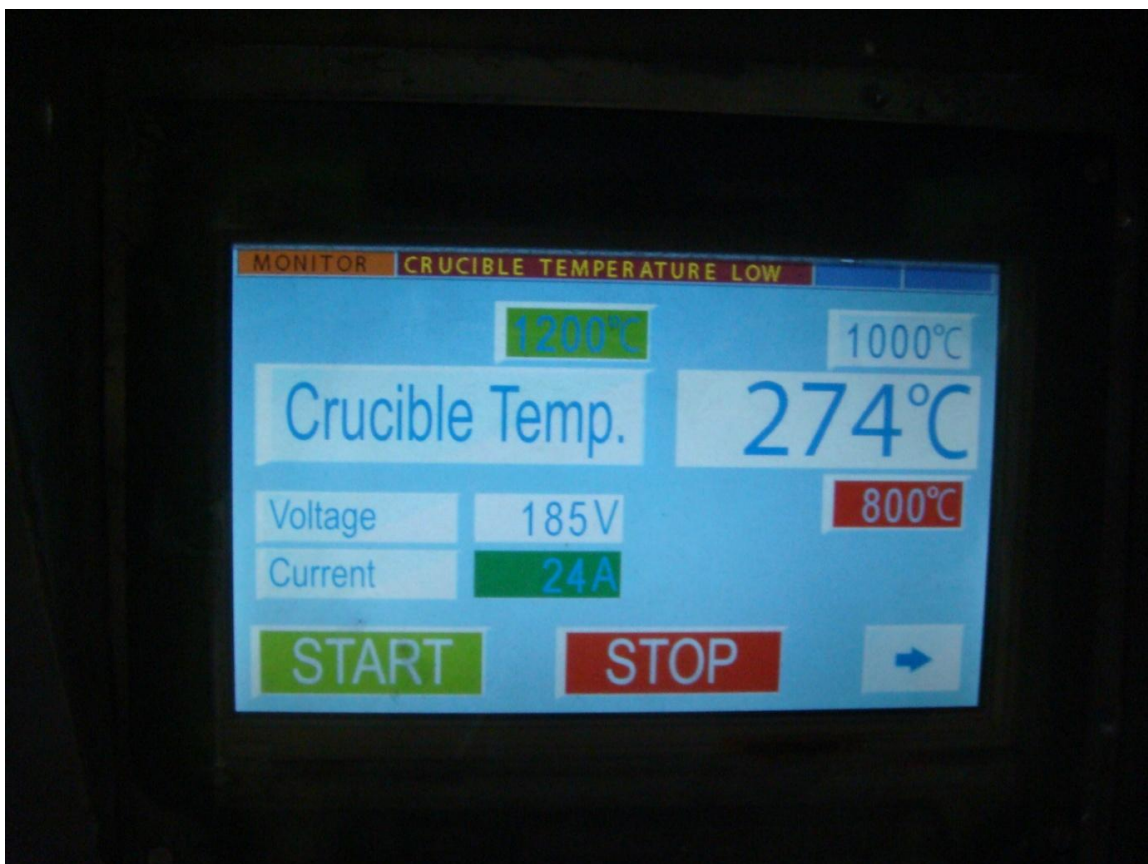


Figure B-7 Monitor Screen of Embedded Controller

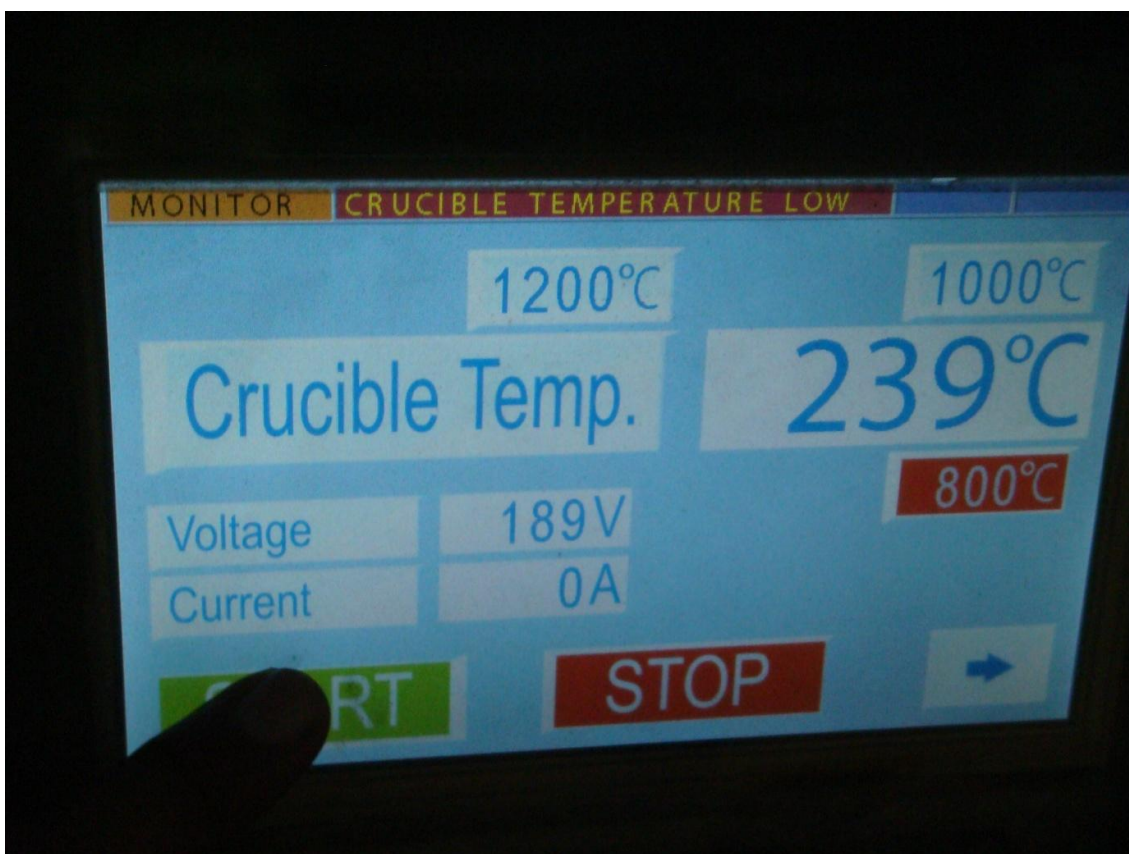


Figure B-8 Screen of Embedded Controller showing START of Melter Power

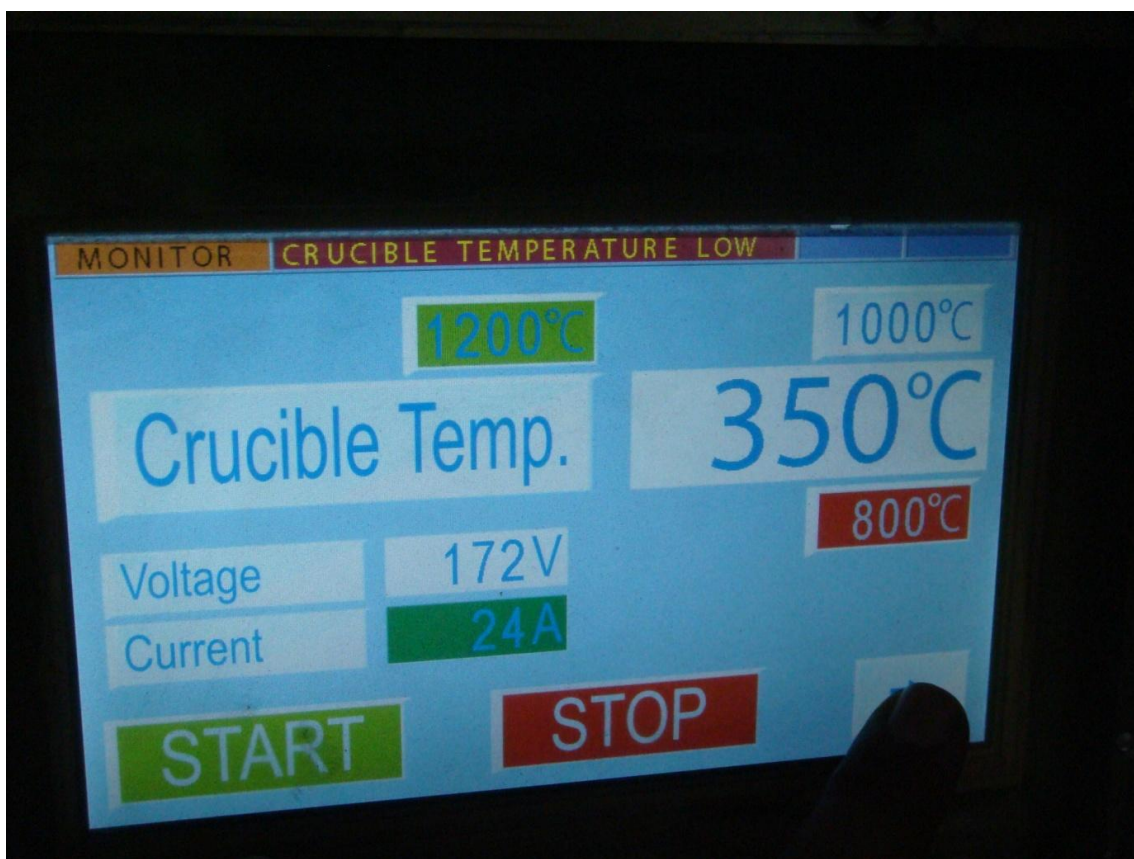


Figure B-9 Screen of Embedded Controller for going into Parameter Menu

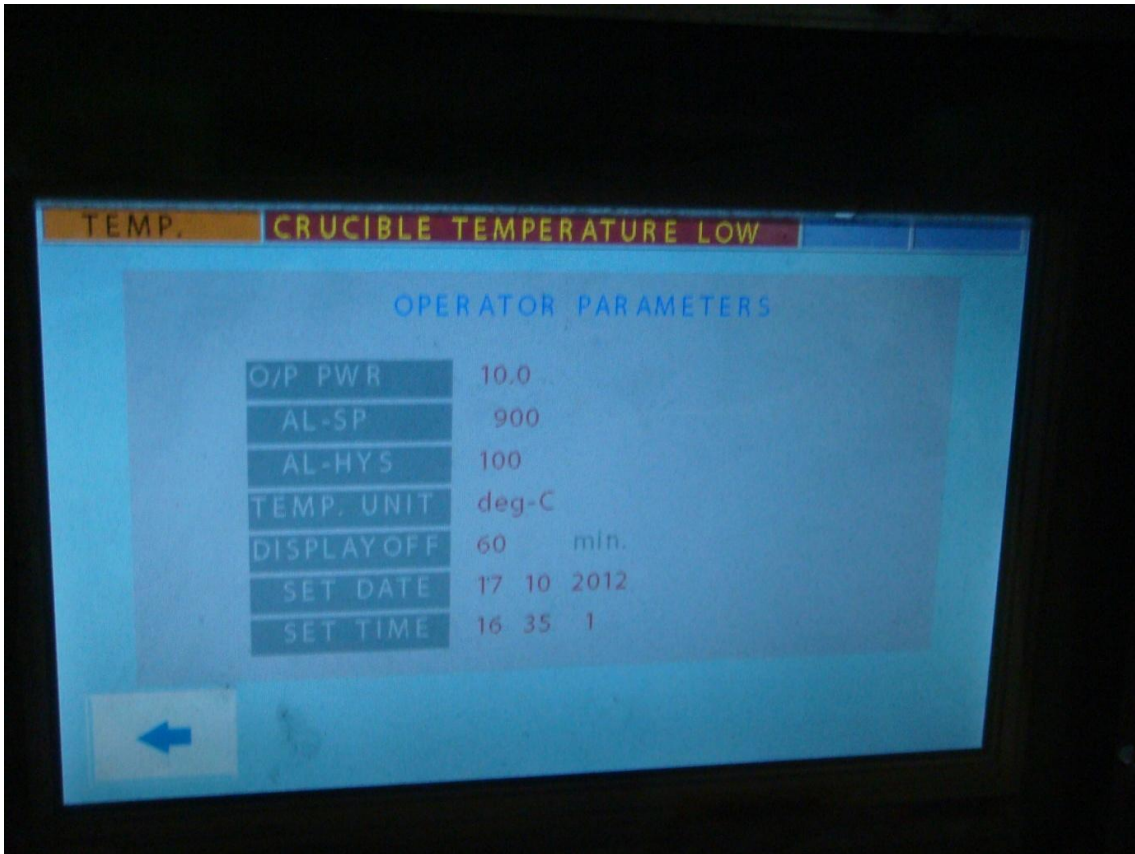


Figure B-10 Parameter Screen of Embedded Controller

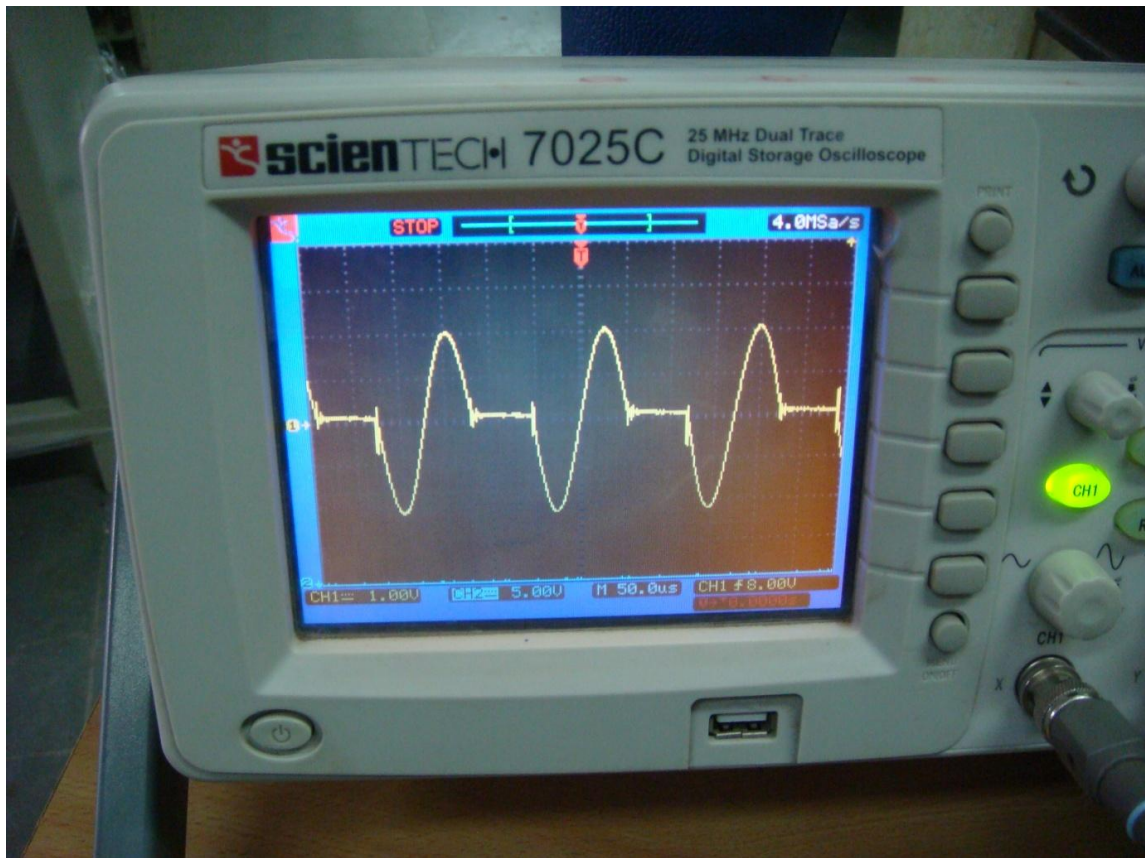


Figure B-11 Snapshot of D.S.O. showing Tank Current



Figure B-12 Whole setup for metering



Figure B-13 Prototype Model of Induction Melter



Figure B-14 Testing of Induction Melter in Progress-1



Figure B-15 Testing of Induction Melter in Progress-2



Figure B-16 Work Pieces of Copper

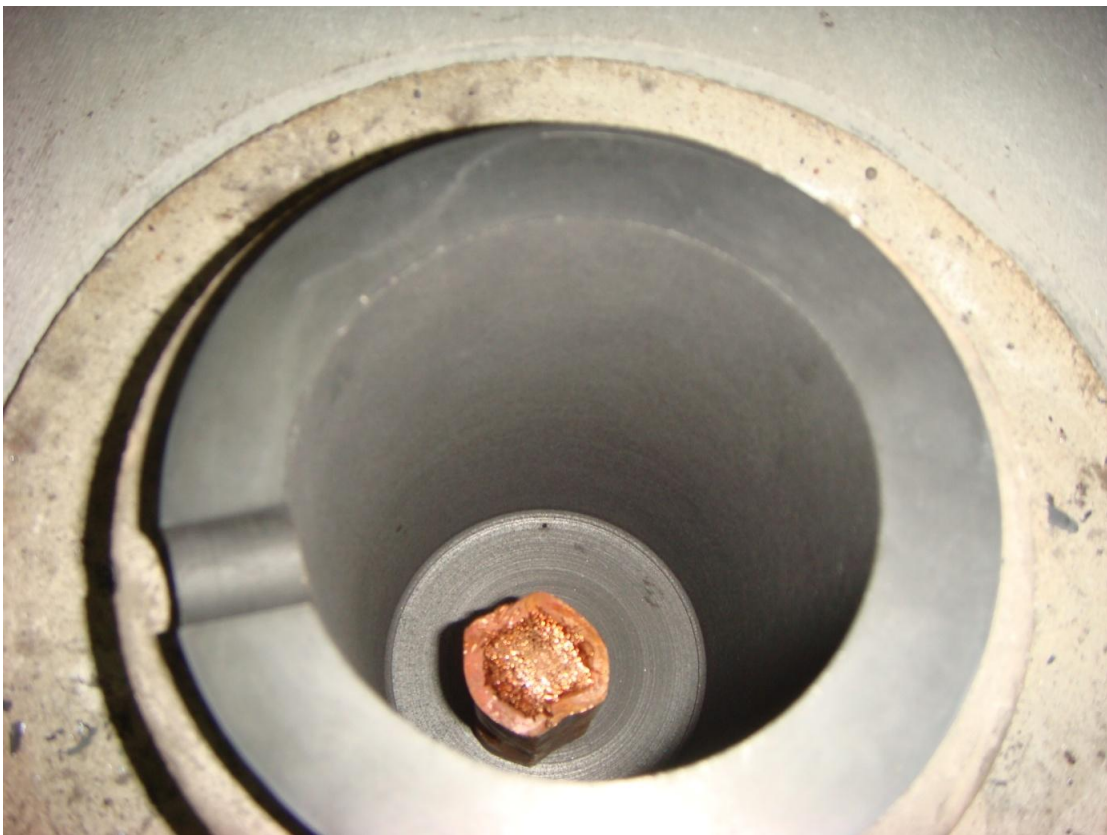


Figure B-17 Work Pieces in Crucible



Figure B-18 Insertion of long copper piece to show effect of load inductance changes



Figure B-19 Melted work pieces